NTNU – Trondheim
Norwegian University of
Science and Technology

2D Vertical Effective Stress Modeling of the Tor Area

Sabrina Berg

Earth Sciences and Petroleum Engineering
Submission date: May 2012
Supervisor: Rune Martin Holt, IPT
Co-supervisor: Stein Haavardstein, ConocoPhillips

Norwegian University of Science and Technology
Department of Petroleum Engineering and Applied Geophysics

Acknowledgments

I would like to thank ConocoPhillips and their employees for giving me the opportunity to write and complete my master thesis in collaboration with their company. Great thanks go to my supervisor at ConocoPhillips, Stein Haavardstein, for assisting and guiding me through the work process leading to the completion of this thesis. Thanks are also given Michael Shaver for being a great help and support in data mining and utilizing Predict. In addition to this, I would like to thank my supervisor at NTNU, Professor Rune Holt, for overseeing the course of my project. Finally, I would like to thank my family and fellow graduates for the support and motivation given throughout the entire process of completing this thesis.

Trondheim
May 2012

Sabrina Berg

"All men by nature desire to know."

-Aristoteles

Sammendrag

I flere tiår har oljeindustrien letet og boret etter hydrokarboner. På norsk sokkel er de fleste oppdagede store felt i sluttfasen, noe som betyr at utvinning av den resterende oljen kan kreve meget komplekse brønner. Disse brønnene kan være av typen med både høyt trykk og høy temperatur, og begrunnet det svært smale borevinduet i slike brønner samt de operasjonelle utfordringene som hører sammen med dem, har de ikke vært mulige å bore tidligere. Nøyaktig estimering av dette borevinduet er derfor helt avgjørende i forhold til planlegging og boring av brønner. Ved å bygge en grundig kalibrert geomekanisk modell er det mulig å estimere de forskjellige trykkgradientene som er til stede, samt predikere det operasjonelle borevinduet.

Denne hovedoppgaven omhandler byggingen av en 2D Tor felt spesifikk lineær elastisk geomekanisk modell. 2D-aspektet av denne modellen kommer av det faktumet at flere nærliggende brønner har blitt brukt til å bygge modellen. I tilfellet der kun en brønn hadde blitt brukt, hadde den resulterende modellen vært 1D. På bakgrunn av loggdata, borehullretningsdata og andre målinger tatt under boring kan den initiale modellen bygges ved hjelp av programvaren Predict. Ved å undersøke diverse dokumenter som beskriver boreprosessen, kan informasjon om operasjonelle hendelser brukes til å kalibrere modellen slik at de modellerte trykkgradientene sammenfaller med de fysiske observasjoner. Denne kalibreringen utgjør en avgjørende del av å bygge en slik modell ettersom den innebærer til finjustering av trykkgradientene, og kan dermed åpne et smalt borevindu og tillate boring av en brønn som tidligere ble ansett som umulig å bore. Under planlegging av fremtidige brønner i dette området, skaleres modellen til å sammenfalle de gjeldende formasjonstopper for å estimere det operasjonelle borevinduet. Initialt anslås denne modellen å ha høy nøyaktighet, dog vil denne øke ettersom flere brønner blir lagt til modellen. På denne måten vil presisjonen av modellen øke og de resulterende gradientene vil være mer nøyaktige.

Dette operasjonelle borevinduet som er gjengitt av modellen kan brukes til å planlegge borevæskedesignet samt foringsrørsdesignet, samt bidra til at brønner kan bores på en både trygg og lønnsom måte.

Abstract

The oil industry has been exploring and drilling for hydrocarbons for decades, and on the Norwegian Continental Shelf (NCS), most of the previously discovered big fields are in their ending phase. The remaining reserves in these fields may require highly complex wells, such as high pressure high temperature (HPHT) wells, and have not been previously drilled due to operational challenges in such a tight drilling window. Precise estimation of this window is therefore crucial when planning and drilling wells, something that may be done by the means of a carefully calibrated geomechanical model, describing the pressure gradients present in the formation of interest.

This thesis involves building a 2D Tor field specific linear elastic geomechanical model, and describes the work process in order to do so. The 2D aspect of the model is due to the fact that several offset wells were utilized in the process of building the model, in the case of using only one well, the model would be 1D. By using log data, survey data and MWD data to build the initial model in the Predict software, operational observations found in daily drilling reports and suchlike documentation are then used to calibrate the model to coincide with these physical observations. This calibration is a crucial part of the modeling, as it will fine-tune the pressure gradients, resulting in the possibility of drilling a well that was previously thought to be close to impossible. When planning future wells in this area, compressing and decompressing the model to fit the formation depths of the planned well will allow an estimation of the safe drilling window. The initial accuracy is presumed to be high, however the more wells that are added to the model will increase the precision of it and lead to a better model.
Based on the drilling window produced by the model, the casing structure and the mud design for the planned well can be estimated. Thus, on the basis of this model, with well estimated and reliable pore pressure gradients, fracture pressure gradients and shear failure pressure gradients, wells can be drilled both safely and cost efficient, allowing an optimal hydrocarbon recovery to surface.

Table of contents

List of figures

List of tables

1. Introduction

1.1. Project Background

Knowledge of the formation surrounding a planned wellbore is crucial. There are several important parameters that must be estimated in order to avoid wellbore stability issues as well as pressure related issues. In order to plan and drill a successful well, oil companies rely on building so-called geomechanical earth models. A geomechanical model consists of earth stresses, rock strengths, pore pressure gradients (PPG) and formation fracture pressure gradients (FG), as well as provide an estimate of the shear failure gradient (SFG) for drilling. The model is built based on a wide collection of data; among these are logs, survey data, drilling data, and geological data. With this data it is possible to give an interpretation of the rock strengths and mechanical properties which will guide the well planner to choose the optimum mud weight, casing and well trajectory design. Also the model may be used to identify risks and recommendations in order to achieve best possible drilling.

ConocoPhillips Norway is one of the biggest operators on the Norwegian Continental Shelf, and with development of new fields as well as re-development of the older, more mature fields, the company is continuously aware of the importance of optimizing the drilling process, both for safety and economic reasons.

1.2. Project Outline

This project involves building the 2D linear elastic effective stress model of the Tor field to use in planning of optimal hydrocarbon recovery to surface. This 2D model consists of several 1D vertical effective stress models, i.e. models based on only one well. By combining all of these 1D models, the final 2D model will be built and can thus be used for future well planning.

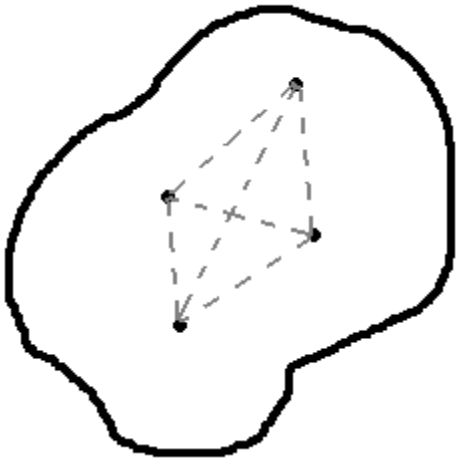

Figure 1.1. Schematic of a field with "connected" wells used to build a 2D model

Figure 1.1 shows how the wells in a specific field may be combined and used to create the 2D model, and as mentioned, this model is a linear elastic vertical effective stress model. In order to build the model, software used to estimate geomechanical properties, namely Predict, will be utilized in order to model earth stresses, pore pressure gradients, fracture pressure gradients as well as shear failure gradients for use when drilling nearby wells.

In summation, a geomechanical model describes the stresses, mechanical properties as well as the pore pressure initially present in the formation, and the construction of such a model is the first step in being able to perform a geomechanical analysis in order to best plan and drill a well (Itasca, 2012). For the purpose of this project, a 1D model will be created by use of well log data, and several exploration and wildcat wells will be modeled and used to create the final 2D field specific model. Hence, the created model will be built based on information and data from offset wells.

This work consists of a literature study and an extensive description of the work done to create the model as well as the achieved results and conclusions that have been drawn.

Section 2 provides an introduction to the Ekofisk area, where the areas the offset wells are located in are briefly described, including date of discovery, water depth and reservoir depth. Section 3 contains a description of the different methods available to estimate the overburden pressure gradient, the pore pressure gradient and the fracture gradient. Following this, section 4 presents a brief, general overview of wellbore stability associated with drilling the well. The theory presented in this section is taken from a previous NTNU project work (Berg, 2011) “Modeling of time dependent instabilities in shale on a real field case using PSI”. However for the usage in this work, it has been revised and edited to suit the current purpose and scope of work.

Section 5 describes the software used in this thesis, Drillworks, and the following section, section 6, contains a detailed description of the work conducted throughout the course of building the model. Section 7 presents the results obtained, including the modeled pressure gradients, rock mechanical properties obtained by using correlations and hemisphere plots showing the variation in mud weight around the wellbore region. These results are discussed in section 8, whereas section 9 provides suggestions as to what further work can be done in order to continue developing the model that has been built. Finally, section 10 concludes the work conducted throughout this thesis.

Appendix A lists the nomenclature used in the equations throughout this work. For the equations, all units are consistent.

2. The Greater Ekofisk Area

As the first major oil field in Norway, the Ekofisk field was discovered in 1969 and started production in 1971. Located in the southern part of the North Sea, the greater area also consists of the Tor, South-East Tor, Tjalve, Embla and Eldfisk fields (ConocoPhillips Company, 2012). For the purpose of this work, several exploration wells drilled in the Tor, South-East Tor and Tjalve will be described and investigated. The locations of these fields are displayed in Figure 2.1.

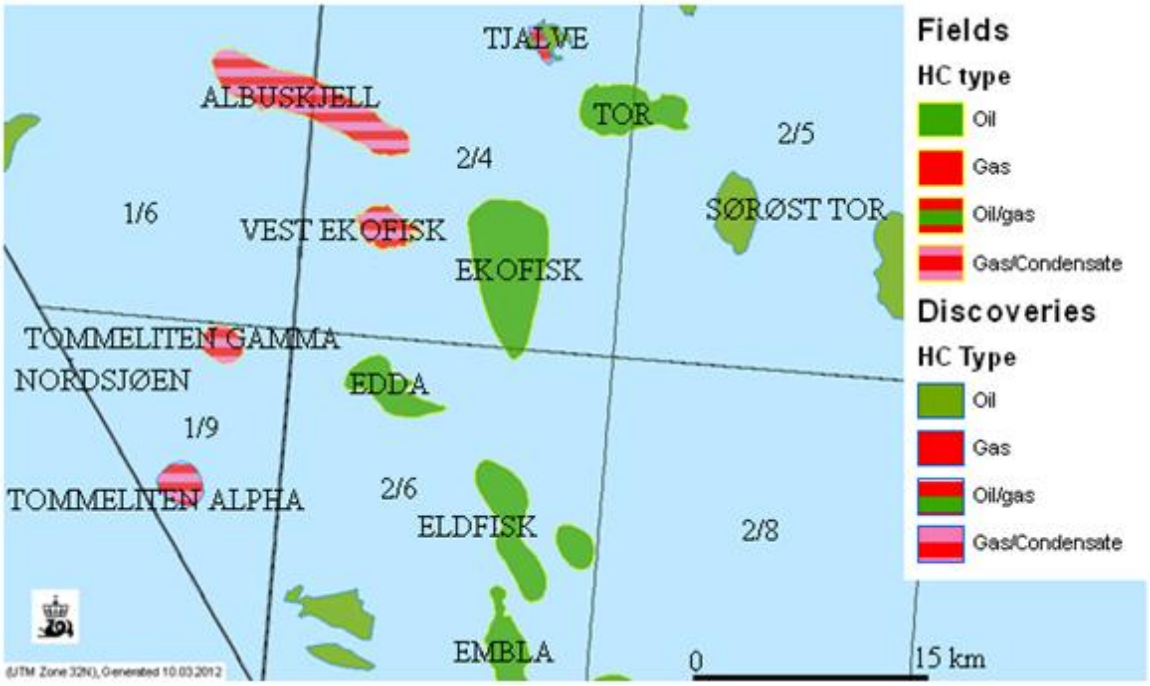

Figure 2.1. The Greater Ekofisk Area. Modified from Norwegian Petroleum Directorate (2012a)

2.1. The Tor Field

Discovered in 1970 with the wellbore 2/5-1, the Tor field is still currently producing. However, the Tor facility has a very limited life expectancy, and currently a redevelopment of the field in order to successfully recover the significant amount of remaining resources in the Tor and Ekofisk formations is being considered (Norwegian Petroleum Directorate, 2012b). Figure 2.2 shows the location of the exploration wellbores for the Tor field.

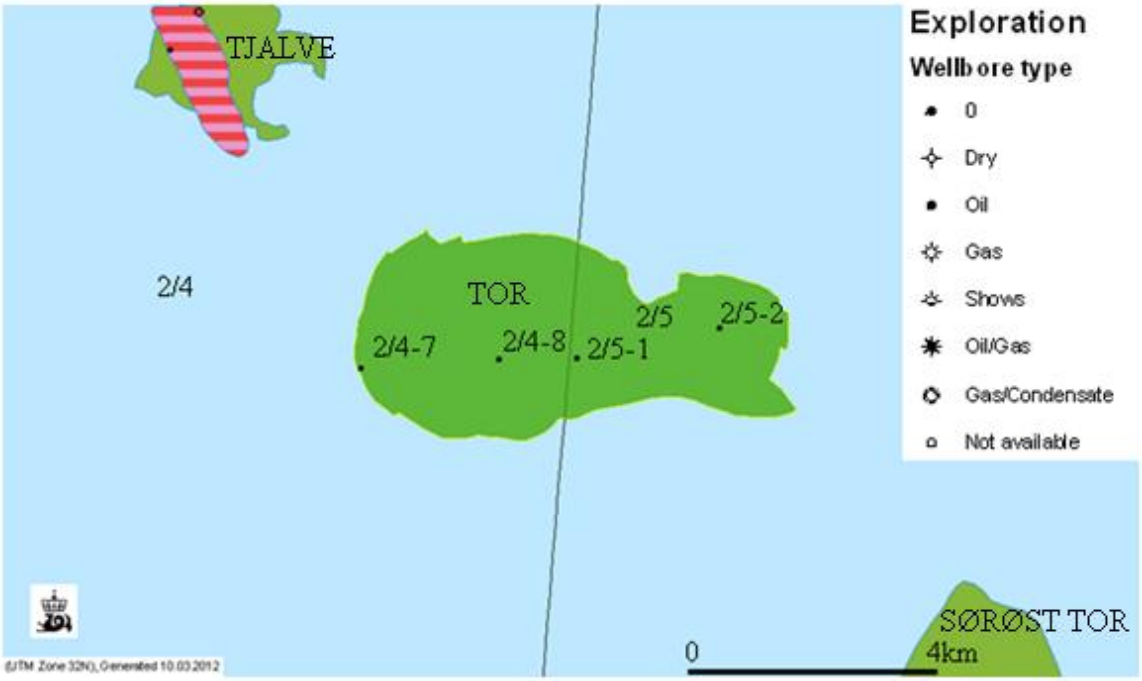

Figure 2.2. The Tor Field. Modified from Norwegian Petroleum Directorate (2012a)

With an average water depth in the area of 230 ft, the main reservoir consists of fractured chalk of the Tor formation that is of Late Cretaceous age. The described reservoir is at a depth of roughly 10,500 ft, and even though the Ekofisk formation of Early Paleocene age also contains oil, this reservoir is of considerably lower quality. For that reason, only minor quantities of oil have been produced from the Ekofisk formation (Norwegian Petroleum Directorate, 2012e).

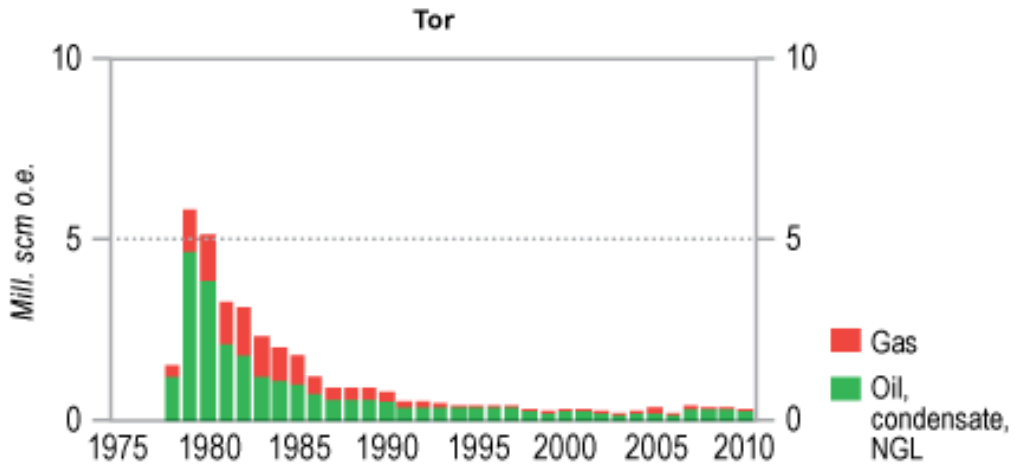

Figure 2.3. Tor Field Production Schematic. From Norwegian Petroleum Directorate (2012e)

As may be observed in Figure 2.3, the Tor field has been producing gas, oil and condensate. Originally, Tor was produced by means of pressure depletion. However as of 1992, water injection was initiated. Now, water injection has been increased, also five wells are producing by the aid of gas lift (Norwegian Petroleum Directorate, 2012e).

According to The Norwegian Petroleum Directorate, as of December 31, 2011, the estimated recoverable reserves of the Tor field are 24.40 million Sm^3 of oil, 10.90 billion Sm^3 of gas and 1.2 million tons of natural gas liquids (NGL) (Norwegian Petroleum Directorate, 2012b).

2.2. The South-East Tor Field

Discovered only two years after the Tor field, the South-East Tor field was discovered in 1971 with the discovery wellbore 2/5-3. The average water depth is similar to the Tor field and development of this field is very likely, however, it is not clarified. Other exploration wells for this field include 2/5-5 and 2/5-8 drilled in 1972 and 1988 respectively. The locations of the exploration wells are shown in Figure 2.4. Well 2/5-3 was a wildcat, while the other two wells were appraisal wells (Norwegian Petroleum Directorate, 2012c).

As according to The Norwegian Petroleum Directorate, the estimated recoverable reserves of the South-East Tor field as of December 31, 2011, are 3.06 million Sm^3 of oil and 0.87 billion Sm^3 of gas. No NGL is assumed recoverable (Norwegian Petroleum Directorate, 2012c).

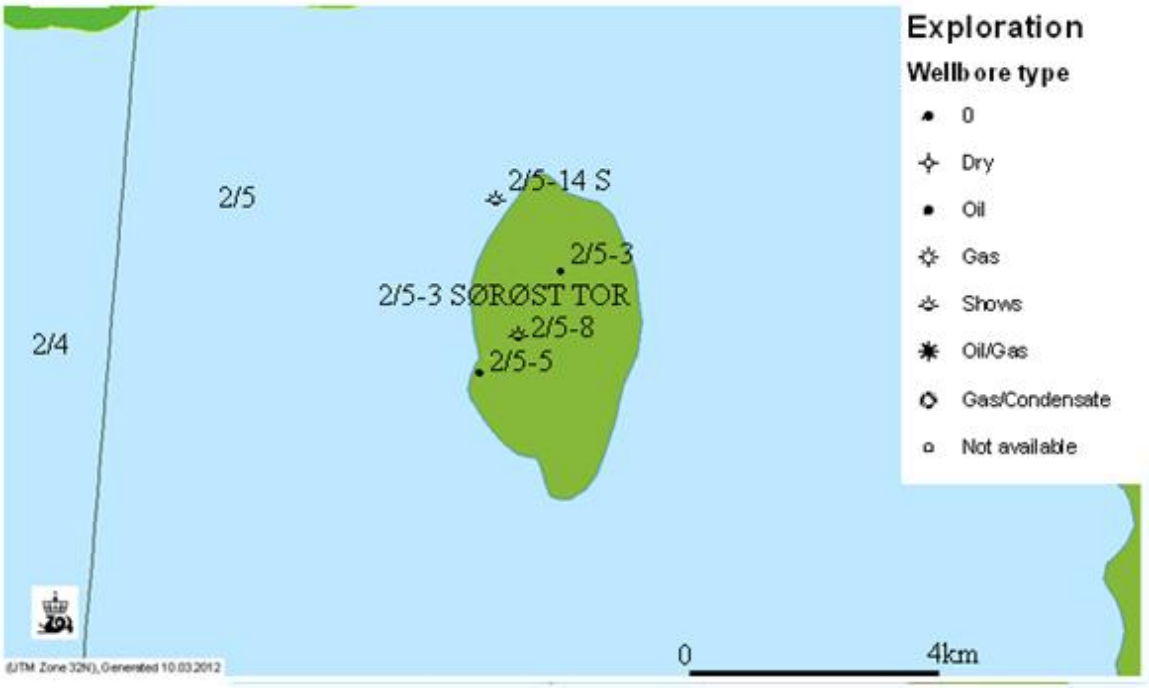

Figure 2.4. The South-East Tor Field. Modified from Norwegian Petroleum Directorate (2012a)

2.3. The Tjalve Field

Discovered in 1992, more than 20 years after the Tor and South-East Tor fields, the Tjalve field was discovered with the wildcat 2/4-17. The water depth at this field is approximately the same as for the Tor and South-East Tor fields. Similarly to the South-East Tor field, development of the Tjalve field is likely but not clarified (Norwegian Petroleum Directorate, 2012d). Figure 2.5 shows the location of the exploration wellbores for the Tjalve field.

The Norwegian Petroleum Directorate assumes the estimated recoverable reserves of the South-East Tor field as of December 31, 2011 to be 0.56 million Sm^3 of oil, 0.99 billion Sm^3 of gas and 0.18 million tons of NGL (Norwegian Petroleum Directorate, 2012d).

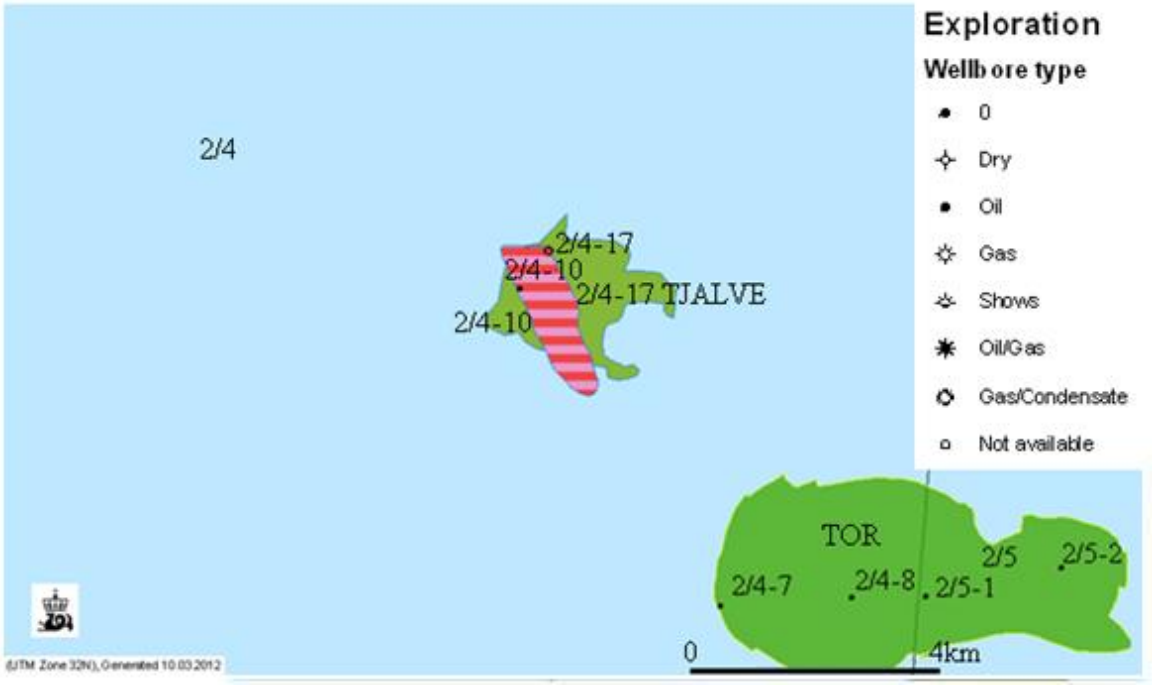

Figure 2.5. The Tjalve Field. Modified from Norwegian Petroleum Directorate (2012a)

3. Estimation of Geopressure

As defined in the Schlumberger Oilfield Glossary (2012), geopressure is "*the pressure within the Earth or formation pressure*". Thus, it may be used in a way that includes overburden-, pore- and fracture pressure (Dutta, 1999).
During the process of planning and drilling a well, determining geopressure is one of the main considerations in order to execute this successfully seeing as its accuracy has a considerable effect on wellbore stability issues that may have a great impact on the total cost of a project. This is of special importance when drilling a high pressure high temperature (HPHT) well, where the margin between pore- and fracture pressure is considerably small (Ward et al., 1995). This narrow drilling window is likely the most well known challenge when it comes to deepwater drilling (Rocha et al., 2004).

The following sections will provide an overview of the various methods available to estimate the pore-, fracture- and overburden pressure.

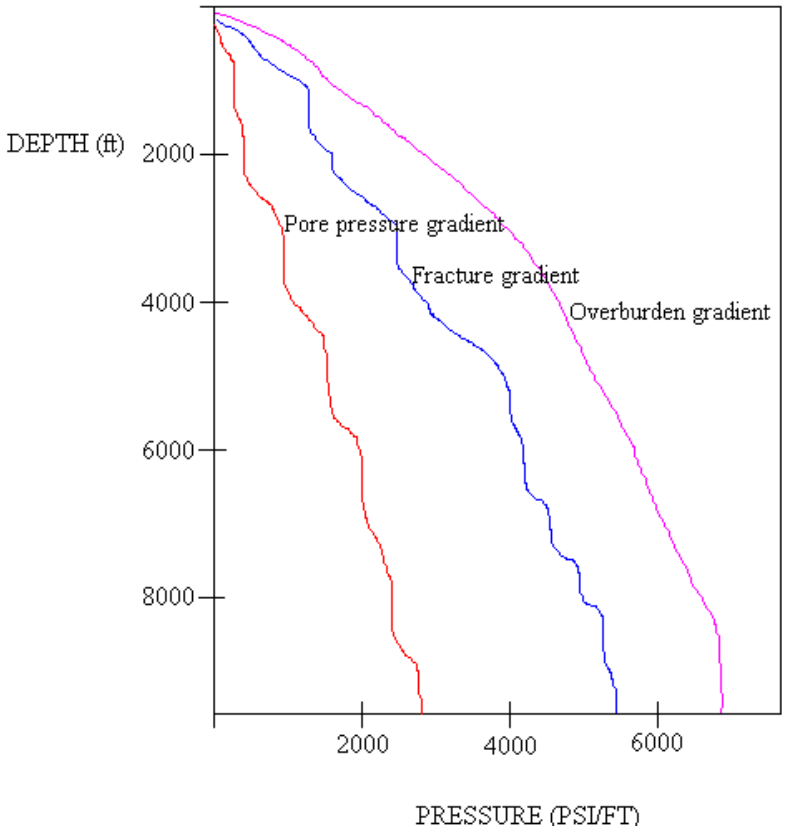

Figure 3.1. Geopressure - Pressure versus depth plot

3.1. Overburden Gradient Estimation

In order to successfully estimate the pore pressure gradient and the fracture gradient, the overburden pressure must be estimated beforehand. If the overburden pressure is incorrectly estimated, this will affect the pore pressure and fracture gradient which both are critical to well design (Hobart, 1999). Ultimately, with the wrong overburden estimate – the shear failure gradient will be incorrect and so will the collapse pressure, leading to an outcome that might be catastrophic.

The overburden stress is a function of depth and density of the sediments lying above the depth of interest. When the density is known, the overburden gradient may thus easily be calculated as shown in equation (1).

$$\sigma_{ob} = \int_0^D \rho_b g dD \tag{1}$$

Where σ_{ob} is the overburden stress, ρ_b the average bulk density of the sediments, g the acceleration due to gravity and D the depth of investigation. For this equation, as well as all the following equations, the symbols that have been used are explained in Appendix A. All units are consistent.

In offshore areas, the above equation must be integrated in two parts as shown below in equation (2). The first part is the integration from the surface to the sea bottom; the second is from the mudline (seabed) to the depth of interest (Bourgoyne Jr. et al., 1986). Hence, the first part represents the overburden stress contribution from the water, the second part the overburden stress contribution from porous rock material.

$$\sigma_{ob} = g \int_0^{D_w} \rho_{sw} dD + g \int_{D_w}^{D} [\rho_g - (\rho_g - \rho_{fl})\phi_0 e^{-KD}] dD \tag{2}$$

The above equation now accounts for the porosity as well as the water depth. ρ_{sw} is the density of seawater, D_w the water depth, ρ_g the grain density, ρ_{fl} the pore fluid density. ϕ_0 is the surface porosity and K is the porosity decline constant, the magnitudes of these two parameters may be determined graphically or by the least-

square method (Bourgoyne Jr. et al., 1986). The remaining parameters are described after equation (1).

However, for wildcats or exploration wells, the density of the overlying sediments is not easily found. The density is first measured when the well has been drilled and logs have been run, and therefore, in order to estimate the overburden gradient for wildcat wells, well planners have to rely on indirect or empirical models of estimation (Hobart, 1999). To this day, there are two main approaches for estimation of the overburden pressure prior to drilling a well that have been used. The first uses the depth parameter in order to create a correlation valid for a specific region for estimating the overburden gradient or density. The second utilizes seismic data, such as velocity and interval transit times, and derives some kind of relationship between this data and the density, so that the deduced density may be used to calculate the overburden gradient as shown previously (Hobart, 1999).

3.2. Pore Pressure Estimation

The estimation and accuracy of the estimation of pore pressure is of high importance as uncertainties of pore pressure may lead to various problems like stuck pipe, wellbore stability problems, formation damage, kicks and in the worst case blowouts. Not only is knowledge of the formation pore pressure indispensable when drilling a safe and cost-efficient well, it is also vital when assessing risk factors associated with exploration drilling, this includes seal integrity and the migration of formation fluids (Tang et al., 2011).

In areas where the formation pore pressure is assumed to be approximately equal to the theoretical hydrostatic head for the vertical depth of investigation, the formation is normally pressurized, i.e. the formation pressure is normal, also referred to as hydrostatic (Bourgoyne Jr. et al., 1986). Thus, for a given area, the normal pore pressure may be estimated by using the hydrostatic gradient that is characteristic for the area of current interest. Table 3.1 shows the hydrostatic pressure gradients for several areas with substantial exploration and drilling activity

Table 3.1. Normal Formation Pressure Gradients for Several Areas of Active Drilling. From Bourgoyne Jr. et al. (1986) p.247

	Pressure Gradient (psi/ft)	Equivalent Water Density (kg/m^3)
West Texas	0.433	1.000
Gulf of Mexico coastline	0.465	1.074
North Sea	0.452	1.044
Malaysia	0.442	1.021
Mackenzie Delta	0.442	1.021
West Africa	0.442	1.021
Anadarko Basin	0.433	1.000
Rocky Mountains	0.436	1.007
California	0.439	1.014

However, most areas do not have normal formation pressure, which implies the pore pressure must be estimated through other methods.

Following the publication of Hottman and Johnson's classic paper "Estimation of Formation Pressures from Log-Derived Shale Properties" (1965), literature on pore pressure estimation has increased extensively. All methods for estimating pore pressure are based on the assumption that pore pressure influences various shale properties such as porosity, density, sonic velocity, and resistivity, i.e. compaction dependent properties. Any wireline or geophysical measurement which is sensitive to pore pressure may be referred to as a "pore pressure indicator", and based on how these measurements are converted into pore pressure measurements, these methods can be divided into two groups: direct methods and effective stress methods (Tang et al., 2011).

The direct methods involve directly relating the amount a pore pressure indictor diverges from its normal trend line to the pore pressure gradient at the depth of

investigation. In general there are two ways by which this can be done; by using crossplots or using overlays.
The effective stress methods are based on Terzaghi's effective stress principal. This principal states that the compaction a geological material experiences is controlled by the difference between the total confining pressure and the pore fluid pressure. The described difference, which is referred to as "effective stress" and denoted by σ', will represent the total stress the rock/sediment grains carry (Tang et al., 2011).

$$\sigma' = p_{confining} - p_f \quad (3)$$

Where $p_{confining}$ is the confining pressure and p_f the pore pressure.

As described in (Bowers, 1999a), the effective stress methods can be separated into vertical methods and horizontal methods. The difference between these is that the vertical methods use the normal trend data at the same pore pressure indicator value as the depth of investigation, i.e. staying along the same vertical line, while the horizontal methods use the normal trend data available at the same depth, i.e. staying along the same horizontal line (Bowers, 1999a).

Special caution should be taken when using porosity based pore pressure prediction methods, as these may not always deliver a satisfactory estimation (Swarbrick, 2001). Methods that utilize porosity only work where there has been developed a reliable normal compaction trend, i.e. an indicator line for a specific petrophysical measurement in a normal compacted rock. Also, these methods may only be used when the overpressure within the formation is due to disequilibrium compaction. Other reasons for these methods failing to provide satisfactory estimates are lateral transfer (tilted reservoirs), shallow top overpressure as well as lithological variations (Swarbrick, 2001).

For the purpose of this work, a handful of methods used to estimate pore pressure will be presented and described. Which methods have been selected is based on the

methods currently used by the industry, as well as attempting to cover all of the different classifications.

3.2.1. Hottman & Johnson Method

In their paper "Estimation of Formation Pressure from Log-Derived Shale Properties", Hottman & Johnson describe how one may use crossplots, i.e. plots of pore pressure gradient versus shale acoustic and resistivity log data, to determine the pore pressure at a given depth (Hottmann & Johnson, 1965). According to their calculations based on data from the Gulf Coast, the method they described provides fluid pressure estimations with an accuracy of ± 0.04 psi/ft, a standard deviation of 0.022psi/ft when using resistivity and a standard deviation of 0.020psi/ft when using sonic transit time data.

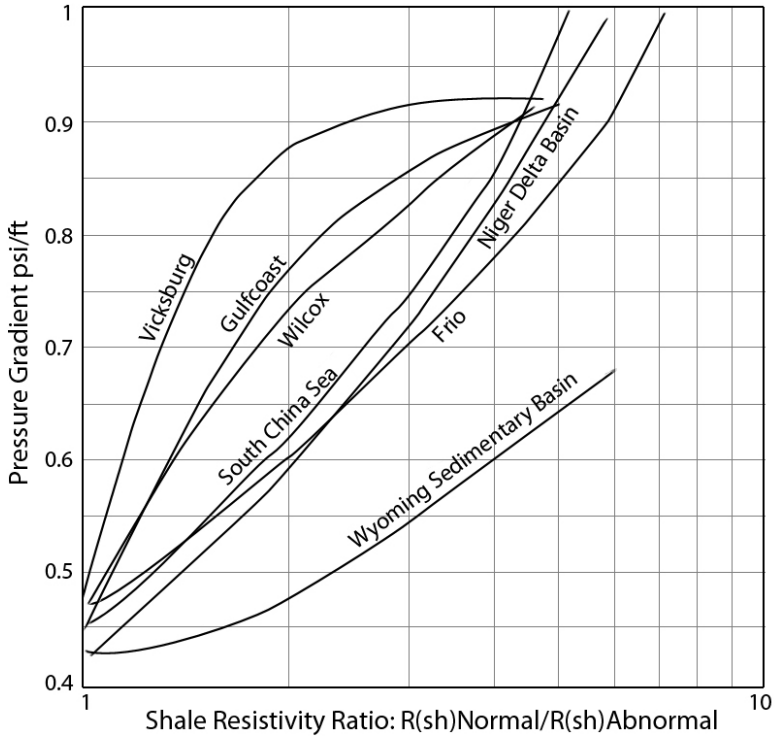

Figure 3.2. Hottman & Johnson crossplots. Pore pressure crossplots for resistivity. After Owolabi et al. (1990)

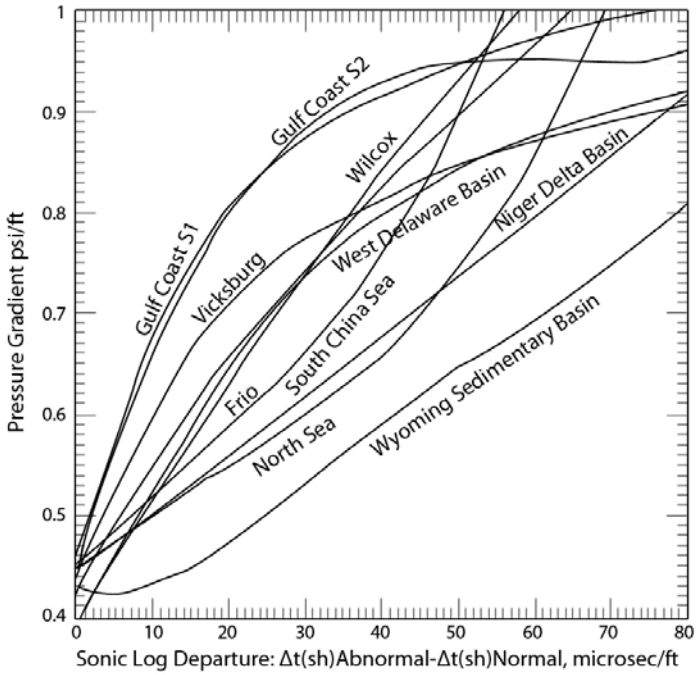

Figure 3.3. Hottman & Johnson crossplots. Pore pressure crossplots for sonic transit time. After Owolabi et al. (1990)

With the pore pressure gradient as the Y-axis, and defining the X-axis as follows in equations (4) and (5) for resistivity and sonic transit time respectively, the crossplots previously described may be created (Bowers, 1999a).

Resistivity:

$$X - axis = \frac{R_n}{R} \tag{4}$$

Sonic Transit Time:

$$X - axis = \frac{\Delta t}{\Delta t_n} \tag{5}$$

Where R is the shale resistivity and Δt the sonic transit time. n denotes the normal compaction trend value.

It is important to keep in mind that the method described by Hottman and Johnson was only developed for the Gulf Coast, still similar crossplots may be developed for other areas with substantial drilling activity. However, their techniques are only applicable in areas where the generation of formation pressure is mainly the

result of compaction due to the overburden stresses (Eaton, 1975). A number of crossplots for several areas that have been published are displayed in Figure 3.2 and Figure 3.3.

3.2.2. Equivalent Depth Method

The Equivalent Depth method is a vertical effective stress method, which assumes that both overpressured and normal pressured formations follow the same effective stress relation. This is the concept The Equivalent Depth method uses to estimate the pore pressure, i.e. assuming that formations with the same velocities, regardless if they are overpressured or normal pressured, will have the same effective stress. Of course, in cases where the overpressured and normal pressured formations do not follow the same effective stress ratio, this method will under predict the pore pressure quite substantially (Bowers, 1999a).

Based on the mathematical relationship shown in equation (6), The Equivalent Depth method graphically solves for the effective stress at the depth of investigation by using the overburden stress and normal pore pressure at a shallower depth (Owolabi et al., 1990)

$$p_f = G_0 D_A - [D_N(G_0 - G_H)] \quad (6)$$

Where p_f is the pore pressure, G_0 the overburden gradient, D_A the depth of interest in the abnormal pressure interval, D_N the normal equivalent depth corresponding to D_A and G_H the normal hydrostatic gradient.

Figure 3.4 shows how The Equivalent Depth method graphically solves for the effective stress at the depth of interest, point A, by using data from the equivalent depth, point N.

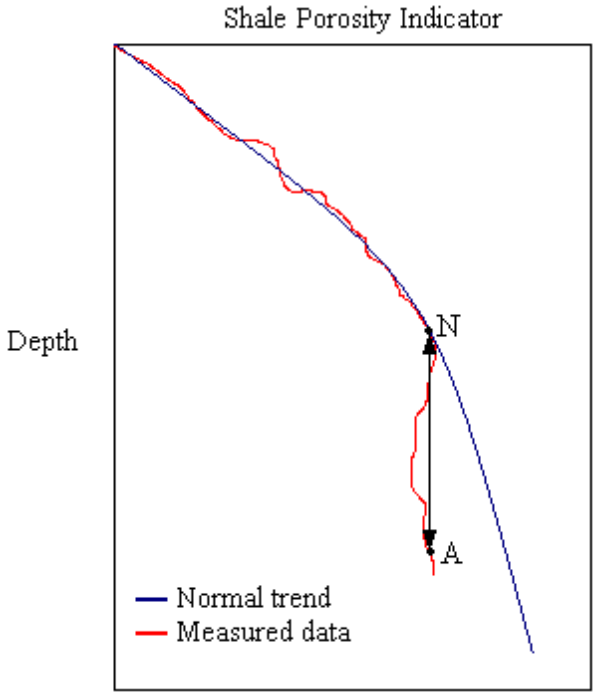

Figure 3.4. The Equivalent Depth method. After Tang et al. (2011)

The x-axis in Figure 3.4 is denoted as Shale Porosity Indicator. This axis may be any pore pressure indicator, which is described in section 3.2.

3.2.3. Eaton's Method

Eaton's method estimates the effective stress based on the normal pressure trend parameters and the normal pressure effective stress at the depth of investigation (Bowers, 1999a). In effect, this means that Eaton's method calculates the effective stress by relating the variation of the effective stress from the normal effective stress to the deviation of a petrophysical measurement from the normal compaction trend line (Tang et al., 2011).

The study done by Eaton and described in his paper "The Equation for Geopressure Prediction from Well Logs", resulted in four equations that allow pore pressure prediction from sonic-travel time, resistivity, conductivity, and corrected "d" exponent data (Eaton, 1975). This "d" exponent is obtained from

various drilling parameters like rate of penetration, weight on bit rotary speed and bit diameter (Bourgoyne Jr. et al., 1986).

Interval transit time

$$\sigma' = \sigma'_n \left(\frac{\Delta t_n}{\Delta t}\right)^3 \quad (7)$$

Resistivity

$$\sigma' = \sigma'_n \left(\frac{R}{R_n}\right)^{1.2} \quad (8)$$

Conductivity

$$\sigma' = \sigma'_n \left(\frac{C_n}{C}\right)^{1.2} \quad (9)$$

d-exponent

$$\sigma' = \sigma'_n \left(\frac{d}{d_n}\right)^{1.2} \quad (10)$$

Where σ' is the effective stress, Δt the sonic transit time, R the resistivity, C the conductivity and d the corrected d-exponent. n denotes the normal compaction trend value (Bowers, 1999a).

Also, according to Eaton, the equation using interval transit time should be valid for predicting effective stress by using seismic data. Thus;

$$\sigma' = \sigma'_n \left(\frac{V}{V_n}\right)^3 \quad (11)$$

Where V is the velocity obtained from seismic data.

When the normal compaction trend line is similar to Eaton's equation, the effective stresses calculated in overpressure by Eaton's method will be close to the normal compaction trend. Thus, Eaton's method and vertical effective stress methods such as The Equivalent Depth method will produce results that resemble one another (Bowers, 1999a). It has been shown that Eaton's method provides the best estimations where the formation pore pressures are low, <1.4g/cc, whereas The Equivalent Depth method is more suitable for high formation pore pressures,

>1.4 g/cc. Also, the accuracy of the estimations provided by The Equivalent Depth method is highly dependent on the accuracy of the normal compaction trend line (Tang et al., 2011).

3.2.4. Bowers Method

Despite the numerous pore pressure estimation methods that had been published, Bowers noticed that none of these formally took into account the actual cause of overpressure. As overpressure may be caused by several mechanisms, among these loading mechanisms, unloading mechanisms and tectonic stresses (Bowers, 2001), he saw the need for a method that in fact accounts for the cause of overpressure.

Recognizing that The Equivalent Depth method failed whenever unloading had occurred, he proposed a modified Equivalent Depth method, which could deal with velocity reversals when unloading was to be expected (Bowers, 2001). His method employs virgin curve and unloading curve relations in order to account for overpressure due to fluid expansion and under compaction (Bowers, 1995).

The virgin curve is given by

$$V = 5000 + A\sigma'^{B} \tag{12}$$

Where V is the velocity and σ' the effective stress. A and B are parameters calibrated with offset velocity versus effective stress data.

The unloading curve is defined empirically, and is given by

$$V = 5000 + A\left[\sigma'_{max}\left(\frac{\sigma'}{\sigma'_{max}}\right)^{1/U}\right]^{B} \tag{13}$$

σ'_{max} is the maximum effective stress, U the unloading parameter and A and B are the same as for the virgin curve and the maximum effective stress is given in equation (14).

$$\sigma'_{max} = \left(\frac{v_{max}-5000}{A}\right)^{1/B} \quad (14)$$

v_{max} is the maximum velocity.

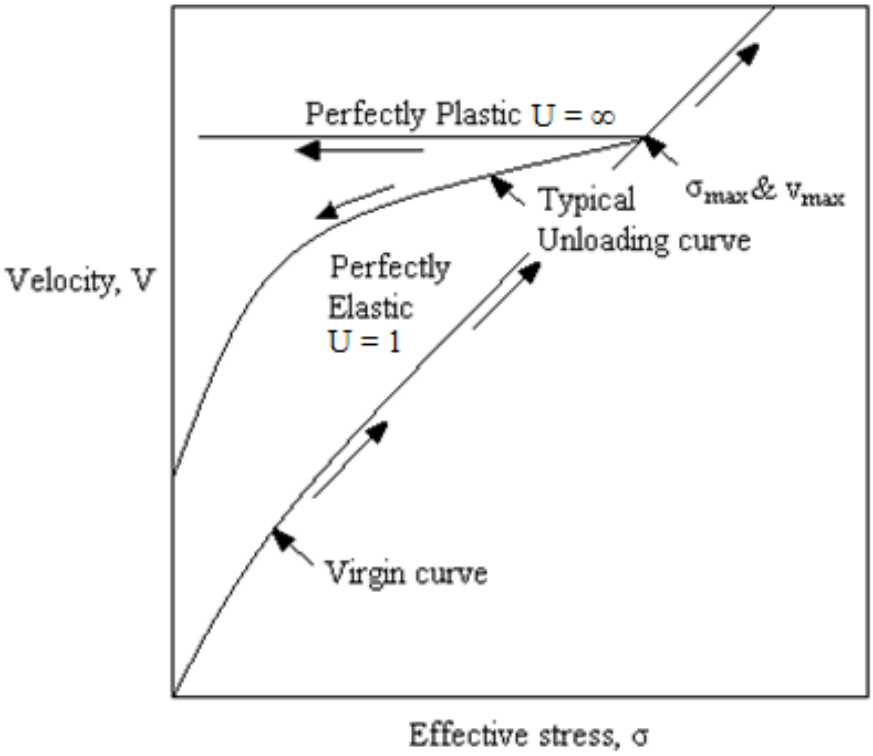

Figure 3.5. The Unloading Parameter, U. After Bowers (1995)

The unloading parameter, U, is a measure of how plastic the sediment is and for most practical purposes, it ranges between 3 and 8. For U = 1, there is no permanent deformation, meaning it is perfectly elastic. U = ∞ implies irreversible deformation.

σ_{max} and v_{max} are estimated at the onset of unloading and the values of σ_{max} , v_{max} as well as U may be determined by fitting the unloading- and loading curve with the velocity versus effective stress data from study wells (Bowers, 1995).

Outside a velocity reversal zone, the effective stresses are calculated by the virgin curve. Inside a velocity reversal zone, data from offset wells may be used to determine which of the two equations are appropriate (Bowers, 1995).

3.2.5. Abnormal Pore Pressure

As mentioned previously in section 3.2, not all areas have normal pore pressure. Usually the pore pressure in areas with *abnormal pore pressure* is higher than the normal pore pressure, hence it may also be referred to as an overpressured zone (Fjær et al., 2008). Drilling in overpressured zones may be hazardous, and it is often in these zones one encounters borehole stability issues. This is due to the fact that in overpressured zones, the drilling window will be narrower.

Abnormal pressures are the result of numerous mechanisms, amongst others temperature increases, tectonics, burial and compaction of sediments as well as hydrocarbon generation (Yassir & Addis, 2002). In the literature, three main reasons for abnormal pore pressure are described. The first is due to a change in the fluid volume as a result of thermal expansion or other chemical processes. These chemical processes include hydrocarbon generation, diagenesis and fluid flow and buoyancy (Osborne & Swarbrick, 1997). Due to the lack of an impermeable seal in most geological circumstances, thermal expansion is not likely to contribute greatly to creating overpressure, neither is diagenesis. Hydrocarbon generation, or kerogen maturation, remains a subject for further investigation as it is unsure if the pressure buildup directly or indirectly slows down the kerogen maturation. Evidence of abnormal pore pressure has also been found in the surrounding area of a hydrocarbon buildup, this is due to the buoyancy of petroleum (Osborne & Swarbrick, 1997).

For a long time, tectonic loading has been considered a cause of abnormal pore pressure. These compressional tectonics are shown to lead to undrained shear stress, and with increasing shear stress pore pressure increases (Fjær et al., 2008).

Skempton's parameter, A, describes the pore pressures reaction to the variation in shear stress (Yassir & Addis, 2002).

$$A = \frac{(\Delta p_f - \Delta\sigma_3)}{(\Delta\sigma_1 - \Delta\sigma_3)} \quad (15)$$

Where p_f the pore pressure, σ_3 and σ_1 the maximum and minimum principal stresses respectively. The above equation assumes an undrained, compressional basin.

The effect of tectonics on pore pressure is most relevant in areas that are currently tectonically active, where overpressure can be quickly created and just as quickly released during fault movements (Osborne & Swarbrick, 1997).

In addition to the two main causes mentioned previously, abnormal pressures may also be the result of disequilibrium compaction. This means that the rate of deposition and compaction of sediments is higher than the rate of fluid migration, leading to the buildup of a pressure (Fjær et al., 2008). This is often the case in shales, where the permeability is quite low. As time passes, the overpressure generated by disequilibrium compaction will dissipate because of fluid movement through the seal or fluid migration (Osborne & Swarbrick, 1997).

The methods that have been described previously in section 3.2.1 through section 3.2.4 on how to estimate pore pressure have a very limited area of usage, as most of them do not properly account for these overpressure mechanisms. With proper knowledge of the overpressure generating mechanisms, the risks and uncertainties in pore pressure estimation may be better assessed.

3.3. Fracture Pressure Gradient Estimation

By definition, fracture pressure gradient is "the pressure gradient that will cause fracture of the formation" (Rocha et al., 2004). As previously mentioned, this means

that if this fracture pressure limit is exceeded, the formation will fracture. One of the most important aspects that must be considered while planning and drilling a well is the fracture pressure gradient. This importance is based on lost circulation problems, and the economic losses connected to this. In extreme cases, the loss of hydrostatic pressure due to lost circulation may in the worst-case scenario result in a blowout.

In general, fracture pressure gradient methods are based on equations derived from rock mechanics theories or on simplified methods (Rocha et al., 2004). The first calls for a number of input data that under normal circumstances are not available, and these methods are normally far too complex. The latter of the two involves several simplifications and hardly resembles subsurface conditions. Despite the lack of accuracy in representing the rocks underground behavior, because of its simplicity the simplified methods are the most popular and preferred amongst drilling personnel (Rocha et al., 2004).

As mentioned earlier in section 3, the pressure margin while drilling in deep water is very small, and the reduction in fracture pressure gradient is a result of numerous mechanisms. One of the main reasons for the reduced fracture pressure gradient is the low stress regime, which is a result of the reduction of the overburden pressure gradient. This gradient may be further reduced by sediments found in the shallower part of the underground that are weak, low compacted and unconsolidated (Rocha et al., 2004).

There are numerous published methods used when determining the fracture pressure gradient, and similar to pore pressure estimation methods, these methods may be separated into two categories, “direct” or “indirect” methods (Rocha et al., 2004). These may also be referred to as verification methods and predictive methods (Bourgoyne Jr. et al., 1986).
The direct (verification) methods are dependent on measuring the pressure required to fracture the rock as well as the pressure necessary to propagate the resulting fracture. These methods are most often based on leak off tests (LOT) or extended leak off tests (XLOT), which are generally performed by most oil companies to calibrate the

previously mentioned simplified methods. Leak off tests are also often performed in vertical wildcat wells where there are no well-established fracture gradients (Rocha et al., 2004). A typical extended leak off test is displayed in Figure 3.6.

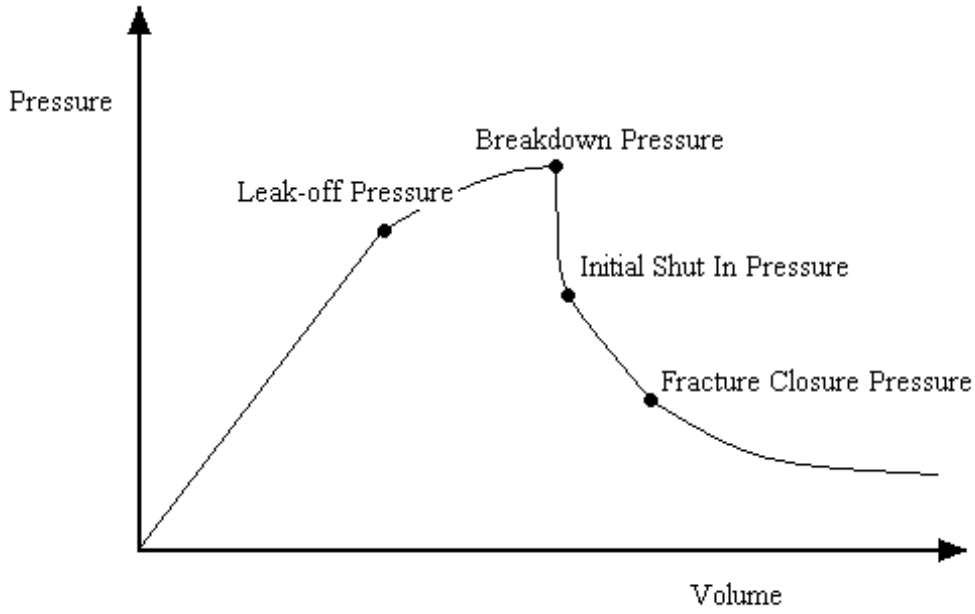

Figure 3.6. Typical Extended Leak Off Test. After Rocha et al. (2004)

Indirect (predictive) methods are based on numerical or analytical models. These models may be used to estimate the fracture pressure gradient along the length of the entire well. A number of these models are very familiar to the oil industry, while other models are developed and built for a very specific area. Common for these models is the fact that they all call for data that in general are very difficult to obtain (Rocha et al., 2004).

Of the numerous methods for estimating fracture pressure gradients that is found in the literature, a handful of methods were selected for further explanation. The selection was based on their relevance as well as which methods are used in the software Predict. An introduction to this software is given later in section 5.

3.3.1. Hubbert & Willis Method

The paper "Mechanics of Hydraulic Fracturing" published by Hubbert & Willis (1957) is considered to be a classic paper, many of the fundamental principals they introduced are still highly relevant. They derived an equation for predicting the minimum well pressure necessary to extend a pre-existing fracture, i.e. the fracture extension pressure, in areas of normal faulting (Hubbert & Willis, 1957). With the fracture pressure gradient as the only dependent variable, they showed the magnitude of this variable was controlled by the independent variables; overburden stress gradient, formation pore pressure gradient and Poisson's ratio (Eaton, 1969). Hubbert & Willis concluded that under these conditions, the smallest principal effective stress, σ'_{min}, is horizontal and equal to approximately 1/3 of the effective overburden stress, σ'_z. The value 1/3 was found by assuming a friction angle, φ, of 30° and using a relation, K_{HW}, given by the following equation (Bowers, 1999b).

$$K_{HW} = \frac{1-sin\varphi}{1+sin\varphi} \tag{16}$$

By using the before mentioned relationship between the minimum principal stress and the effective overburden stress they arrived at the following expression for the fracture extension pressure, p_{ff}.

$$p_{ff} = \sigma'_{min} + p_f = \frac{\sigma'_z}{3} + p_f = \frac{\sigma_{ob}+2p_f}{3} \tag{17}$$

Where p_f is the pore pressure.

Hubbert & Willis' method is based on the minimum in situ stress, as many other methods for predicting the formation fracture pressure gradient are. All the methods based on the minimum in situ stress are based on the principle that the minimum horizontal and vertical effective stress, σ'_h and σ'_v, are related through a so-called "effective stress ratio" denoted by K_{eff} (Rocha et al., 2004).

$$K_{eff} = \frac{\sigma_h'}{\sigma_v'} = \frac{\sigma_h - p_f}{\sigma_v - p_f} \quad (18)$$

Under the assumption that a fracture will be initiated when the fracture stress is equal to the minimum in situ stress, one arrives at an expression for the fracture pressure, p_{ff}.

$$p_{ff} = K_{eff}(\sigma_v - p_f) + p_f \quad (19)$$

Where σ_v is the vertical stress and p_f the pore pressure.

What differentiates the several fracture pressure estimation methods from one another is the approach taken to estimate the effective stress ratio, K_{eff} (Rocha et al., 2004). For Hubbert & Willis' method, the effective stress ratio is estimated by the relation K_{HW}.

3.3.2. Matthews & Kelly Method

In general, equation (17) is not valid for deeper formations (Bourgoyne Jr. et al., 1986). With this knowledge, Matthews & Kelly replaced assumption of the effective stress ratio, K_{eff}, being 1/3, with the relation shown in equation (20)

$$K_{eff} = F_\sigma \rightarrow \quad \sigma_h' = F_\sigma \sigma_v' \quad (20)$$

They determined the matrix coefficient, F_σ, empirically from field data obtained from normally pressured formations. The values that were obtained for F_σ are shown in Figure 3.7. In the case of wanting to use this relation in abnormally pressured formations, the matrix stress coefficient must be determined at the depth at which a normally pressured formation would have the same vertical effective stress as found in the abnormally pressured formation (Matthews & Kelly, 1967). This depth is denoted D_i. Under these premises, the fracture extension pressure estimation procedure becomes as shown in equations (21) through (23).

$$\sigma_n = \sigma_{ob} - p_{fn} = G_0 D_i - G_H D_i \tag{21}$$

$$\rightarrow D_i = \sigma_n \frac{1}{G_0 - G_H} = \frac{D - p_f}{G_0 - G_H} \tag{22}$$

Where σ_n is the normal vertical matrix stress, p_{fn} the normal formation pore pressure, p_f the pore pressure, G_0 the overburden gradient and G_H the normal hydrostatic gradient.

Using D_i, the matrix coefficient can be determined graphically, allowing the fracture extension pressure to be estimated (Bourgoyne Jr. et al., 1986).

$$p_{ff} = \sigma'_{min} + p_f = \sigma'_h + p_f = F_\sigma \sigma'_v + p_f \tag{23}$$

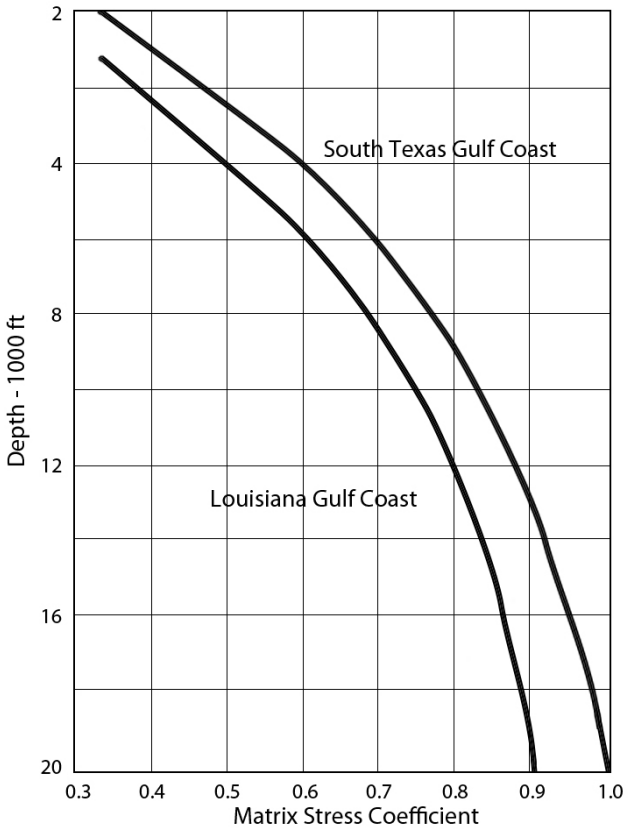

Figure 3.7. Matthews and Kelly matrix-stress coefficient for normally pressured formations. After Eaton (1969)

3.3.3. Eaton‘s Method

Eaton’s method assumes the “effective stress ratio”, here denoted K_E, is given as a function of Poisson’s ratio, ν (Bourgoyne Jr. et al., 1986).

$$K_{eff} = K_E = \frac{\nu}{1-\nu} \tag{24}$$

$$\sigma_h' = K_E \sigma_v' = \frac{\nu}{1-\nu} \sigma_v' \tag{25}$$

$$p_{ff} = \sigma_h' + p_f \tag{26}$$

Where σ_h' is the minimum horizontal effective stress, σ_v' the vertical effective stress, p_{ff} the fracture pressure and p_f the pore pressure.

In Eaton’s paper, “Fracture Gradient Prediction and its Application in Oilfield Operations”, he points out that the effective stress ratio of 1/3 presented by Hubbert & Willis (1957) corresponds to a Poisson’s ratio of 0.25. This value may be valid for some areas, however it will lead to erranous estimations of the fracture pressure gradient when used as a standard due to the fact that this value may vary from lower than 0.25 up to 0.50 (Eaton, 1969).

By collecting and analysing data from the Texas and Louisiana gulf as well as from west Texas, correlations for Poisson’s ratio were obtained. One correlation was created by assuming a constant vertical overburden gradient of 1psi/ft, the other by assuming a variable overburden gradient obtained by the integration of the bulk density log (Bourgoyne Jr. et al., 1986). These correlations were presented in Eaton’s paper published in 1969 and are shown in Figure 3.8.

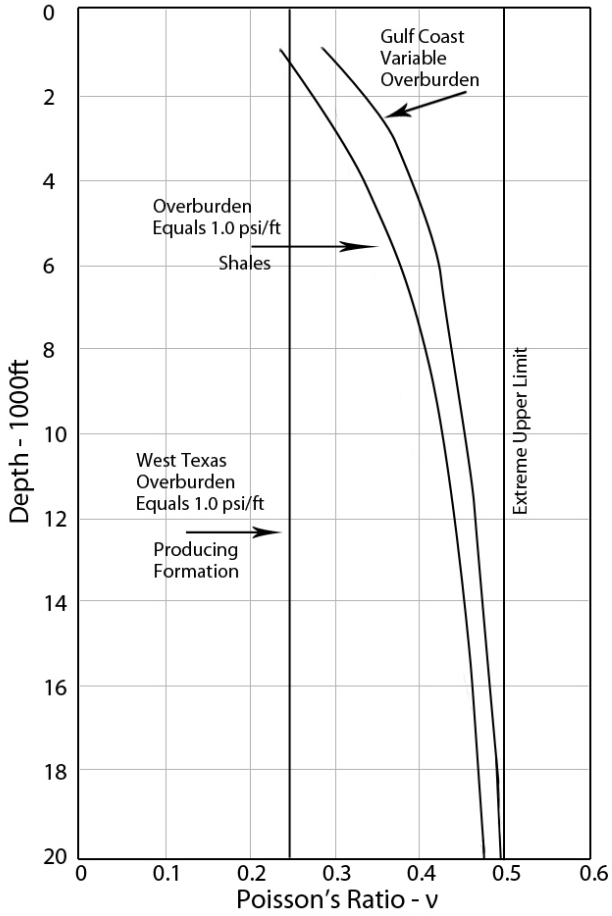

Figure 3.8. Eaton correlation for Poisson's ratio. After Eaton (1969)

However, as pointed out by Bowers (1999) in "State of the Art in Fracture Gradient Estimation", both the static and the dynamic estimations of Poisson's ratio may be inadequate when using them in Eaton's method. To avoid inaccurate estimates, one may use leak off test data to provide fictitious Poisson's ratios. First the effective stress ratio is estimated by use of equation (18), and then Eaton's definition of the effective stress ratio is solved with respect to Poisson's ratio (Bowers, 1999b). When leak off data is not available, Poisson's ratio may be estimated by the use of analytical relations (Eaton & Eaton, 1997). These were published by Eaton & Eaton in 1997, and may be found in their publication.

3.3.4. Daines' Method

Daines' method may be regarded as a continuation of Eaton's method. By adding an extra term, β, to the effective stress ratio, Daines accounts for the effect of

tectonic stresses on the fracture pressure gradient (Bowers, 1999b). The magnitude of β is determined from leak off tests, and is assumed to be constant for a single well (Zhang et al., 2008). The resulting ratio is denoted as K_B.

The equation for estimating the fracture pressure gradient then becomes

$$\sigma_h' = \left(\frac{\nu}{1-\nu} + \beta\right)\sigma_v' = K_B\sigma_v' \quad (27)$$

Where

$$\beta = \sigma_t/\sigma_1' \quad (28)$$

Thus

$$K_{eff} = K_B = \frac{\nu}{1-\nu} + \beta \quad (29)$$

$$p_{ff} = \sigma_h' + p_f \quad (30)$$

Where σ_h' is the minimum horizontal effective stress, σ_v' the vertical effective stress, ν Poisson's ratio, σ_t the superposed horizontal tectonic stress, σ_1' the maximum in situ effective stress, p_{ff} the fracture pressure and p_f the pore pressure (Daines, 1982).

In his paper, Daines provided numerous tabulated values of Poisson's ratio that may be used for several different rock types. These values are shown in Table 3.2.

Table 3.2. Typical values of Poisson's ratio for numerous rock types. After Daines (1980)

Rock Type	Poisson's Ratio
Clay, very wet	0.50
Clay	0.17
Conglomerate	0.20
Dolomite	0.21
Greywacke:	
Coarse	0.07
Fine	0.23
Medium	0.24
Sandstone:	
Coarse	0.05
Coarse, cemented	0.10
Fine	0.03
Very fine	0.04
Medium	0.06
Poorly sorted. clayey	0.24
Fossiliferous	0.01
Limestone:	
Fine, micritic	0.28
Medium, calcarenitic	0.31
Porous	0.20
Stylolitic	0.27
Fossiliferous	0.09
Bedded fossils	0.17
Shaley	0.17
Shale:	
Calcareous (<50% $CaCO_3$)	0.14
Dolomitic	0.28
Siliceous	0.12
Silty (<70% silt)	0.17
Sandy (<70% sand)	0.12
Kerogenaceous	0.25
Siltstone	0.08
Slate	0.13
Tuff, glass	0.34

3.3.5. Breckels and Van Eekelen Method

Breckels and van Eekelen created a method for estimating the fracture pressure gradient by establishing a direct relationship between depth and minimum principal in-situ stress (Breckels & van Eekelen, 1982). This relationship was established on the basis of available field data as well as data found in previously published literature. By combining correlations for minimum horizontal total stress versus depth and the effects of abnormal pore pressure on horizontal total stress, they deduced a correlation that may be used to estimate the horizontal total stress in abnormally pressured formations in various areas (Breckels & van Eekelen, 1982). This is provided the pore pressure is known.

The established correlation for the U.S. Gulf coast is provided below

For $D < 11{,}500\ ft$

$$\sigma_h = 0.197D^{1.145} + 0.46\left(p_f - p_{fn}\right) \tag{31}$$

For $D > 11{,}500\ ft$

$$\sigma_h = 1.167 - 4{,}596 + 0.46\left(p_f - p_{fn}\right) \tag{32}$$

Where D is the depth, $\sigma_h$the minimum in-situ horizontal total stress, p_f the pore pressure and p_{fn} the normal pore pressure.

By utilizing this method, the minimum in-situ horizontal total stress is directly estimated, and can be inserted in the equation for fracture pressure estimation.

$$p_{ff} = \sigma_h' + p_f \tag{33}$$

The equation for transforming total stress into effective stress is given by equation (3) in section 3.2.

For the Breckels & van Eekelen equations, the depth reference point was not provided in their governing paper, however other publications (Bowers, 1999b)

indicate that all depths should be measured in total vertical depth (TVD) from sea level. For deep water wells, this results in having to treat the depth as TVD below mudline/sea bottom, and assign the hydrostatic head due to the water column to the minimum horizontal stress term, σ_h (Bowers, 1999b).

4. Wellbore Stability

Prior to drilling a well, there are compressive stresses present in the formation. These compressive stresses are known as *in-situ stresses* and consist of the minimum and maximum horizontal stress, σ_h and σ_H , which in most cases are unequal, and the vertical/overburden stress σ_v/σ_o. In addition to this, pore pressure, p_f, is also present. After drilling the well, these stresses in the vicinity of the borehole wall will be redistributed into so-called hoop stress, σ_θ, axial stress, σ_z, and radial stress, σ_r. If the well is deviated, an additional shear stress, $\tau_{\theta z}$, is created (McLean & Addis, 1990).

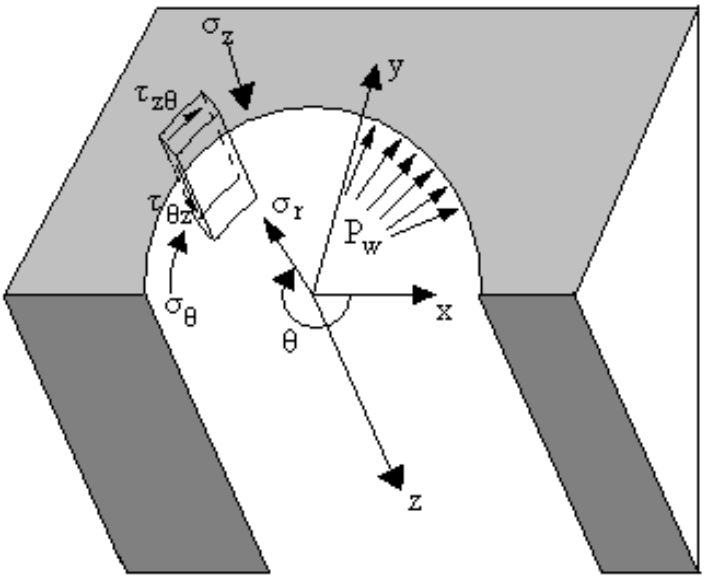

Figure 4.1. Stress state at the wall of a deviated wellbore. After McLean & Addis (1990)

While drilling the well, rock material is being removed from the hole and the drilling fluid replacing it must therefore have a certain weight in order for the hole to remain stable and intact. Attaining this correct mud weight is therefore critical as an incorrect mud weight may lead to tensile or shear failure in the wellbore. In the case of a mud weight that is too low, the stresses around the wellbore will be too high and the rock may fail in shear failure, also known as wellbore breakout. In the case of overestimating the mud weight, i.e. a mud weight too high, one may experience lost circulation or mud losses (Li et al., 2012). Thus, the rock will remain intact and borehole failure will be

avoided as long as the rock stresses are kept below a certain limit. However, from an operational point of view, the accepted failure limit may be higher than what wellbore stability models predict, meaning that initial borehole failure is not necessarily critical (Fjær et al., 2008).

The required mud weight necessary to avoid failure may be estimated by using several wellbore stability models, where the goal is to create a mud weight window, referred to as a drilling window, allowing safe operations. This drilling window provides us with a mud weight/fluid density that will be high enough to obtain wellbore stability and low enough to prevent fluid losses (Zhang et al., 2008).

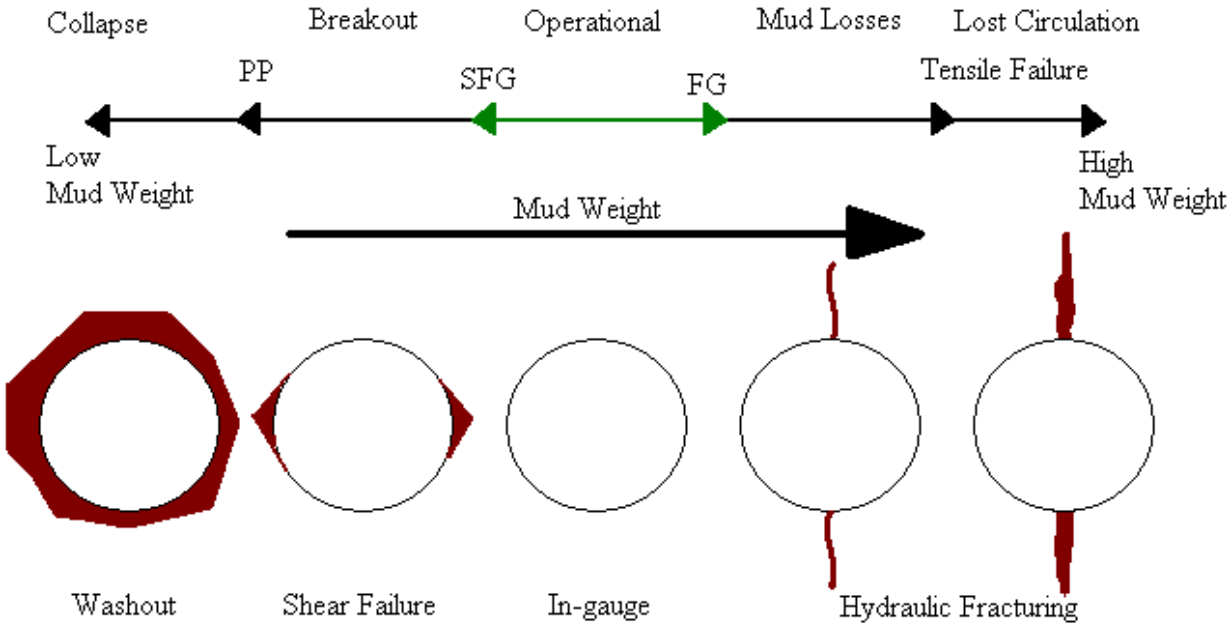

Figure 4.2. Mud weight and wellbore failure relationship. After Li et al. (2012). MW = Mud Weight, PP = Pore Pressure, SFG = Shear Failure Gradient, FG = Fracture Gradient

Figure 4.2 provides a schematic overview of the relationship between mud weight and wellbore failures. With an insufficient mud weight, i.e. a mud weight that is too low, the hole will collapse. If the mud weight is lower than the shear failure gradient, but higher than the pore pressure gradient, the hole will breakout in shear failure. When operating with a mud weight higher than the fracture gradient the hole may experience hydraulic fracturing, i.e. tensile failure, and there will be loss of mud ultimately leading to lost

circulation if the mud weight reaches a certain value. As Figure 4.2 indicates, the safe operational mud weight window will be between the shear failure gradient and fracture gradient.

In order to determine the functional mud weight window, it is intuitive that the shear failure gradient and the fracture gradient must be determined. The fracture gradient is estimated as described in section 3.3, while the shear failure gradient may be estimated by numerous wellbore stability models, which depend on the total stress state of the borehole. In most cases, the total stress state is described by using the three principal effective stresses ($\sigma_1, \sigma_2, \sigma_3$) which are determined by transposing the axial, radial and hoop stress as shown below (McLean & Addis, 1990). One of the principal stresses is the well pressure, P_w, which acts perpendicular to the borehole wall.

$$\sigma_1, \sigma_2, \sigma_3 = \begin{Bmatrix} \frac{\sigma_\theta + \sigma_z}{2} \pm \sqrt{\left(\frac{\sigma_\theta + \sigma_z}{2}\right)^2 + \tau_{\theta z}^2} \\ P_w \end{Bmatrix} \quad (34)$$

Several wellbore stability models used to estimate the shear failure gradient (SFG) are found in the literature. The following will describe the mechanisms governing shear and tensile failure as well as briefly list and describe some of the models used to estimate the SFG.

4.1. Shear Failure

Shear failure occurs when the shear stress along a plane in a rock sample reaches the maximum limit the rock can take. After shear failure has been initiated, and a sufficient amount of time has passed, a fault zone will develop allowing the two sides of the fault to move against each other. Thus, the critical shear stress for which shear failure will be initiated is dependent on the normal stress that acts over the failure plane (Fjær et al., 2008).

It is indicated in literature that the most common models used to predict wellbore shear failure are Mohr-Coulomb, Modified Lade and Drucker-Prager, which all assume linear elasticity prior to failure (Islam et al., 2010).

When modeling shear failure pressure, and thus the minimum mud weight required to prevent this, numerous data is required. Amongst these are overburden- and pore pressure, horizontal stresses, in-situ stress orientation, rock strength data and the wellbore trajectory (Zhang et al., 2008).

4.1.1. The Mohr-Coulomb model

Applying the Mohr-Coulomb model to estimate the minimum mud weight possible, the shear failure gradient (SFG) in a vertical well is given as

$$SFG = \frac{1}{2}(3\sigma_H - \sigma_h)(1 - \sin\varphi) - S_0 cos\varphi + p_f sin\varphi \quad (35)$$

Where σ_H is the maximum horizontal stress, σ_h the minimum horizontal stress, φ the friction angle and S_0 the cohesion.

The above equation shows that the shear failure pressure is directly related to the pore pressure (Zhang et al., 2008), and is only valid for vertical wells with impermeable walls.

Another way of expressing the Mohr-Coulomb criterion is shown in equation (36).

$$\sigma_1' = C_0 + \sigma_2' \tan^2\beta \quad (36)$$

Where C_0 is the unconfined compressive strength, σ_1' the maximum principal effective stress, σ_3' the minimum principal effective stress, and β the failure angle.

The above relationship illustrates how the Mohr-Coulomb neglects the effect of the intermediate principal stress, thus it only represents rock failure under triaxial stress states, i.e. $\sigma_2 = \sigma_3$. This will result in a relatively conservative prediction of

wellbore stability, meaning a narrower drilling window. When estimating if a wellbore will fail, experimental data indicates that all three principal stresses should be included in the estimation, thus the intermediate principal stress should not be neglected. This is shown in the following section 4.1.3. Therefore, it is clear there must exist a 3D failure criterion model that can account for polyaxial stress effects (Islam et al., 2010).

4.1.2. The Drucker-Prager model

In difference from the Mohr-Coulomb model, the Drucker-Prager model assumes the three principal stresses all contribute (Ewy, 1999).

$$(\sigma_1' - \sigma_2')^2 + (\sigma_1' - \sigma_3')^2 + (\sigma_2' - \sigma_3')^2 = C_1(\sigma_1' + \sigma_2' + \sigma_3' + C_2)^2 \qquad (37)$$

C_1 and C_2 are material parameters, which are related to cohesion and internal friction.

The Drucker-Prager model has been reported to overestimate the influence of the intermediate stress, leading to incorrect stability predictions (Islam et al., 2010).

4.1.3. The Modified Lade model

The original Lade criterion was first formulated in 1977 and was based on the behavior of soils. This criterion was later modified and presented by Ewy in "Wellbore-Stability Predictions by Use of a Modified Lade Criterion" (1999). The criterion is given as follows.

$$\frac{(I_1")^3}{I_3"} = 27 + \eta \qquad (38)$$

where

$$I_1" = (\sigma_1 + S_1 - p_f) + (\sigma_2 + S_1 - p_f) + (\sigma_3 + S_1 - p_f) \qquad (39)$$

$$I_3" = (\sigma_1 + S_1 - p_f)(\sigma_2 + S_1 - p_f)(\sigma_3 + S_1 - p_f) \qquad (40)$$

S_1 and η are material parameters, p_f is the pore pressure.

$$S_1 = \frac{S_0}{tan\varphi} \tag{41}$$

$$\eta = 4\tan^2\varphi\frac{9-7sin\varphi}{1-sin\varphi} \tag{42}$$

Given a general stress state, i.e. $\sigma_1 \neq \sigma_2 \neq \sigma_3$, it is assumed that the Modified Lade criterion is the criterion that most accurately describes the intermediate stress influence on the rock strength. This model initially predicts a strengthening effect when the intermediate stress, σ_2, increases and in addition to this the model predicts a decrease in strength in the case of σ_2 being excessively high (Ewy, 1999). Because of these abilities, it is deduced the Modified Lade criterion properly accounts for the influence of the intermediate principal stress when modeling wellbore stability.

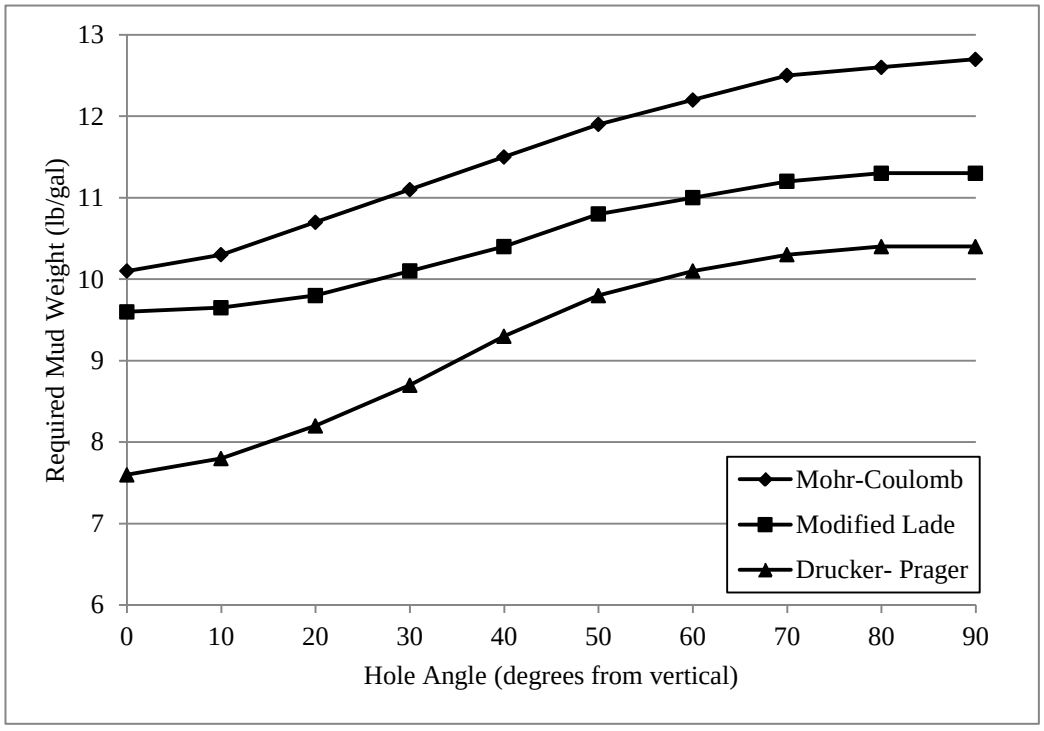

Figure 4.3. Required mud weight versus hole angle for MC, ML and DP models. After Ewy (1999)

Figure 4.3 shows the difference in the modeled required mud weight governed by the Mohr-Coulomb, Modified Lade and the Drucker-Prager criterions. As one may observe, the Mohr-Coulomb is the most conservative of the three. The Modified Lade criterion is not quite as conservative as the Mohr-Coulomb criterion, however it estimates a higher mud weight than the Drucker-Prager criterion, meaning it is more conservative. Another observation that may be made from the above figure is that the Modified Lade predicted mud weights are not as sensitive to variation in well angle as the mud weights predicted by the other two methods (Ewy, 1999).

4.2. Tensile Failure

Another type of failure that may occur in a wellbore is tensile failure. This type of failure will happen when the minimum effective stress around the wellbore is exceeded by the tensile strength of the formation, T_0, and as a result of this, the formation will fracture. This criterion may be expressed as follows,

$$\sigma_3' = \sigma_3 - p_f = -T_0 \tag{43}$$

Where σ_3' is the minimum effective principal stress, σ_3 the minimum total principal stress and p_f the pore pressure.

It is easily observed that the criterion for tensile failure is considerably more simple than the criterion for shear failure.

The typical reaction for a rock sample experiencing tensile failure is to split along few fracture planes – in some cases the rock splits along only one fracture plane. These fracture planes are most often perpendicular to the direction of the tensile stress (Fjær et al., 2008).

Following the start of tensile failure, i.e. hydraulic fracturing, there is a chance this fracture may grow and extend, the probability of this occurring must be further

explored for each specific case. Occasionally, when the magnitude of the smallest principal stress, σ_3, is larger than the required fracture pressure in the well, only minor fluid losses will be experienced. This is due to the fact that the tensile fracture propagation length is no larger than only a few radii from the borehole wall (McLean & Addis, 1990).

4.3. Fatigue Failure

Although a material has withstood a load applied once, there is no guarantee the material will be able to avoid failure when the same load is reapplied several times. When a material is repetitively stressed with a stress magnitude not necessarily higher than the maximum stress the material can withstand, it is said the material is undergoing “cyclic fatigue” (Cardu et al., 1989). The behavior of rock material under such cyclic loading differs from rock behavior under conditions where stress is only applied once. The cyclic loading often causes failure of the rock, even below the rocks static strength (Cho & Haimson, 1987). Hence, it is understood that cyclic loading may cause fatigue of the rock and ultimately lead to failure, which is referred to as fatigue failure. For an applied amount of stress lower than the static strength, referred to as “fatigue strength”, there is a corresponding amount of cycles that will cause fatigue failure. This number of cycles is referred to as the “fatigue life” (Cho & Haimson, 1987).

By expressing the fatigue strength as the ratio of the applied maximum stress to the static strength, governing values between 0 and 1, the fatigue life may be determined for values of the fatigue strength. As reported by Cho & Haimson (1987) experimental results indicate that for rocks in uniaxial compression, at a fatigue strength level of 0.7, fatigue failure will occure when the fatigue life is of the magnitude of hundreds of thousands. However, in the case of a rock in uniaxial tension, for the same fatigue strength, the corresponding fatigue life is tens of thousands or so. In the case of alternating compression and tension, the fatigue life is decreased to merely several hundreds (Cho & Haimson, 1987).

In the case of drilling a well, the circular rock opening is subjected to a cyclic internal pressure that will cause simultaneous tensile tangential stresses and compressive radial stresses in the near borehole wall area. Experimental results provided by Cho & Haimson (1987), show a conventional fatigue strength – fatigue life relationship, that means as the fatigue strength is reduced, the fatigue life will increase. This is as expected, as it is fairly intuitive that by applying a lesser load, the material will last longer. These results were obtained by keeping the remaining parameters constant. The results obtained also strongly suggest that the dominant form of fatigue failure is tensile fatigue failure (Cho & Haimson, 1987). Thus, under drilling operations it it fairly obvious that one should operate in such a manner to limit the stresses inflicted on the borehole wall.

4.4. Effect of Plasticity on Wellbore Stability

One observation that is often made when drilling a wellbore is that the borehole is considerably more stable than primarily estimated when using the elastic-brittle theories. The theories previously described in this thesis are elastic-brittle theories, and do not account for the non-elastic behavior of the material which is in fact the reason for this increased strength. When accounting for this non- elastic behavior, the concept of plasticity is introduced. By utilizing such elasto-plastic behavior one assumes the material may continue to hold its load after failure has been initiated. This differs from the elastic-brittle theories where the material presumably loses its entire load bearing capacity after failure initiation. Figure 4.4 displays this difference, and shows the stress versus strain curves for both elasto-plastic and elastic-brittle behavior of a load bearing material.

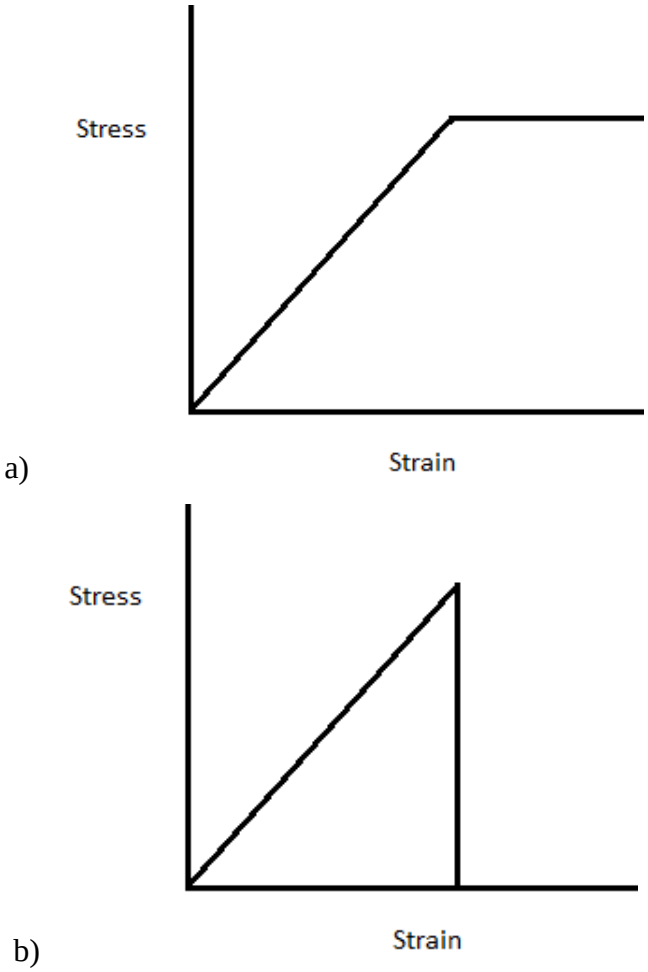

Figure 4.4. a) Elasto-plastic behavior. b) Elastic-brittle behavior.

After failure has been initiated around the wellbore, a zone with elasto-plastic characteristics will develop. This zone is in fact softer than the non-plastic zone, but surprisingly it may strengthen the behind laying rock (Fjær et al., 2008).

In order to determine the radius of this plastic region, and account for the effect of plasticity on the near wellbore stresses, one may use a slightly modified version of the Mohr-Coulomb criterion. For further reading regarding the physics and mathematics behind this, the reader is referred to the book “Petroleum Related Rock Mechanics” by Fjær et al., 2008.

5. Drillworks

The following section will provide an overview of the software used to complete the modeling in this thesis.

5.1. Drillworks Predict – Pore Pressure Analysis

As mentioned in the previous sections, pore pressure related issues are a main cause to many drilling problems that are both time consuming and expensive. Inadequate accuracy regarding the estimated value of pore pressure as well overburden pressure and fracture pressure, may result in fluid losses and kicks, and in some cases the well may be lost due to poor casing design (Knowledge Systems, 2006a).

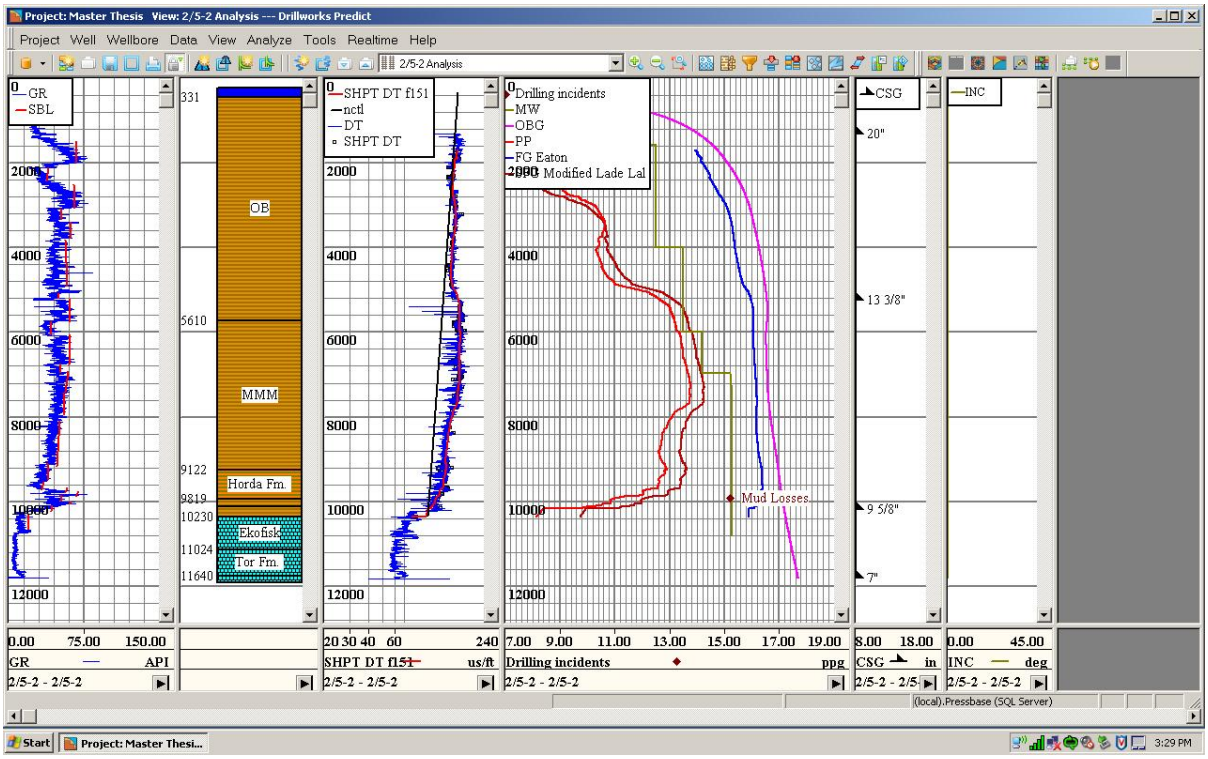

Figure 5.1. Predict output window

This software, namely Predict, provides a reliable pore pressure forecast, assuming correct input values have been used. With numerous models and correlations available

for pressure estimation, Predict offers a pre-drill, real-time as well as a post-drill analysis in order to enhance drilling performance and avoid difficulties throughout the entire drilling process. The pre-drill analysis assists in choosing the optimal mud weight design and casing setting depths for a successful well. If the pre-drill analysis turns out to be erroneous in any way, the real-time analysis allows the well planner to implement modifications to the pre-planned model in order to maintain an optimal drilling process. With the option to perform a post-drill analysis, the planning and drilling of future wells may be improved through calibrating the prior estimated pressure gradients (Knowledge Systems, 2006a).

One of the main advantages with the Predict software is the interactive aspect of it. Predict allows the user to make changes to various trend lines while viewing the output window, and immediately shows the consequence of the variation of this parameter. This function provides a well planner the possibility to vary parameters that may be uncertain and investigate what outcome this will have on the safe drilling window, i.e. the margin between the shear failure gradient and the fracture gradient.

5.2. Drillworks Geostress – Wellbore Stability Analysis

Geostress allows the user to assess wellbore stability issues before drilling, as well as in real-time, i.e. during drilling. This software is a geomechanical analysis tool, and may be used to plan the most suitable well path as well as fine tune and create the best mud weight design possible (Knowledge Systems, 2006b). This implies fewer wellbore stability problems during drilling and thus a safer and more cost efficient drilling process. For the use in this thesis, the software has been used to investigate the safe wellbore trajectory, i.e. how variations of azimuth and inclination will affect the wellbore stability.

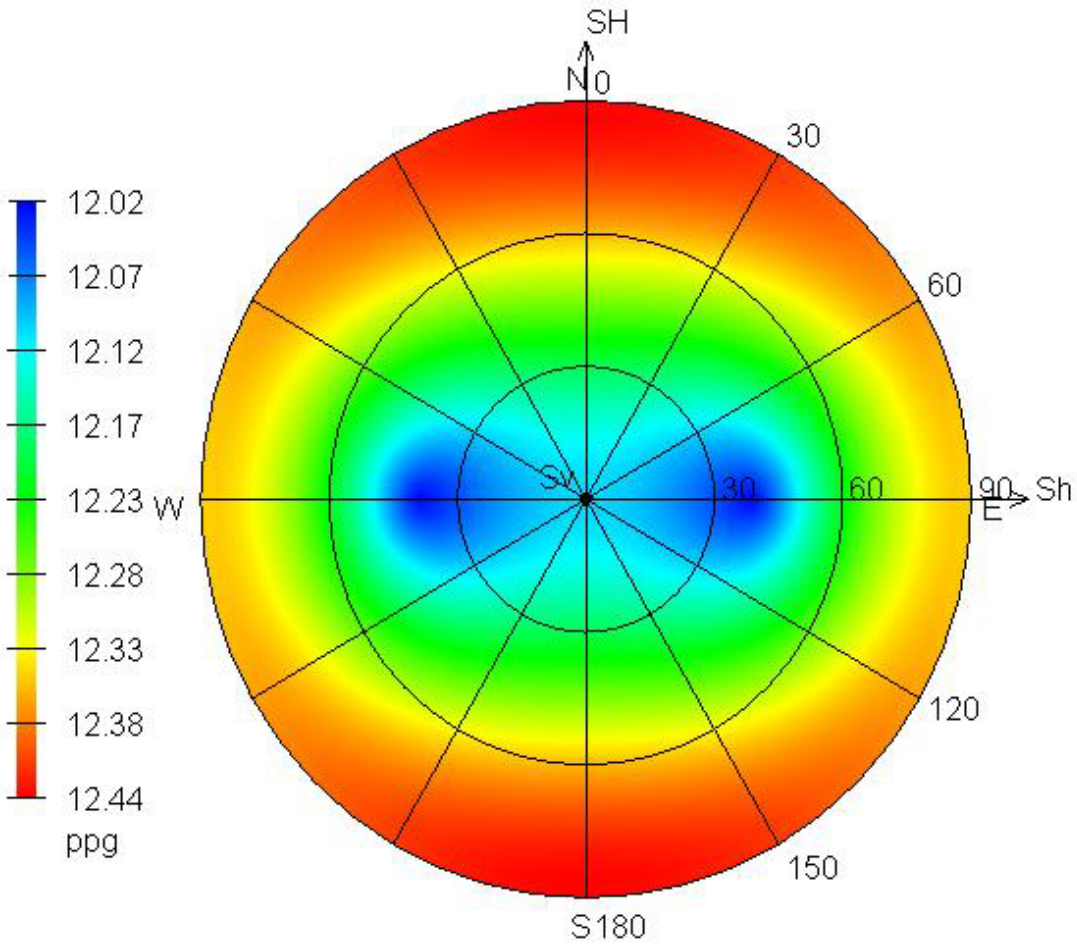

Figure 5.2. Hemisphere plot generated by Geostress illustrating the Safe Wellbore Trajectory.

6. Geomechanical Modeling

As mentioned earlier, this work involves creating a 2D Tor field specific geomechanical model by utilizing log data and documentation describing observed drilling incidents from the surrounding area. This geomechanic model will be built by using the software described in section 5, Predict. Building a model of this kind is the practical way of combining the theory discussed in the previous sections of this thesis with the common procedures used in the oil industry today.

A large part of this project consists of collecting relevant log data as well as locating and collecting data such as daily drilling reports, final well reports and other well operation data that contain information regarding relevant events and observations throughout the course of drilling and completing the well. Taking into consideration the age of the exploration wells chosen to build this geomechanic model, this is a task that may prove to be quite challenging.

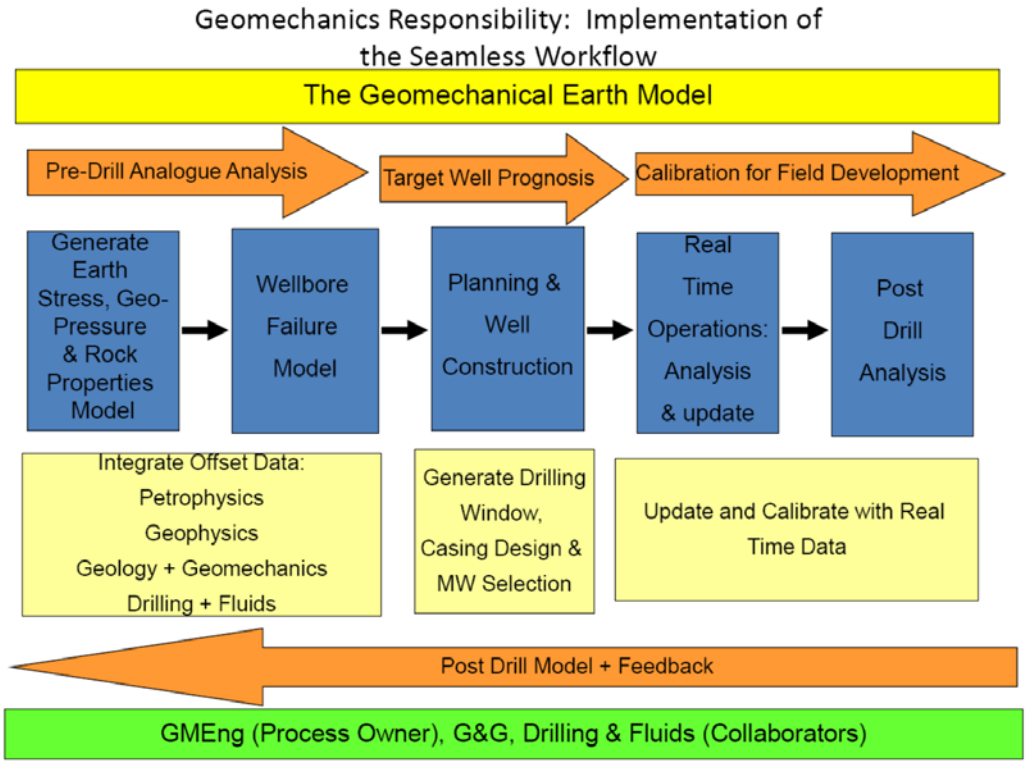

Figure 6.1. Geomechanic Earth Model Work Flow. Adapted from Michael Shaver, personal communication, April 18, 2012

Figure 6.1 shows the general work flow when building a geomechanical earth model. The chart shows how various data, i.e. petrophysical data, MWD data, real time data etc., may be used together to build a post drill geomechanical model.
The first step in the process of building the geomechanical model that may be used in the planning of future wells in the Tor field is to collect all data that will be relevant to building the model. This includes log data, survey data and documents describing the drilling operations and the physical observations made during the operations. Following this the model can be built based on raw log data, i.e. the data from wireline logging or MWD measurements. Prior to using this log data, it is important that the data is thoroughly quality checked to ensure the magnitudes of the measurements are plausible, as well as ensuring there is an adequate amount of data available in order to build the most accurate geomechanical model possible. After estimating an initial pore pressure gradient and fracture gradient, a shear failure stress gradient can be estimated and in order to do this a wellbore failure model must be chosen. After choosing the model and estimating the shear failure gradient, the estimation of the pressure gradients is complete. As shown in Figure 6.1 the next step after choosing the wellbore failure model is to plan the well construction, meaning the mud weight and casing design is planned based on the generated drilling window. However, this thesis involves a post-drill analysis of several wells, so the planning & well construction step as well as the real time operations analysis and update step is not relevant for this case. These particular steps are important when using a geomechanical model for planning and drilling a well, which would allow real time analysis. Hence, for the work conducted in this thesis, the step following constructing the shear failure gradient is to calibrate the model against operational observations made when drilling the well. This will be done by locating actual drilling incidents by examining the daily drilling reports and other documents describing the drilling operations. By performing such an analysis, the estimated drilling window will be validated.

This section of the master thesis work will contain detailed descriptions of the work done in order to build a Tor field specific geomechanical model as well as observations that have been made while doing so.

6.1. Data Collection

After locating survey data and available log data for each of the ten wells, the collected data was imported into Predict. These data will be the base of the model that will be created later on. The log data collected for the different wells include gamma ray logs (GR), resistivity logs (RES), sonic logs (DT), density logs (RHOB), caliper logs (CAL) and total gas cut logs (TGAS). The mentioned logs all measure important parameters of the formation. In brief, the gamma ray log measures a formations natural radiation of gamma rays, the resistivity log measures the resistivity, the sonic log measures the P-wave travel time, the density log measures the density, the caliper log measures the borehole diameter and the total gas cut log measures the amount of gas in the drilling mud (Schlumberger, 2012).

After importing the data, a track view of the log input data was created for each well in order to provide a simple overview of what depths there is available data for each well. An example of such a view, referred to as a *track view,* is displayed in Figure 6.2.

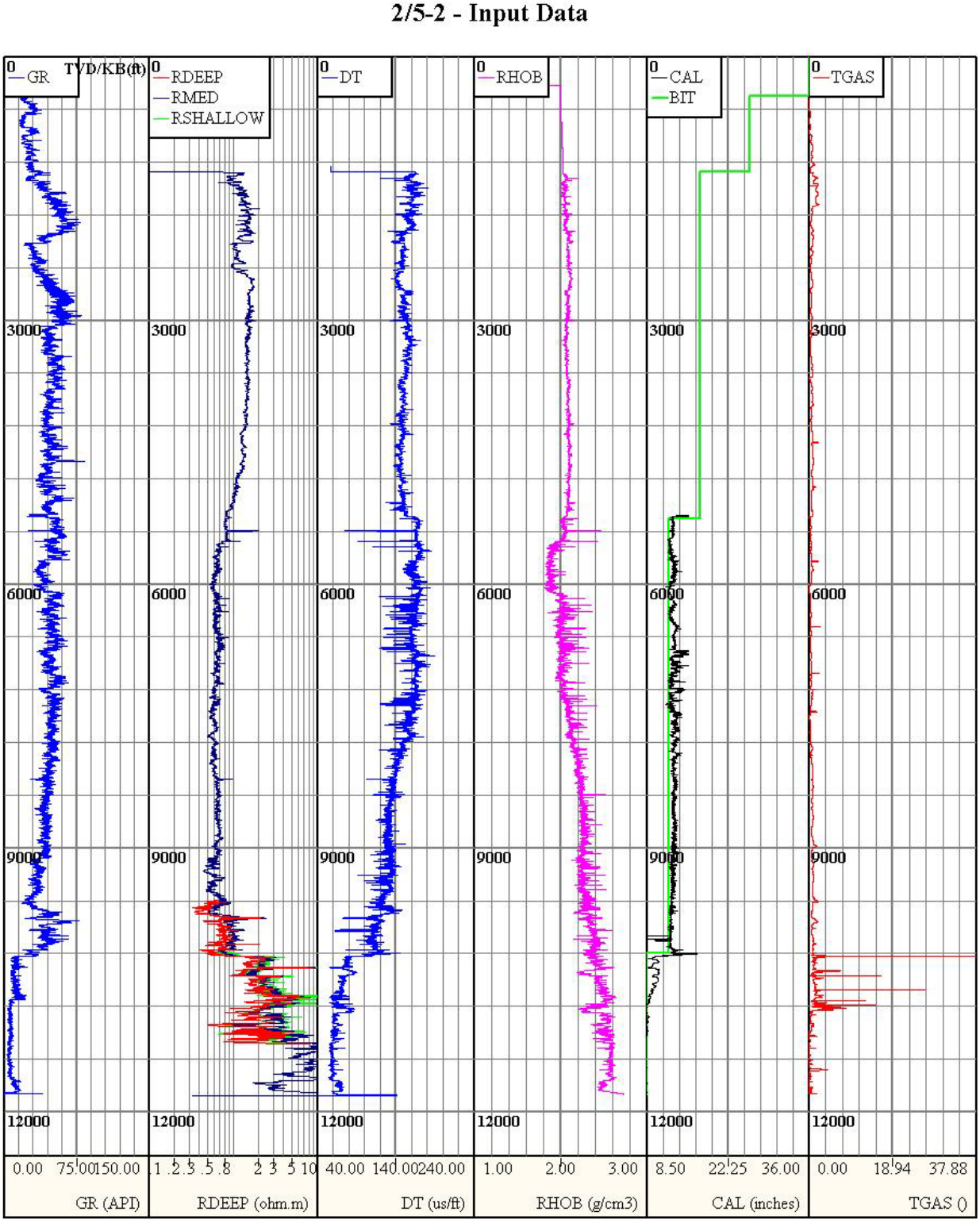

Figure 6.2. Example of input data track view. Depth in ft

Following an initial study of the data, a table showing the available log data for each well was assembled and is provided in Table 6.1. For further analysis of the data and

building of the model, it is important that the gamma log and the sonic log cover as large a depth interval as possible.

Table 6.1. Overview of available log data. Y – available data, N – unavailable data

	Well name									
Available Log Data	2/4-10	2/4-17	2/4-7	2/4-8	2/5-1	2/5-2	2/5-3	2/5-5	2/5-8	2/5-14S
Caliper	Y	Y	Y	Y	Y	Y	Y	Y	Y	Y
DT - Sonic	Y	Y	Y	Y	Y	Y	Y	Y	Y	Y
DTs - Shear Sonic	N	N	N	N	N	N	N	N	N	Y
DTc - Compressional Sonic	N	N	N	N	N	N	N	N	Y	N
Gamma Ray	Y	Y	Y	Y	Y	Y	Y	Y	Y	Y
Density	Y	Y	Y	Y	Y	Y	Y	Y	Y	Y
Resistivity - deep	Y	Y	Y	Y	Y	Y	Y	Y	Y	Y
Resistivity - medium	Y	Y	Y	Y	Y	Y	Y	Y	Y	Y
Resistivity - shallow	Y	Y	Y	Y	Y	Y	Y	Y	Y	N
Total Gas Cut	Y	N	N	Y	Y	Y	N	N	Y	N

As may be observed in Table 6.1, all the wells have available caliper, acoustic, gamma ray, density and resistivity log data. Some wells also have the total gas cut data, as well as shear or compressional sonic measurements.

After further review of the log data available, a decision to disregard several wells was made. This is due to the available data being limited to a very short depth interval, therefore proving to be inadequate to utilize for modeling. The disregarded wells are shaded red in Table 6.1. An example of such a well is provided in Figure 6.3. The wells that were disregarded are listed on the following page by their well name, the area in which they are drilled is also included.

- 2/4-8 (Tor field)
- 2/5-5 (South-East Tor field)
- 2/5-8 (South-East Tor field)
- 2/5-14S (South-East Tor field)

The wells left which are available and have a sufficient amount of data are listed below.

- 2/4-7 (Tor field)
- 2/4-10 (Tjalve field)
- 2/4-17 (Tjalve field)
- 2/5-1 (Tor field)
- 2/5-2 (Tor field)
- 2/5-3 (South-East Tor field)

With the data in a similar overview it is also simple to perform a quality check, this is shown in Figure 6.4 for the sonic data. The reason this is done is to make sure no measured values are obviously wrong. This is fairly simple to detect as these logs should be quite similar since they were logged in the same area. In our case, the logs show conformity.

Survey data, i.e. measured depth (MD), inclination and azimuth, was also collected in order for the true vertical depth (TVD) to be calculated for wells where the TVD data is missing. Data regarding formation tops was located, and displayed in lithology columns to assist in creating a complete overview. The sea level is further referred to as the mean sea level (MSL) and the formation overlying the first formation top simply referred to as overburden (OB). Table 6.2 shows the formation tops for well 2/5-2, similar tables exist for all the other wells.

Table 6.2. Formation tops for well 2/5-2

Pick Name	TVD (ft)	MD (ft)
Sea bottom	331.4	331.4
Horda Formation Top	9122.4	9122.4
Sele Formation Top	9819.5	9819.5
Lista Formation Top	9996.7	9996.7
CHALK GROUP Top	10377.3	10377.3
Tor Formation Top	10731.6	10731.6
Hod Formation Top	11640.4	11640.4
ROGALAND GROUP (CNS) Top	9780.2	9780.2
HORDALAND GROUP Top	5725.1	5725.1

In addition to this, the depths of the Middle Miocene Markers (MMM) were located and are also displayed on the lithology columns shown later in the thesis. It is of special interest to locate the Middle Miocene Marker as this is where a large percent of losses occur according to historical data. The Middle Miocene Marker marks the top of shale with density lower than 2 g/cc, and previously this has been the mark where casing is set to ensure borehole stability. This shale can however handle pressures, it is the work associated with drilling the well that causes it to fail. With the final model built in this thesis, it is of interest to see if there is a possibility of reducing the mud weight and pushing the casing shoe further down for future wells.

Apart from collecting log data, survey data and formation tops, documents describing real time drilling incidents were located and examined for all the relevant wells. These documents consist of daily drilling reports (DDR’s) and final well reports, the relevant sections of the final reports being the daily operations summary.

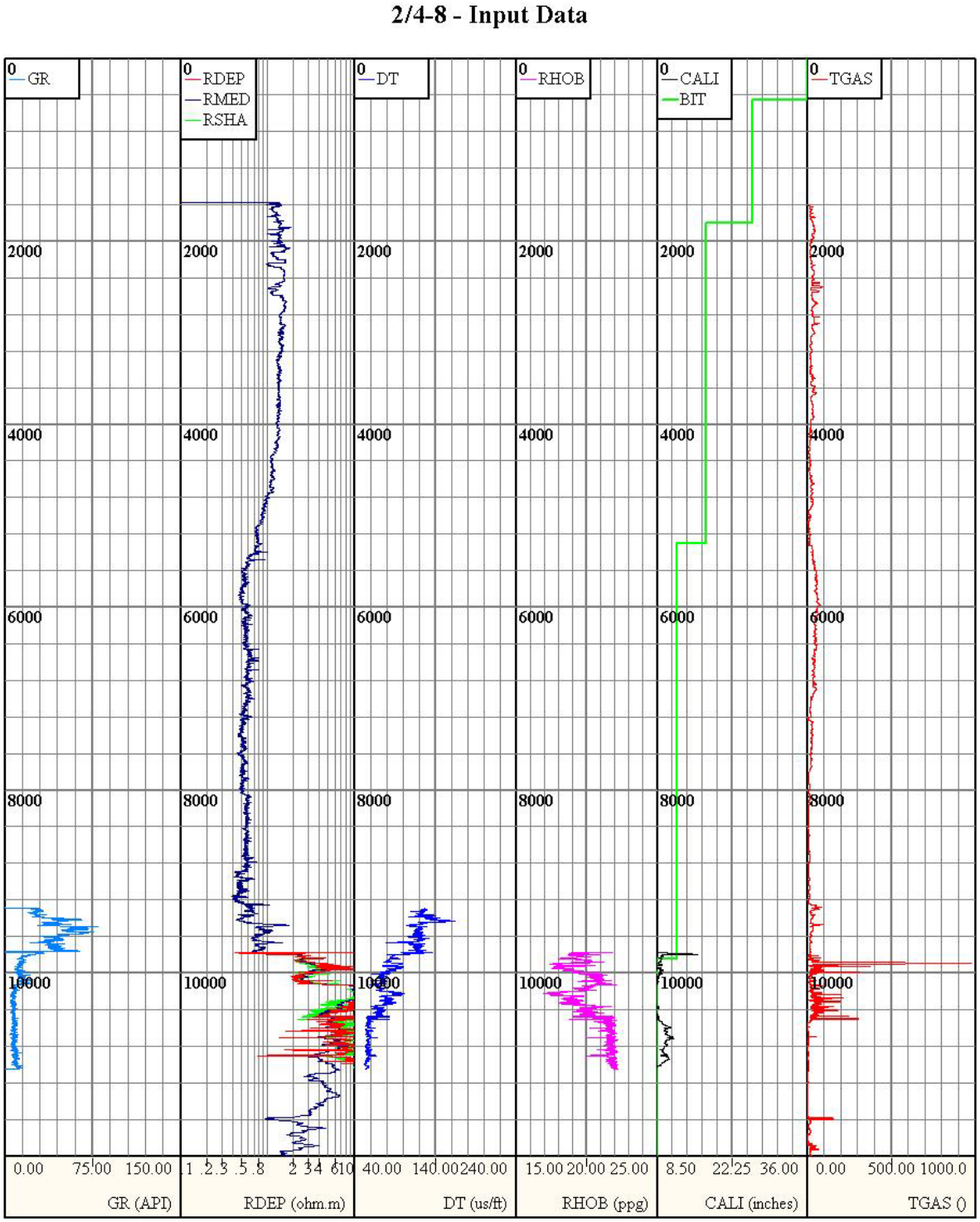

Figure 6.3. Well with inadequate log data. Depth in ft

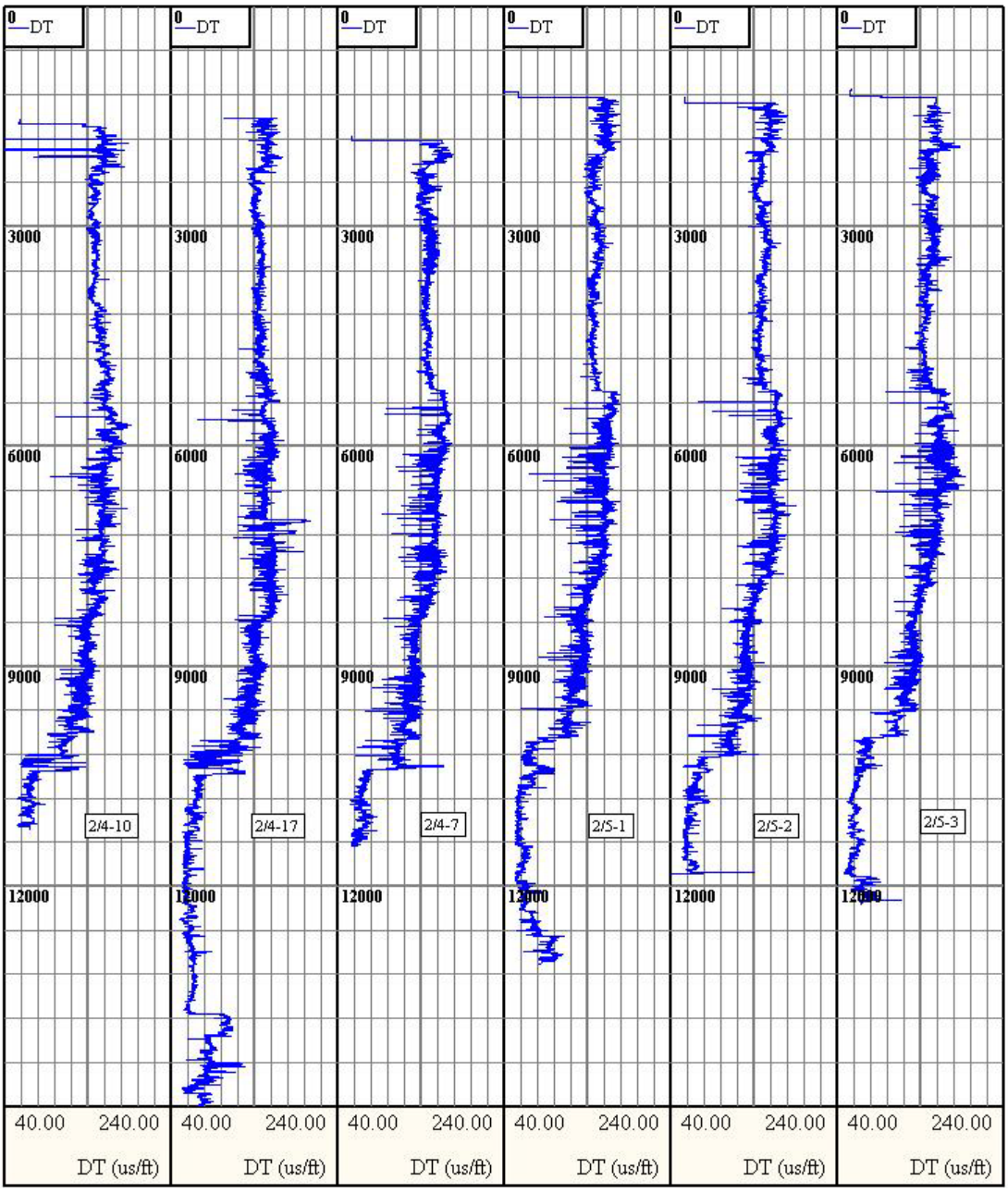

Figure 6.4. Sonic log data audit. Depth in ft

6.2. Overburden Gradient Estimation

In order to estimate the overburden gradient, as previously explained in section 3.1, density data is needed. For the remaining six wells this is provided and sufficient data is available, thus the overburden gradients may be easily estimated by Predict. In the case of a well with insufficient density data, i.e. density data only available for short depth intervals, the sonic log can be used to estimate the density through a Gardner transformation and thus also used to calculate the overburden pressure gradient. This is of course given there is more sonic data available than density data. For exploration wells, it is common to log both sonic and density logs, while for other types of wells the density log is more common to log than the sonic.

The equation used to do this, i.e. Gardner's equation, is shown as follows (DiSiena & Hilterman, 1994).

$$\rho = 0.23V^{0.25} \tag{44}$$

The velocity is given in ft/sec and the density in g/cc.

One of the overburden pressure gradients produced by Predict is shown as follows in Figure 6.5, using well 2/5-2 as an example. Included in the track view is the resulting density of the transformation of sonic data as shown in equation (44). It may be observed that the Gardner transformation yields approximately the same values apart from an interval between 7000-10000ft where the Gardner transformation yields a lower density than the density log.

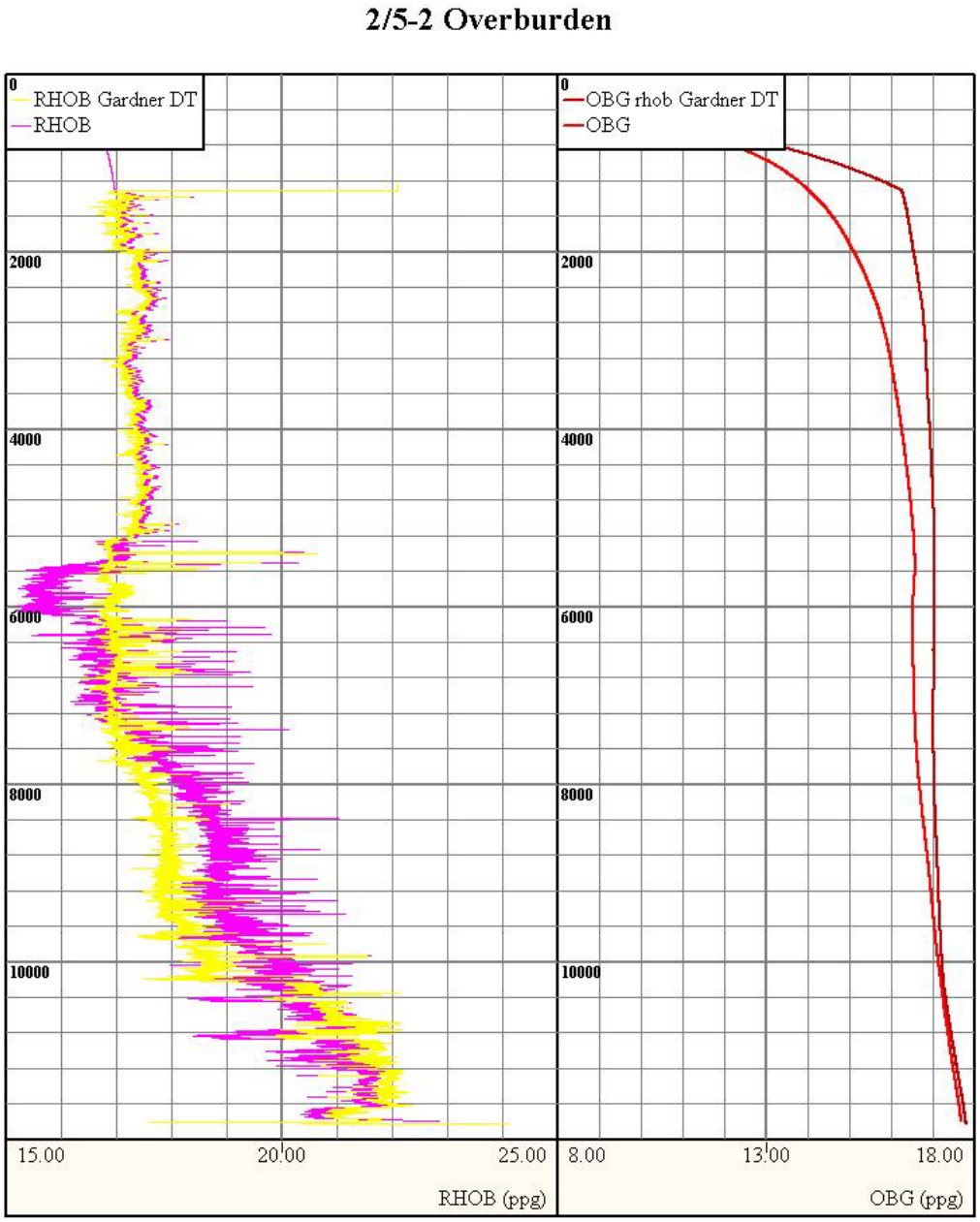

Figure 6.5. Overburden gradient estimation well 2/5-2. Depth in ft

It is of the utter most importance that the input data and the process of determining the overburden gradient is done correctly and with precision. An imprecise overburden gradient will lead to uncertainties in both the pore pressure gradient and the fracture gradient, ultimately leading to an incorrect shear failure gradient and a collapse pressure that does not resemble the actual collapse pressure. As mentioned previously this will lead to well stability issues, which can evolve into a potential loss of the well.

6.3. Pore Pressure Gradient Estimation

Following the prediction of the overburden gradient, the shale base lines for each well were located, and according to where these shale base lines were placed, the shale points are plotted on the sonic curve. This is based on the decision to use the sonic as the porosity indicating dataset. The resistivity measurements may also be used to estimate the porosity, however the resistivity data is sensitive to numerous factors, amongst them temperature, salinity and lithology. Thus, the sonic measurements were chosen to calculate the pore pressure.

For an optimal pore pressure prediction, a refined porosity indicating dataset is needed. This dataset may be created by applying a filter to the raw shale points, hence filtering the noise and creating a somewhat smooth line. The new and refined dataset will in turn contribute to creating a smoother pore pressure gradient. For this work, a boxcar filter was used, and a filter point number of 151 was chosen. Hence, every 151 data points will be selected and used to create the new dataset. Such a high number was chosen in order for the resulting dataset to be smooth.

After this refined porosity indication dataset was created, the Normal Compaction Trend was developed. This was done manually using a mudline sonic of 160µft/s and a value of 100µft/s at the base of the interval, i.e. directly over the reservoir zone. The mudline sonic value was chosen based on the fact that the shallower sediments have experienced an accelerated porosity reduction due to glaciation. This leads to over compaction/consolidation of the sediments. The areas under investigation for this work therefore have a lower velocity than areas like the Amazon or the Gulf of Mexico (fluvial deposits) where typical values will be 195-200µft/s (Shaver, 2012).

Under the premise that all the previous analyses described in this section have been completed, Predict will allow you to analyze the pore pressure. The methods available in the Predict software are Eaton, Bowers, Miller and Equivalent Depth, some which have been described in section 3.2. For the purpose of this project the chosen method was Eaton’s sonic. This is because Bowers, Miller and The Equivalent Depth method

are very similar, and are most reliable for quickly deposited depositional environments. Also, these methods call for top hole measurements, something that is not available in our case. Thus, by using one of these methods, the pore pressure will be overestimated. Eaton on the other hand, is good for all depositional environments, including the slowly deposited depositional environments. However, regardless of which method is chosen, the pore pressure gradient will later be calibrated against drilling events, such as kicks, losses, cavings etc., ultimately leading to this data taking precedence over the chosen method. As to which of Eaton's equations should be used, the Eaton's sonic was chosen. This is due to the fact that sonic data consists of grain-to-grain measurements, thus the method may be transposed and used in different areas.

Using Eaton's sonic method the pore pressure gradient for the relevant wells were successfully estimated. An example, well 2/5-2, is shown in Figure 6.6. The chosen casing depths of the wells as well as the inclination are plotted and shown in the same track view in order to provide a complete overview of the well situation.

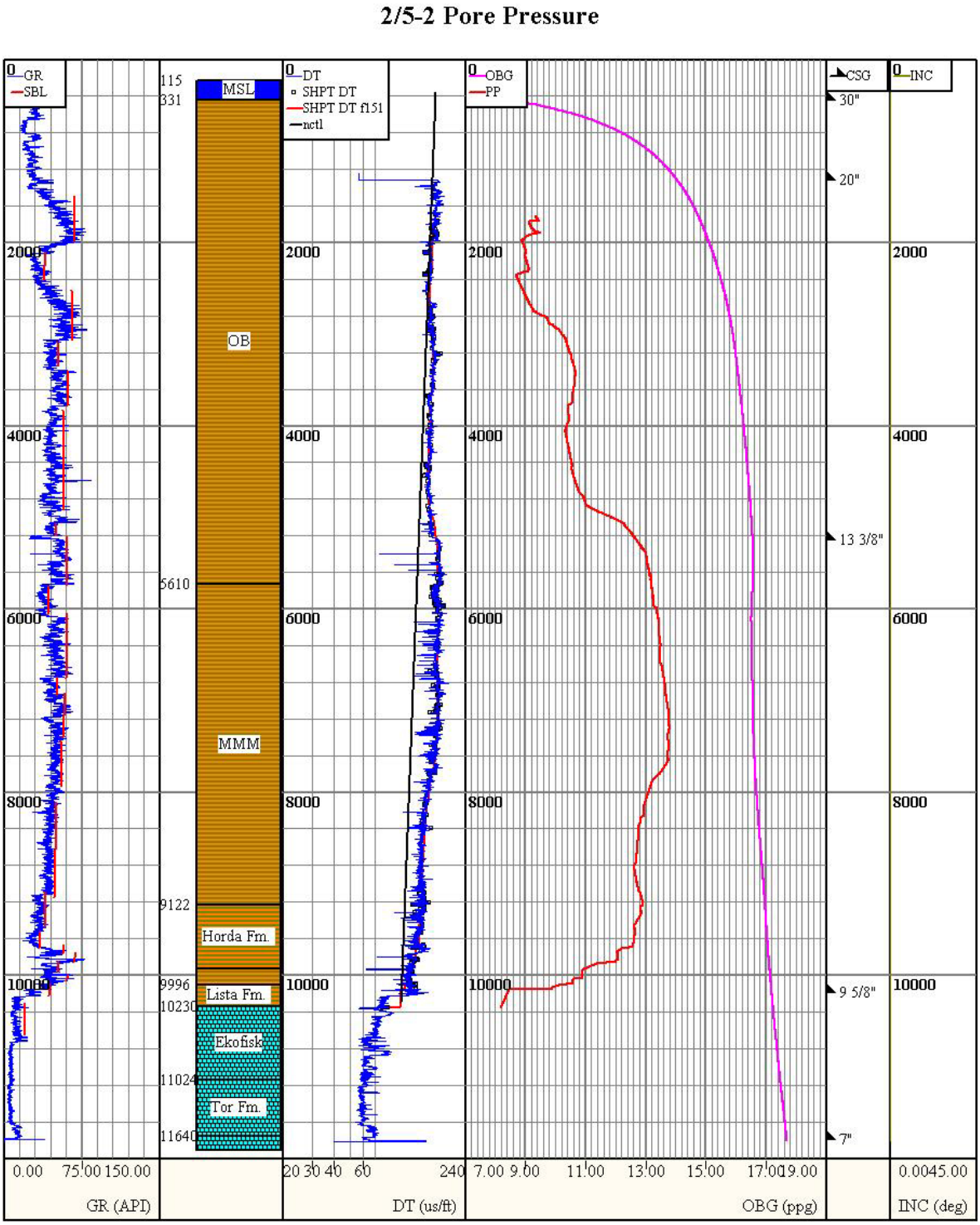

Figure 6.6. Pore pressure gradient estimation well 2/5-2. Depth in ft

6.4. Fracture Gradient Estimation

Similarly to the procedure of estimating the pore pressure gradient, Predict provides the option to choose between several methods in order to estimate the fracture gradient. As was done for estimating the pore pressure, the appropriate method for the current conditions must be chosen in order to achieve the most accurate estimate possible.

The methods offered by Predict for this purpose are Eaton, Daines, Matthews & Kelly and Breckels & Van Eekelen. These have been described in detail in a previous section, section 3.3, where the pros and cons of each method was mentioned. For the purpose of this work, given the geological conditions, the chosen method is Eaton's method. This decision was made on the grounds of several reasons. Due to the lack of tectonic activity in the greater Ekofisk area, there is no need to account for tectonic activity as Daines method does. Hubbert & Willis' method and Matthews & Kelly's method are very similar to Eaton's method, the difference being the manner of how the "effective stress ratio" is defined. Where Eaton uses Poisson's ratio to calculate the effective stress ratio, Hubbert & Willis assume an effective stress ratio of 1/3, which is found using a constant friction angle of 30°, a value that most likely is incorrect in our case. Matthews & Kelly's method calls for a matrix coefficient found directly through an empirical correlation, a correlation which is not available for the greater Ekofisk area. Similarly, a Breckels and Van Eekelen correlation has yet to be derived for this area. However, as mentioned in section 6.3, a calibration of the gradients will be performed later, ultimately leading to the data derived from drilling incidents to take precedence over the chosen method.

As mentioned in section 3.3.3, Eaton's method calls for Poisson's ratio, ν, in order to estimate the "effective stress ratio", K_{eff}. From leak-off tests and other historical data, an effective stress ratio equal to 0.8 is indicated, leading to the possibility to back out a Poisson's ratio value of $\nu = 0.46$ as described in section 3.3.3. Similarly for the sands and carbonates, an effective stress ratio of 0.6 is estimated from historical data, leading to a Poisson's ratio of approximately 0.3 (Shaver, 2012).

For the estimation of fracture gradients in this thesis, the same constant value of 0.46 for Poisson's ratio will be used as the overburden in the Ekofisk area consists of mainly shale.

Using the overburden gradient and the pore pressure gradient previously estimated as well as the constant Poisson's ratio value of 0.46, fracture gradients were estimated and plotted for each of the six wells involved in this work. An example of a track view containing the work conducted up to this point is shown in Figure 6.7 using well 2/5-2.

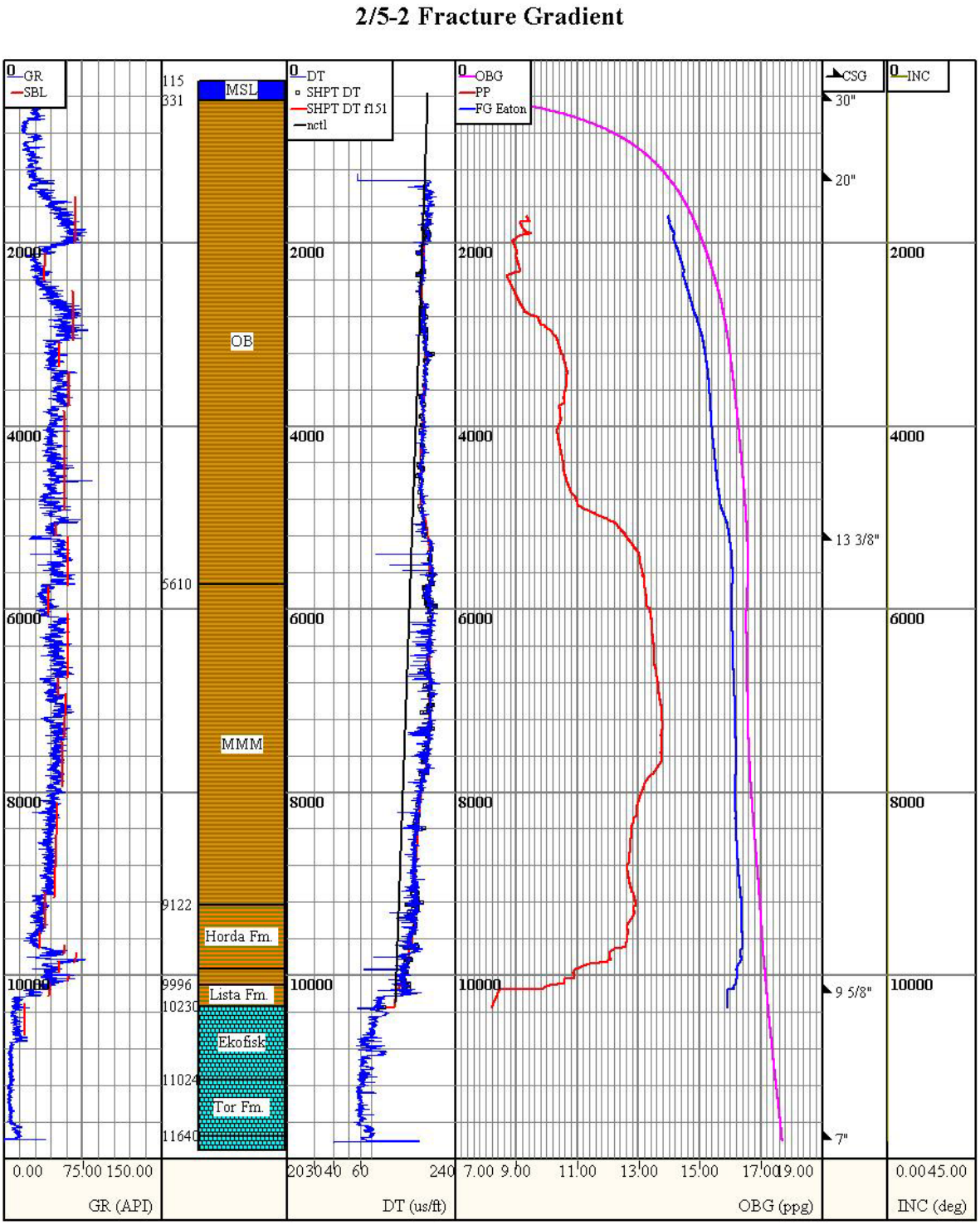

Figure 6.7. Fracture gradient estimation well 2/5-2. Depth in ft

6.5. Shear Failure Stress Gradient Estimation

Preceding the estimation of the pore pressure gradient and fracture gradient, the shear failure stress gradient (SFG) may now be estimated. As mentioned previously, the shear failure gradient is the lower bound of the safe drilling window, and it is important to stay above this restriction in order to maintain a safe drilling process. Similar to the estimation of the pore pressure and fracture pressure, Predict offers several methods commonly used to estimate the shear failure stress gradient; Mohr-Coulomb, Drucker-Prager, Stassi-d'Alia and Modified Lade failure criterion. As mentioned previously in section 4.1.3, the Modified Lade criterion is the criterion that is assumed to best describe the influence of the intermediate stress on wellbore stability, assuming a general stress state, $\sigma_1 \neq \sigma_2 \neq \sigma_3$. On the Norwegian Continental Shelf it is common practice to assume anisotropy of the horizontal stresses and a horizontal stress ratio, σ_H/σ_h, of approximately 1.02, thus resulting in a general stress state as mentioned earlier. For these reasons, the decision was made to use the Modified Lade criterion to estimate the shear failure stress gradient.

For the estimation of the shear failure gradient, predict calls for a number of parameters, amongst these the unconfined compressive stress (UCS) and friction angle. These are values that may be obtained by performing various tests on core samples from offset wells, however these values are not representative for the whole depth of the well, and for that matter they are not representative for the same formation at different geological coordinates. From a practical drilling well construction point of view, the values must reflect the fact that there is a continuous formation change over the whole depth in order to provide a satisfactory estimation of the shear failure gradient. In our case, the overburden consists mostly of shale, and there have been developed several correlations between the petrophysical properties, which may be obtained from log data and MWD, and the mechanical properties. Predict allows the user to either input a rock strength dataset, use a correlation data set as previously mentioned or simply use a constant. Lacking a rock strength dataset, the decision was made to use a correlation dataset. Predict provides the option to use the same correlation for shale and sand, use different correlations for shale and sand or

only apply a correlation to the shale. For this project, given that the overburden is mainly shale, the same correlation is used on shale and sand. Following this, the shale correlation law must be chosen, where Predict offers three choices; Lal's law, Horsrud's law and Lashkaripour and Dusseault's law. These correlations are listed in the following table, Table 6.3, and the governing papers are listed in the bibliography in case of the need for further reading. For the purpose of this work, the correlations based on petrophysical properties will be listed, as it is these correlations Predict uses.

Table 6.3. Petrophysical and mechanical properties correlation from various authors

Correlation	Author
$C_0 = 0.77 v_p^{2.93}$	Horsrud (2001)
$C_0 = 243.6 \phi^{-0.96}$	Horsrud (2001)
$C_0 = 193.4 \phi^{-1.143}$	Lashkaripour and Dusseault (1993)
$sin\phi = (v_p - 1)/(v_p + 1)$	Lal (1999)
$C_0 = 5(v_p - 1)/\sqrt{v_p}$	Lal (1999)

Where C_0 is the unconfined compressive strength in MPa, v_p the P-wave velocity normal to bedding given in km/s and ϕ is the porosity in percent.

Lashkaripour and Dusseault's law was based on 13 data points obtained from public sources as well as data obtained by own testing on shales that were somewhat more porous with a higher strength than the shales Horsrud based his correlations on (Horsrud, P., 2001). Horsrud based his correlations on soft North Sea shales, while the correlations reported in Lal (1999) showed to be fairly good estimates for sonic-log derived velocities for different core depths in the North Sea (Lal, 1999; Horsrud, P., 2001).

For estimation of the shear failure stress gradient in this thesis, Lal's equations are the chosen correlations. The method used to calibrate rock strength will, as for calibration of the pressure gradients and shear failure stress gradient, be taken precedence over by the operational observations used for the following calibration.

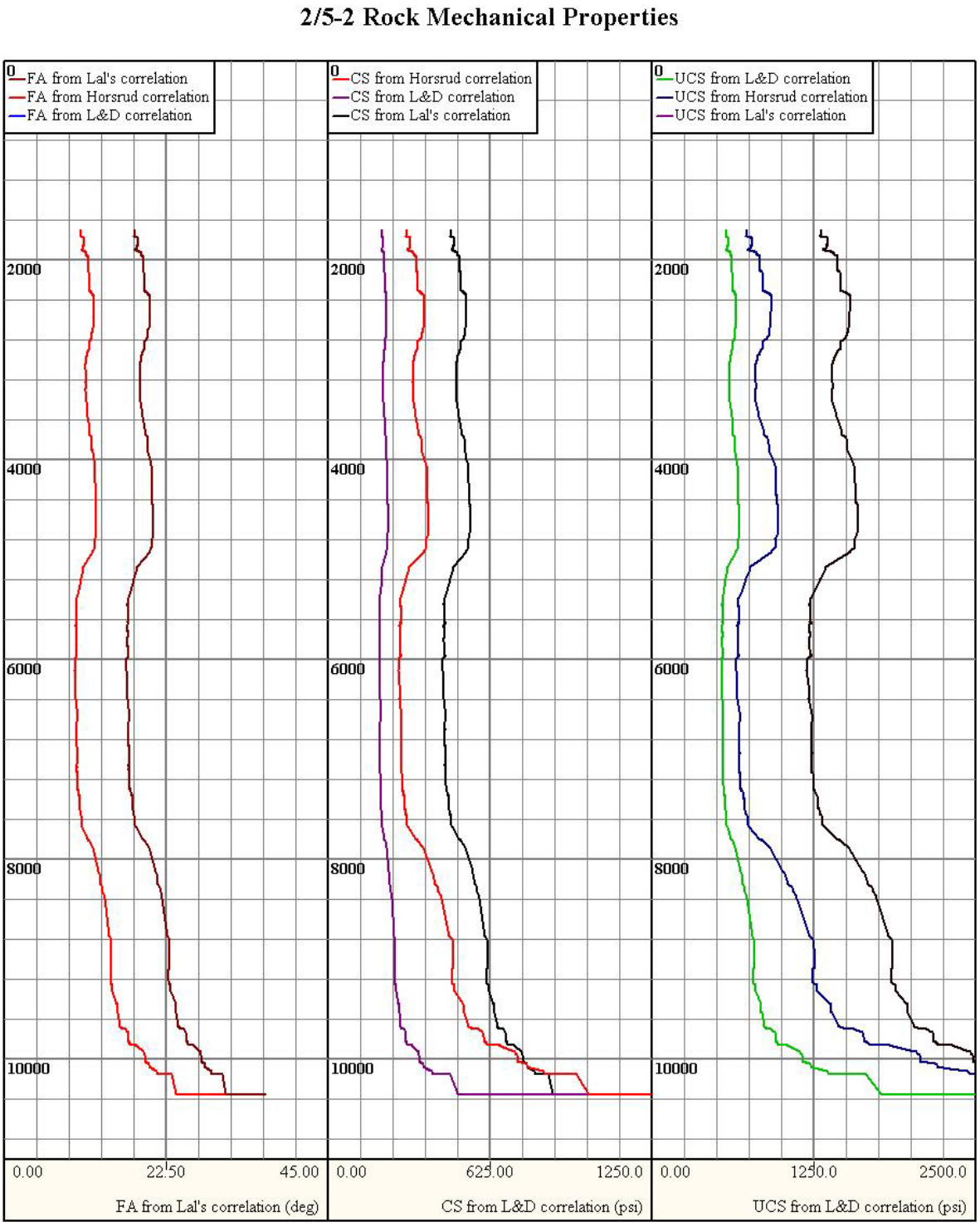

Figure 6.8. Comparison of methods used to estimate mechanical properties. Depth in ft

Figure 6.8 shows the variance in mechanical properties the different correlations yield. For the friction angle, FA, Lashkaripour and Dusseault's law and Lal's correlation yield the same values, while Horsrud's correlation yields a lower friction

angle than the two other methods. For the cohesive strength and the unconfined compressive strength it is evident for both parameters that Lal's correlation predicts the highest strength while Lashkaripour and Dusseault's law predicts the lowest. This is further discussed towards the end of this section.

In order to calculate the shear failure gradient, the horizontal stress gradients are needed. For this modeling, the fracture gradient dataset is used as the minimum horizontal stress gradient (ShG), and for the maximum horizontal stress gradient (SHG) dataset, Predict provides a formula that will calculate the maximum horizontal stress gradient based on the minimum horizontal stress gradient and tectonic factor. The tectonic factor is a ratio that is dependent on the stress regime. Normal faulting stress regimes have a tectonic factor that varies between 0 and 1, whiles other stress regimes will have a tectonic factor, tf, higher than 1 (Halliburton, 2009). In our case, this factor is 1.02, assuming the maximum horizontal stress is 2% higher than the minimum horizontal stress. The function used by Predict is shown below in equation (45)

$$SHG = ShG * tf \tag{45}$$

By using the Modified Lade criterion for shear failure, the shear failure gradients were estimated and plotted in the same depth plot as the pore pressure gradient and the fracture gradient in order to complete the first main part of building the model. An example of a track view containing the work conducted up to this point is shown in Figure 6.9 using well 2/5-2.

From the observation made regarding the rock mechanical properties it is evident the shear failure gradient will be affected by which method is chosen. The variance in the shear failure gradient is shown in Figure 6.10. Clearly, Horsrud's correlations for the rock mechanical properties will result in the most conservative drilling window and Lal's correlations the least conservative window. However, as described earlier, when calibrating the model the gradients will be shifted to coincide with observed drilling

events, hence these observations will take precedence over the method chosen to estimate the rock mechanical properties.

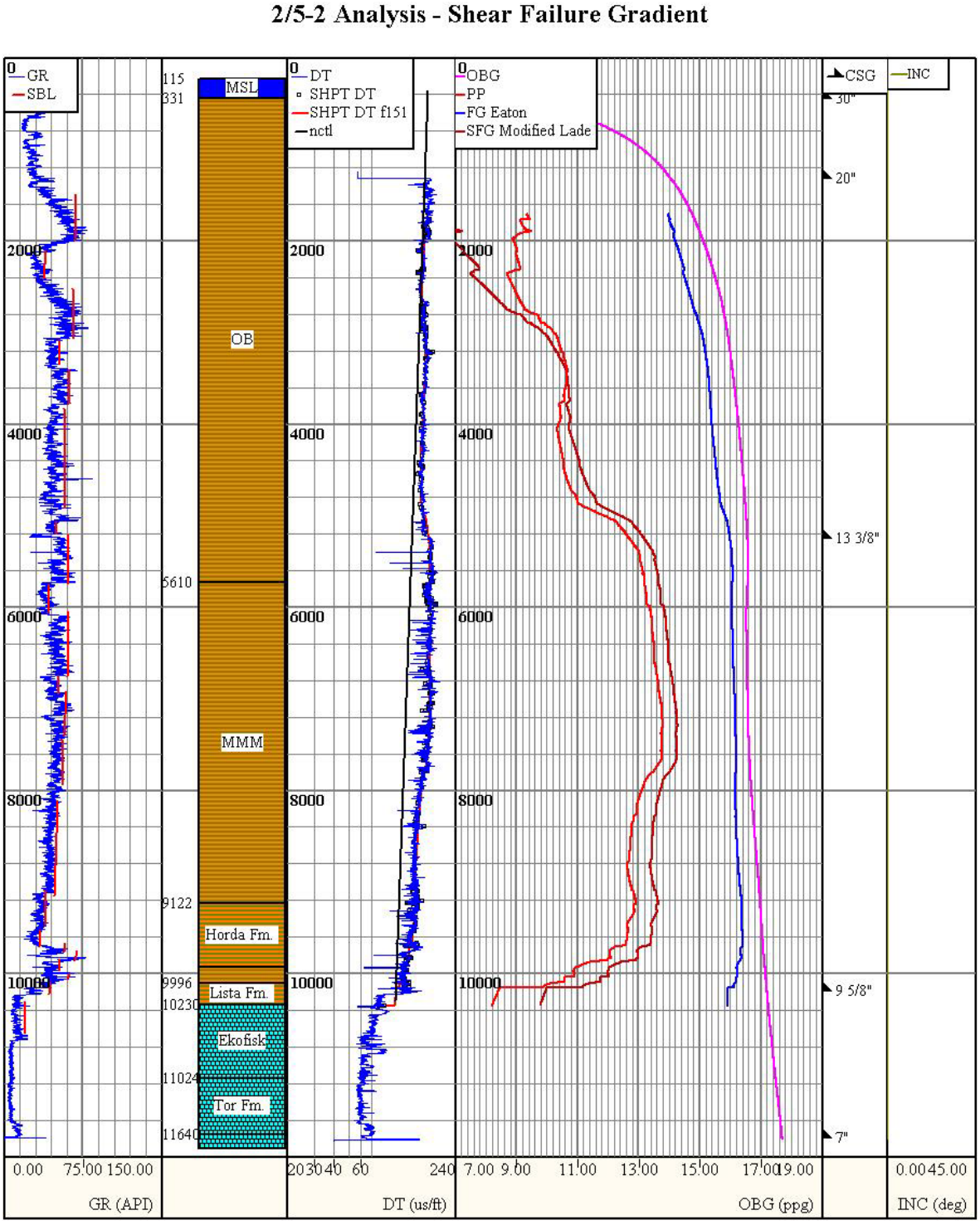

Figure 6.9. Shear Failure gradient estimation well 2/5-2. Depth in ft

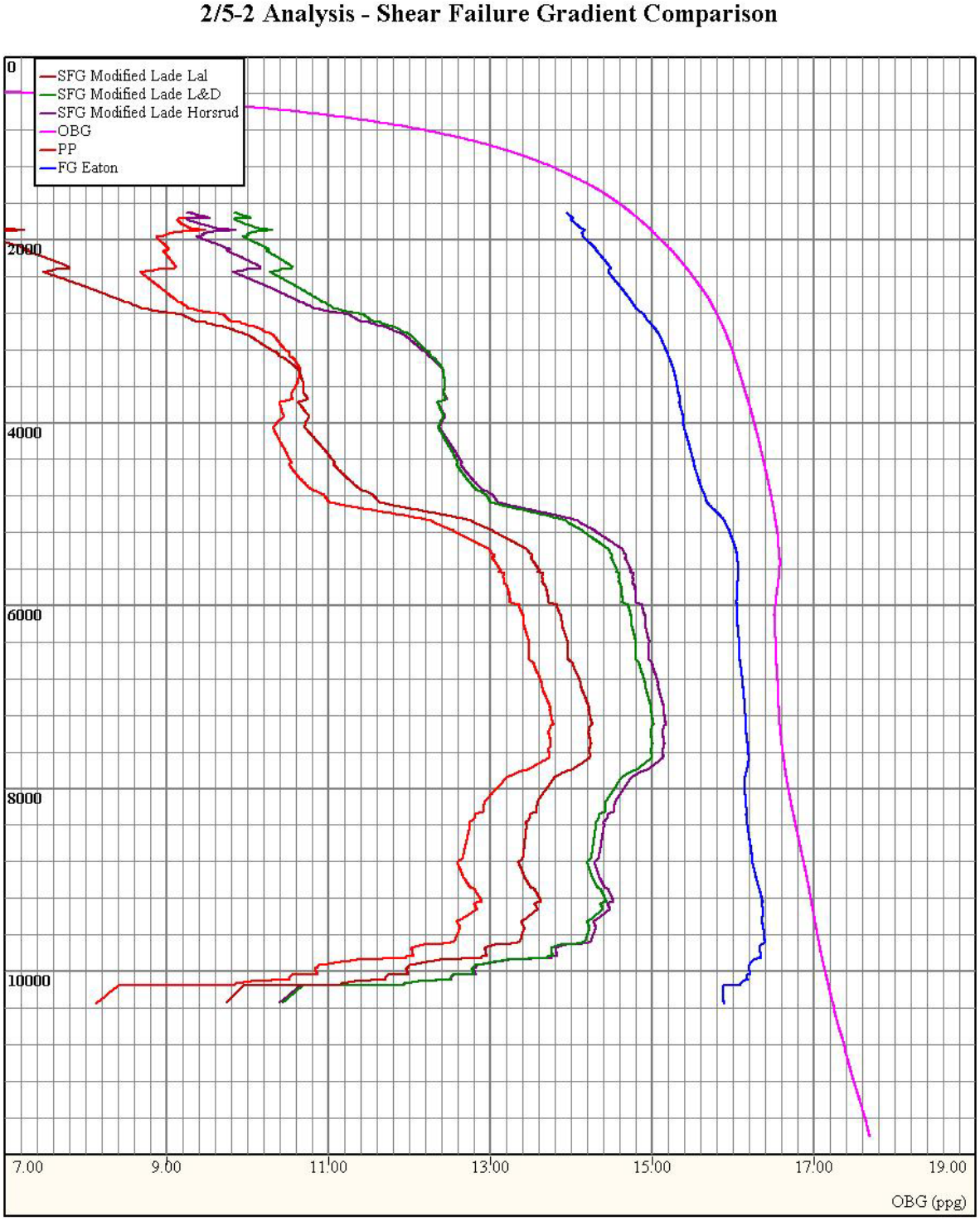

Figure 6.10. Shear Failure gradient comparison well 2/5-2. Depth in ft

6.6. Post Drill Analysis & Calibration

As mentioned in section 6, well planning is not relevant for this work, as the analysis performed is a post-drill analysis, i.e. the well has already been drilled.

One of the most important parts of this work is to calibrate the estimated curves to fit actual observed drilling incidents such as losses, kicks or leak-off test and formation integrity test information. This calibration takes precedence over the models used to estimate the pressure gradients as described in sections 6.2, 6.3, 6.4 and 6.5. With such data, i.e. observations made during the drilling process that may be related to the pressure gradients, it is possible to associate drilling events to pressure gradient values for a specific wellbore to determine whether or not the curve is actually located where one primarily believed it to be. By reviewing the daily drilling reports and several other sources of documentation describing observations made throughout the drilling process, information regarding the previously mentioned incidents was collected and the pore pressure gradients and fracture pressure gradients may be calibrated, i.e. shift the curves to coincide with observed fracture and pore pressures. This calibration is a way of ensuring the geomechanical model built resembles reality as closely as possible.

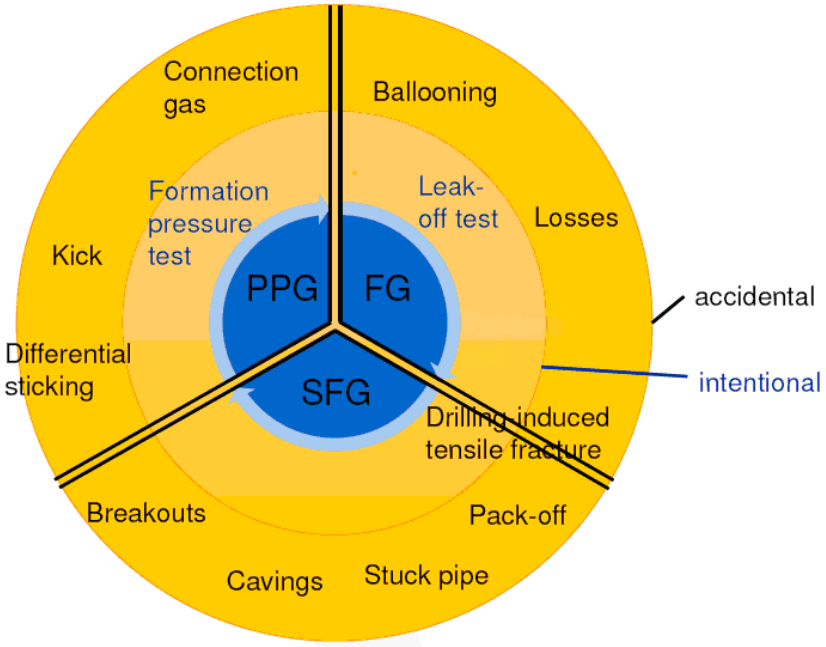

Figure 6.11. Schematic showing various calibration sources. Adapted and slightly modified from Baker Hughes Inc. (2011)

Figure 6.11 shows the different calibration sources that may be used for calibrating the drilling window. These sources can be categorized as either accidental or intentional, i.e. if the pressure indicator was the result of a planned test or if it was an observed, unplanned incident while drilling the well. There are several sources of calibration for each pressure gradient that has been estimated earlier in this thesis, most of the sources shown in Figure 6.11, dependent on their relevance, will be described as well as the importance the respective source has to the calibration.

When performing the calibration, it is important to start calibrating the pore pressure gradient, as both the fracture gradient as well as the shear failure gradient is based on the estimated pore pressure. As Figure 6.11 shows, the Formation Pressure test is the only intentional calibration source for pore pressure gradients. This can be done by running wireline or MWD and gives a direct measurement of the formation pressures in permeable formations, meaning this is not possible in shale. The accidental sources consist of connection gas, which involves a brief influx of gas into the mud when making a connection. This happens because the pumps are stopped to make this connection, leading to a lower bottom hole pressure (Schlumberger, 2012).

Differential sticking typically occurs in sand layers with very high permeability, and because of a high differential pressure between the formation and the wellbore, the drillstring sticks to the borehole wall, leading to an unmovable pipe (Schlumberger, 2012). These two sources do not provide a direct value that the gradients may be calibrated against, both because it is difficult to pinpoint exactly where this problem occurred and what pressure it happened at. Taking a kick is when an influx of formation fluids occurs in the well while drilling, a scenario that may ultimately lead to a blow out. However, for the purpose of calibrating a geomechanical earth model, a kick is the main calibration source as it provides a direct indication to what the pore pressure is. A kick is a strong and exceptionally good indicator, proving that the modeled pressure was underestimated, i.e. too low. Due to political reasons and regulations, it is not possible to intentionally take a kick, as it may develop into an uncontrolled situation (Haavardstein, 2012).

In the case of the fracture pressure, experiencing ballooning or observing losses are two “accidental” pressure indicators. Ballooning involves an initial fluid loss to the formation due to an operation involving considerably high pressures, followed by an increase in mud when the pressure returns to “normal”. The increase in fluid resembles an influx of formation fluids and is often confused to be a kick (SPE, 2011). In the case of fluid losses to the formation, this is an indication that the fracture pressure has been exceeded, and the wellbore is now experiencing a loss of drilling fluid to the formation, something that may lead to a kick due to the reduction in hydrostatic pressure. By performing a leak off test, you may gain information that can be used to calibrate the fracture gradients. The results from a leak off test are shown in Figure 3.6, where the leak off pressure is the value that should be used to calibrate the fracture gradient. Obtaining accurate and representative fracture pressure values by performing a leak off test is dependent on the test being done correctly. In some cases, the fracture pressure is read as the breakdown pressure instead of the leak off pressure, leading to an assumed value of the fracture gradient that is too high.

Drilling induced tensile fractures, found by examining borehole image logs, can be used as a pressure indicator for both the shear failure gradient and the fracture

pressure. It does not provide an exact pressure which causes the fractures, but may be used as an indicator to see whether you are over or under the fracture gradient or shear failure gradient, based on the fracture characteristics.

There are currently no intentionally obtained sources for calibrating the shear failure gradient, however there are several accidental sources. Breakouts, cavings, stuck pipe and pack-offs are all indicators that the shear failure gradient has been underestimated. In order to obtain sufficient information regarding the shear failure, the cavings size and shape must be investigated. However, these events are merely indications as to "which side of the shear failure gradient you are", and do not provide us with enough information about the current drilling situation to calibrate the shear failure gradient to a specific pressure value.
Collecting data to perform a calibration of the six wells under investigation proved to be a very challenging task as the wells are significantly old of age and documentation regarding drilling events on these wells is therefore scarce or simply non-existent. However, the data regarding the drilling incidents that was found was utilized in the building of the model and will be shortly summarized in the following sub-sections. Because of the interactive feature of Predict, once the data has been collected, the calibration of the pressure curves is straight forward, any change to the shale base line or normal compaction trend line will reflect on the modeled pressure gradients. Thus, the calibration is performed by shifting these line segments.

6.6.1. Well 2/4-7

The documentation regarding well 2/4-7 was not very descriptive, lacking leak-off test data and describing one stuck pipe incident as the only operational observation that may be used for calibration. However, the stuck pipe incident occurred at a depth deeper than the interval appropriate for the analysis performed in this thesis, meaning it cannot be used for calibration.
The mud weights that were used at different depths are described in the reports, and these may therefore be used to validate that the model predicts safe drilling with the mud weights that were chosen.

6.6.2. Well 2/4-10

Regarding well 2/4-10, the situation is fairly similar. As for well 2/4-7 only a few incidents were recorded, implying scarce information for this well to be calibrated against. The mud weights that were used are recorded, and these may be used to validate the gradients.

6.6.3. Well 2/4-17

Well 2/4-17 is the well with most data available for use when calibrating. The well was primarily drilled to almost 7000 ft using a much lower mud weight than the model predicts possible. In addition to this, several incidents of loss of returns were observed and the leak-off test data is documented. The observed loss of returns occurred at a depth than is not possible to calibrate against. This well seems to be the well that will best calibrate the model, thus validating or invalidating our predictions. Similarly to the two previously described wells, the used mud weights are documented and may also be used for calibration.

6.6.4. Well 2/5-1

The daily drilling reports obtained for well 2/5-1 contain very little detail, providing merely a one sentence summary of the daily drilling status. For this well, the main calibration source will be the used mud weights.

6.6.5. Well 2/5-2

Some loss of returns were observed when drilling well 2/5-2, allowing us to use this data to calibrate the modeled gradients accordingly. However, similar to well 2/4-7 these incidents occurred too deep to be included in the calibration. In addition to this, the mud weight program is tabulated and may also be used in the calibration.

6.6.6. Well 2/5-3

Well 2/5-3 is the well with the least information. No valuable information was obtained by investigating the daily drilling reports, and the Norwegian Petroleum Directorates fact pages also contained very little to no information that can be used.

7. Results of Post Drill Analysis

In the previous section the method by which the model was built was described, providing an understanding of the process of building a geomechanical model. The following section will provide an overview of the results obtained throughout the modeling and observations made from these results. The resulting track views after calibration showing the models that have been built are displayed and described.

7.1. Well 2/4-7

The modeled pressure gradients prior to calibration are shown in Figure 7.1. As mentioned in section 6.6.1, the data available for calibration is not very extensive, and provides the mud weight design that was actually used to drill the well as the main calibration source. After performing the calibration by shifting the normal compaction trend line, all the pressure gradients are shifted to the left, i.e. towards the lower mud weights. This was done in order to achieve a situation where the given mud weights are of a higher value than the estimated shear failure gradient, thus avoiding shear failure. The same is done for all the wells throughout section 7. An increase in the margin between the shear failure pressure gradient and the pore pressure gradient is also observed. To obtain the correct gradients, the normal compaction trend line was shifted from 100μs/ft to approximately 125μs/ft. The resulting pore pressure gradient, fracture pressure gradient and shear failure gradient are shown in Figure 7.2.

In addition to this, the resulting rock mechanical properties obtained by using Lal's correlations are shown in Figure 7.3. From this overview it is clear that the friction angle, FA, cohesive strength, CS, and unconfined compressive strength, UCS, increase with depth, especially close to the wells total depth (TD).

For wellbore stability issues regarding the wellbore trajectory, a hemisphere plot showing variations in mud weight due to wellbore trajectory position relative to minimum and maximum horizontal stress is shown in Figure 7.4. The parameters used in the analysis are presented in Table 7.1. The plot is displayed for a depth of 5000ft, however this depth is arbitrary as the same plot can be produced for all depths of the well.

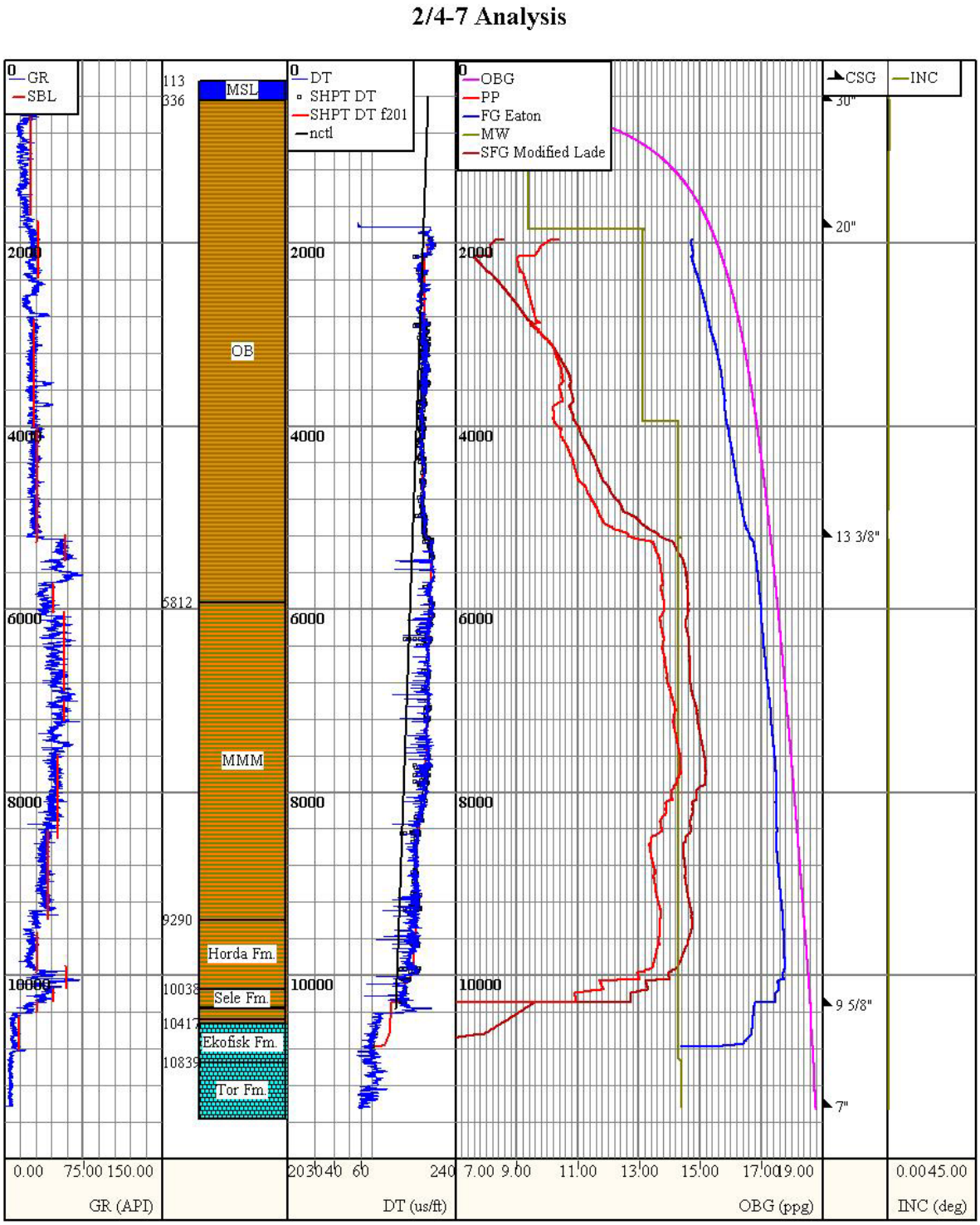

Figure 7.1. Modeled pressure gradients for well 2/4-7 prior to calibration. Depth in ft

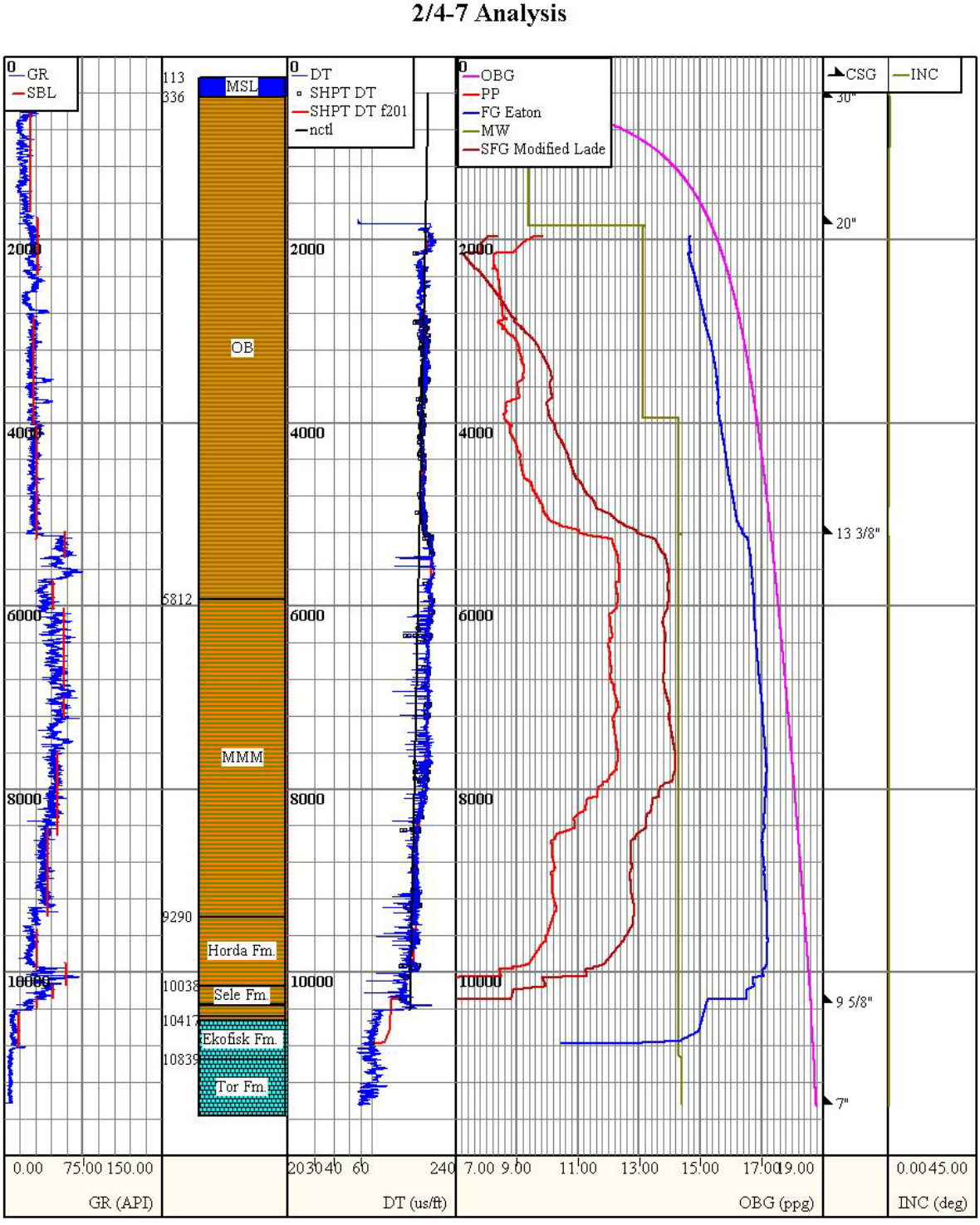

Figure 7.2. Modeled pressure gradients for well 2/4-7 post calibration. Depth in ft

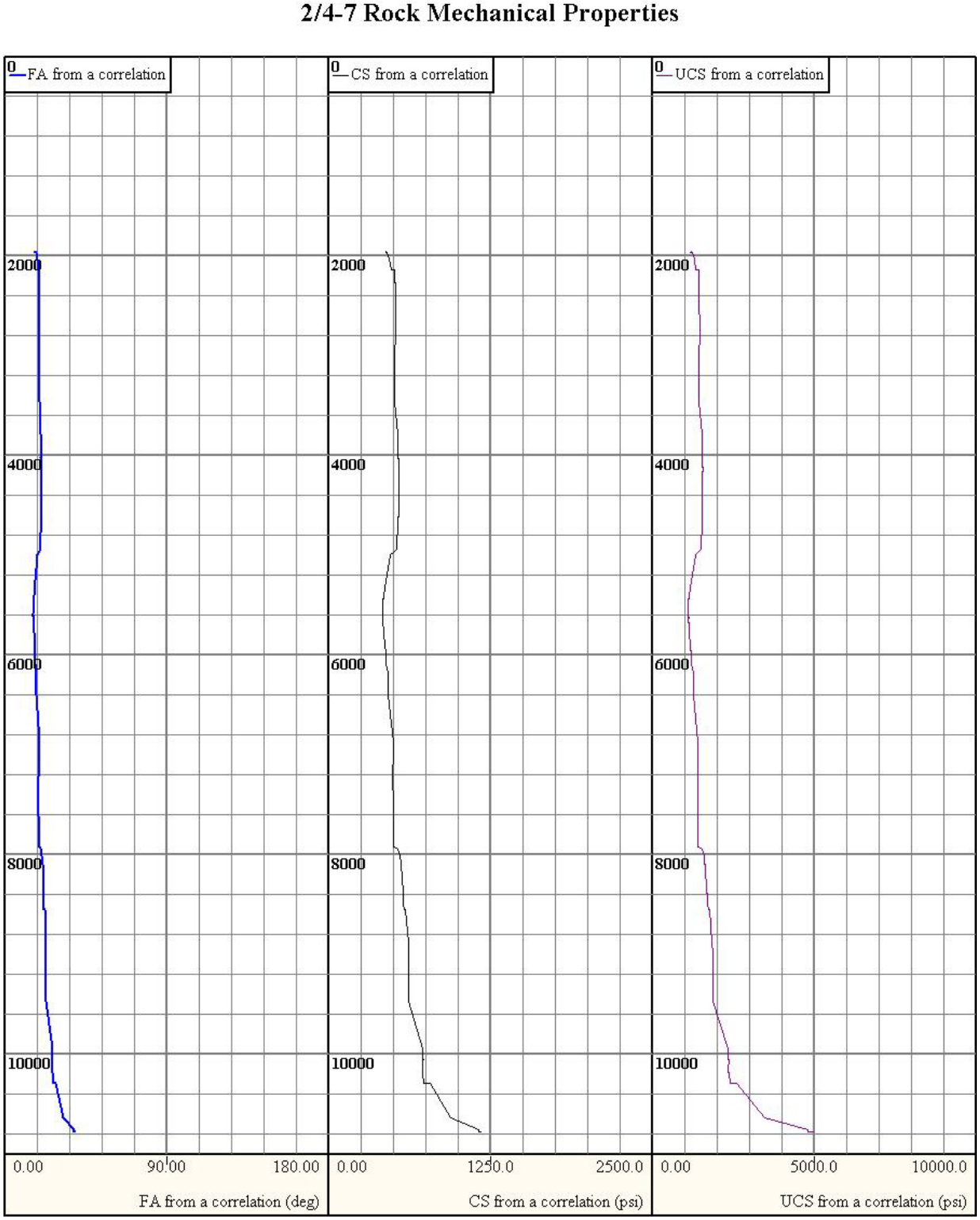

Figure 7.3. Rock mechanical properties for well 2/4-7. Depth in ft

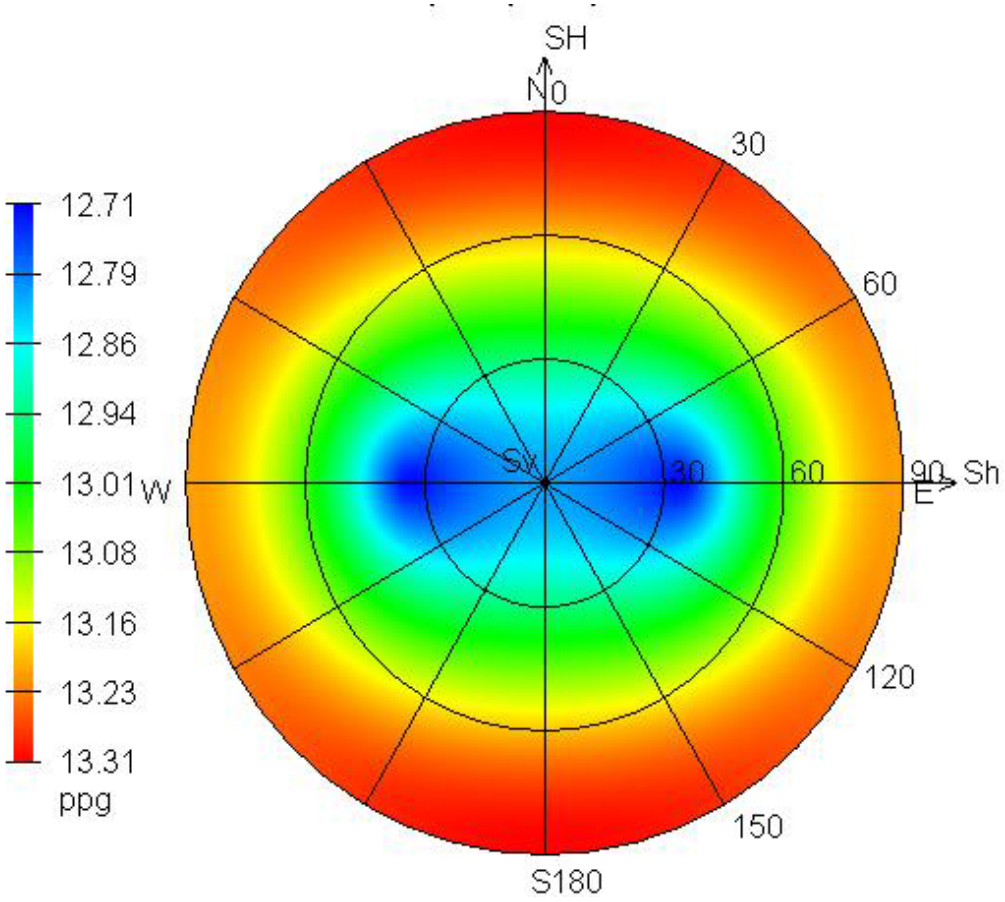

Figure 7.4. Hemisphere plot for well 2/4-7 at 5000ft

Table 7.1 Parameters used for safe wellbore trajectory analysis of well 2/4-7

Depth (ft)	5000
Failure criterion	Modified Lade
Overburden Gradient (ppg)	17.28
Pore Pressure Gradient (ppg)	11.52
Minimum Horizontal Stress Gradient (ppg)	16.40
Maximum Horizontal Stress Gradient (ppg)	16.73
Maximum Horizontal Stress Azimuth (ppg)	0.00
Poisson's ratio	0.46
Friction Angle (deg)	18.42
Cohesive Strength (psi)	482.81

7.2. Well 2/4-10

The pressure gradient curves without calibration are shown in Figure 7.5, Similar to well 2/4-7, there were very few sources to base the calibration on. As may be seen from Figure 7.5, the curves need to be shifted to the left towards the lower mud weights, thus the normal compaction trend line needs to be shifted towards higher values. Figure 7.6 shows the pressure gradients post calibration. The normal compaction trend line end point has been shifted from 100μs/ft to 125μs/ft, leading to the mud weight design and pressure curves to predict wellbore stability.

The estimated rock mechanical properties for this well are presented graphically for the whole depth of the well in Figure 7.7. Similar to well 2/4-7, the friction angle, cohesive strength and the unconfined compressive strength show a stable trend, i.e. show approximately the same values until close to the wells TD, where the values show an increase.

The hemisphere plot, shown in Figure 7.8, is also similar to that of well 2/4-7. However, close to the bulls' eye for well 2/4-10 the hemisphere plot shows more variation in the mud weight in the minimum horizontal stress direction than for well 2/4-7.

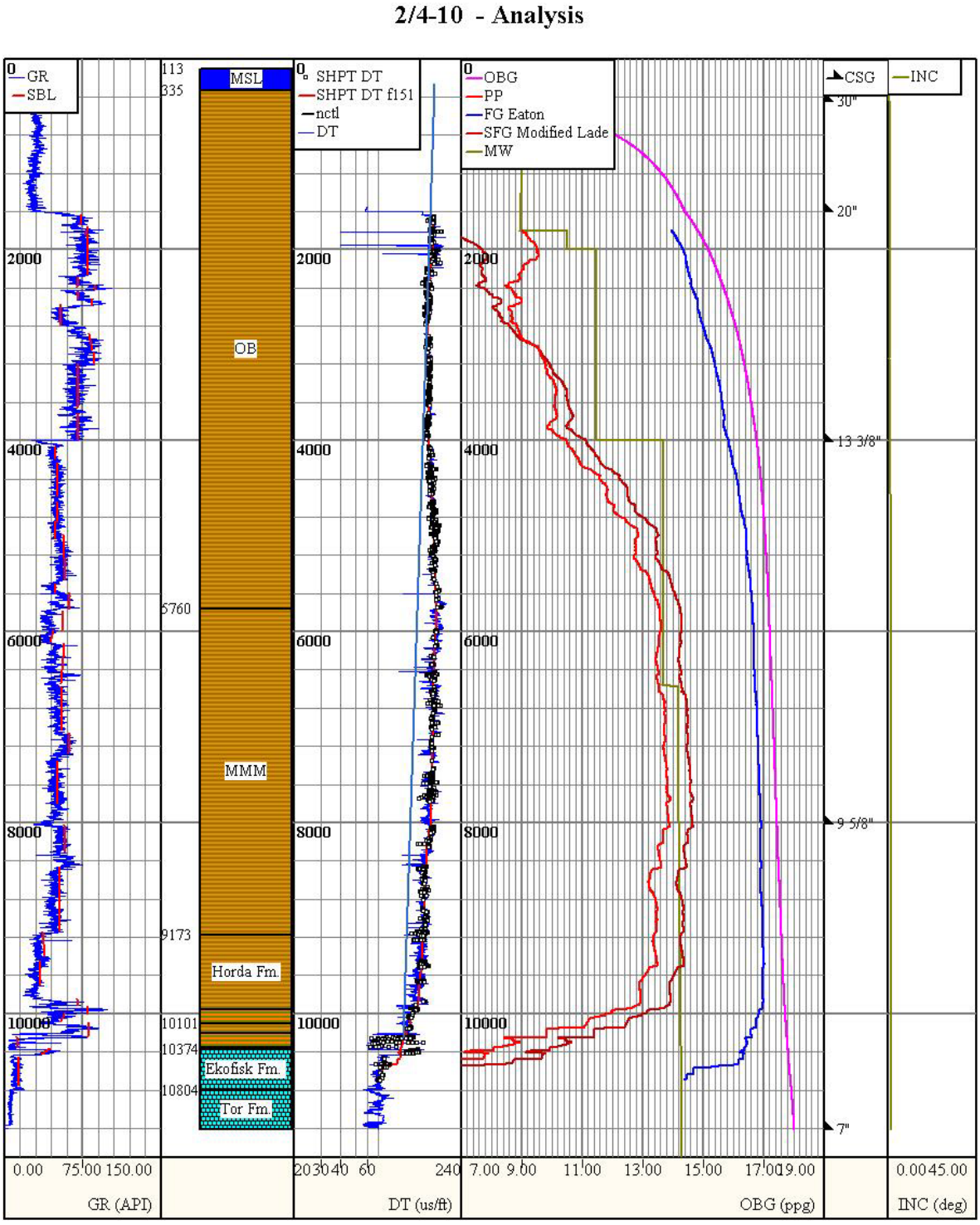

Figure 7.5. Modeled pressure gradients for well 2/4-10 prior to calibration. Depth in ft

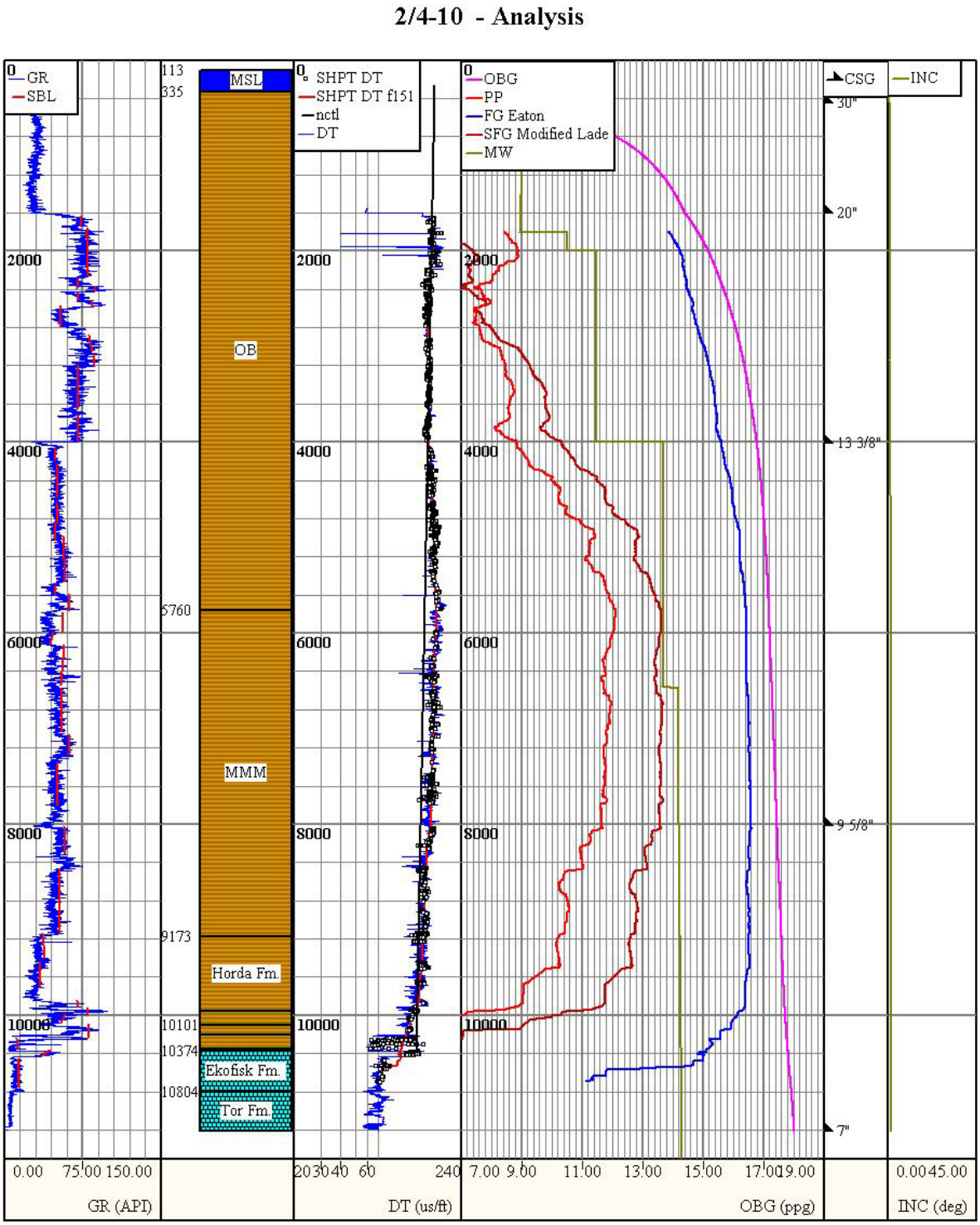

Figure 7.6. Modeled pressure gradients for well 2/4-10 post calibration. Depth in ft

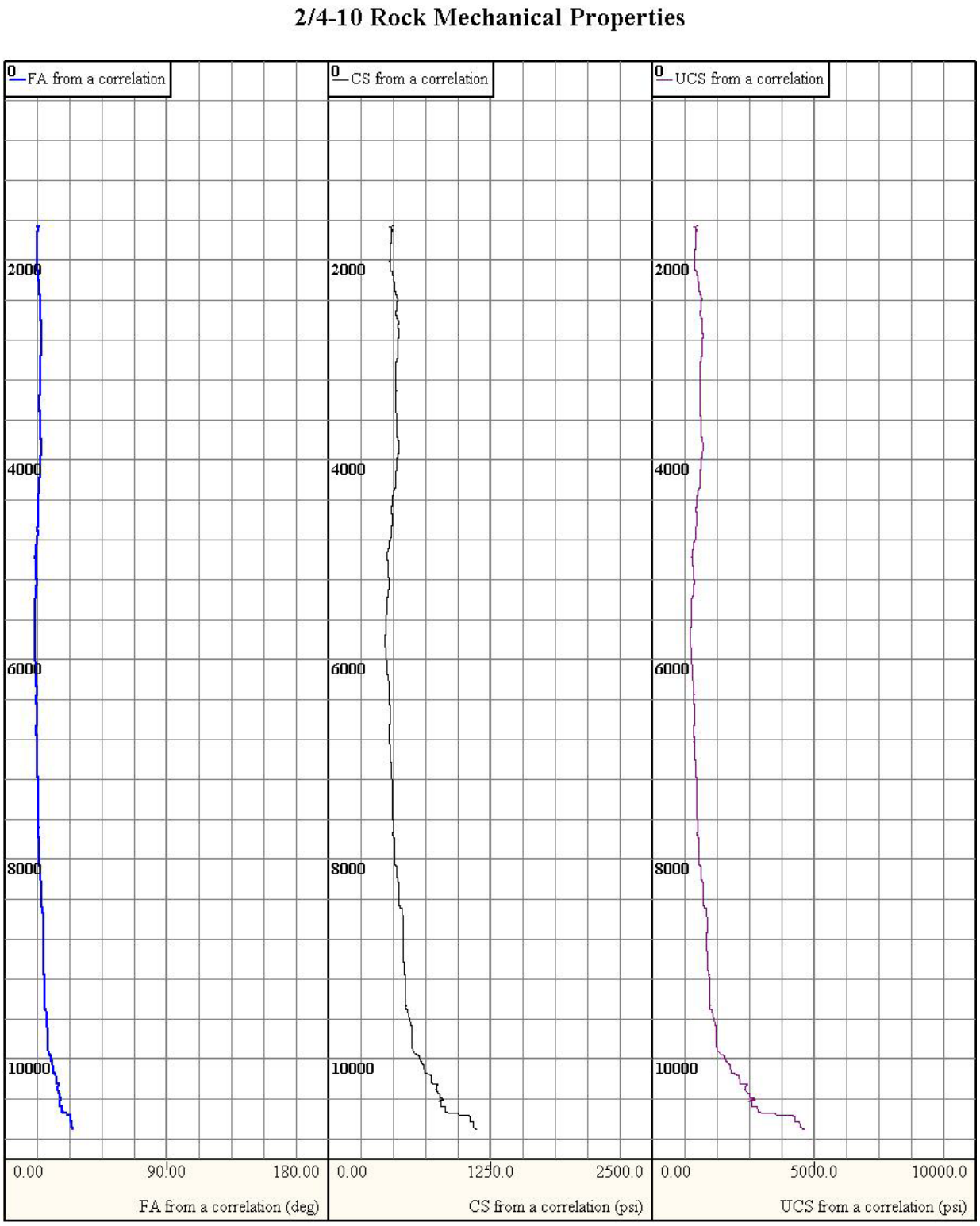

Figure 7.7. Rock mechanical properties for well 2/4-10. Depth in ft

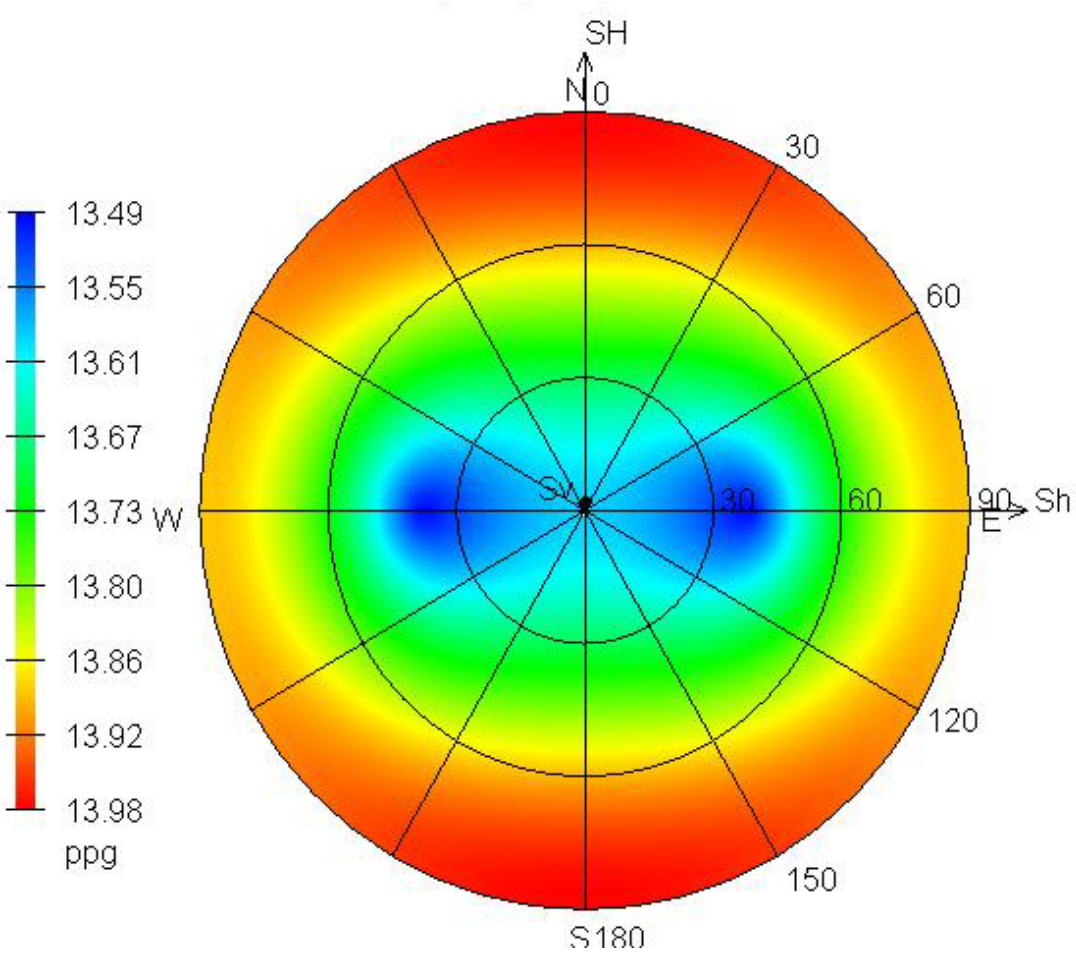

Figure 7.8. Hemisphere plot for well 2/4-10 at 6000ft

Table 7.2. Parameters used for safe wellbore trajectory analysis of well 2/4-10

Depth (ft)	6000
Failure criterion	Modified Lade
Overburden Gradient (ppg)	17.19
Pore Pressure Gradient (ppg)	12.00
Minimum Horizontal Stress Gradient (ppg)	16.45
Maximum Horizontal Stress Gradient (ppg)	16.78
Maximum Horizontal Stress Azimuth (ppg)	0.00
Poisson's ratio	0.46
Friction Angle (deg)	17.24
Cohesive Strength (psi)	450.05

7.3. Well 2/4-17

Well 2/4-17 was the well with most available calibration sources. This well was also drilled to a substantial depth using a mud weight of 12.6ppg before needing to drill a sidetrack in order to reach TD. Also, there was available leak off test data for this well, leading to a possible calibration of the fracture gradient. As for the previous wells, the pore pressure and shear failure gradient exceed the mud weight that was used. These initial gradients are displayed in Figure 7.9. As may be seen in Figure 7.10, by shifting the normal compaction trend line from 100µs/ft to 135µs/ft, the pore pressure gradient and the shear failure gradient fall below the mud weight, and the fracture gradient coincides with the leak off test data. As mentioned previously, a pack off is merely an indication as to whether the pressure in the well was lower or higher than the shear failure pressure gradient, it does not provide a specific pressure value to use in order to calibrate the gradients.. For well 2/4-17 the main calibration source is the leak off tests, and the pressure data for the hole pack off is used to verify that the estimated gradients are correct. After the calibration, it may be observed that the margin between the shear failure gradient and the pore pressure gradient increases substantially. In difference from the previous wells, a considerable decrease in the pore pressure is observed, at around 6500ft the pore pressure has been reduced from 13ppg to 9ppg.

As for the rock mechanical properties that are shown in Figure 7.11, they show an approximately constant value until approaching the wells TD, where they show an increase starting at around 9600ft.

As shown in Figure 7.12, the hemisphere plot shows the same trend as the previous wells. For well 2/4-17 the hemisphere plot shows a close to concentric trend, i.e. a similar mud weight variation in the minimum and maximum horizontal stress direction as the radial distance from the bulls' eye increases.

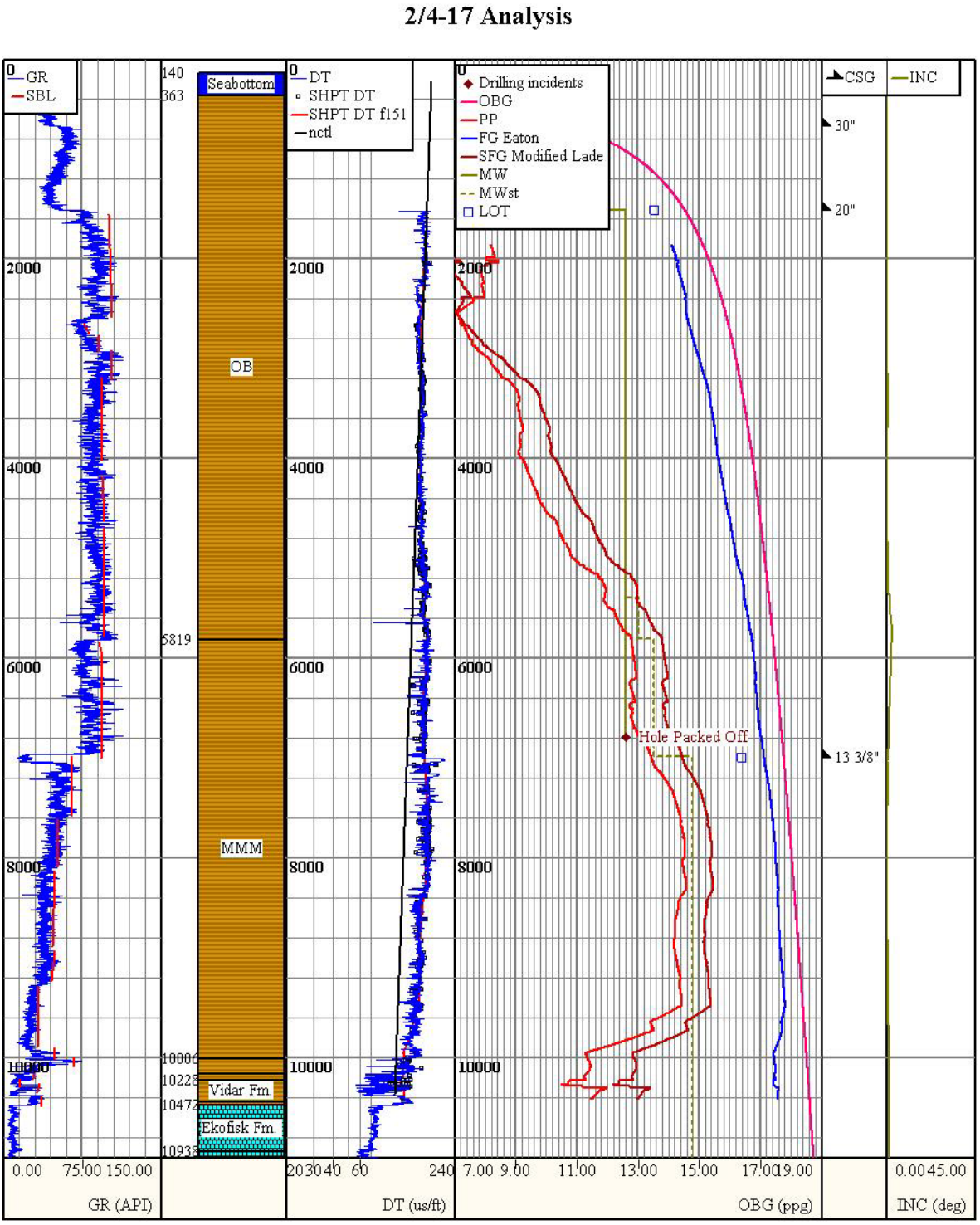

Figure 7.9. Modeled pressure gradients for well 2/4-17 prior to calibration. Depth in ft

2/4-17 Analysis

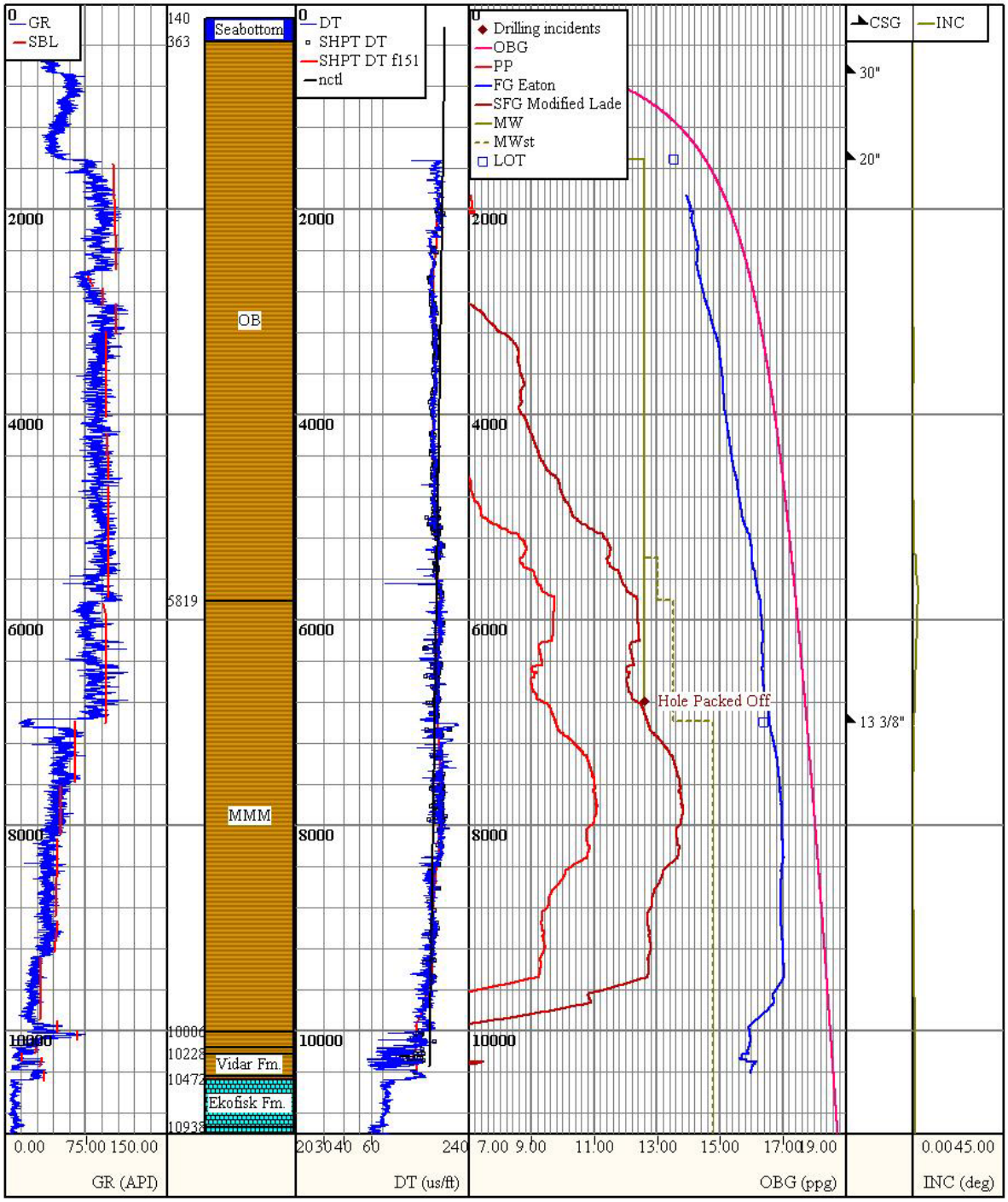

Figure 7.10. Modeled pressure gradients for well 2/4-17 post calibration. Depth in ft

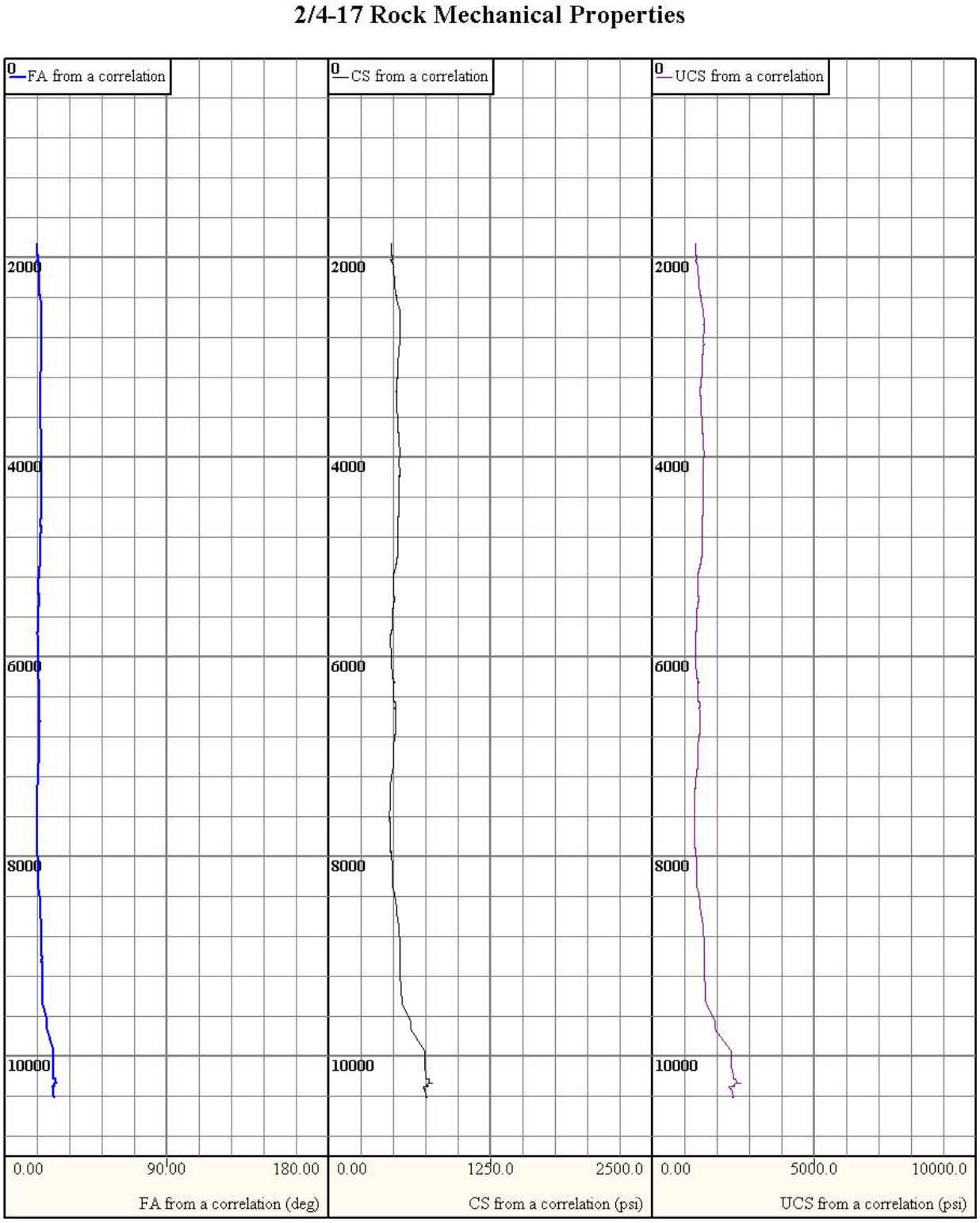

Figure 7.11. Rock mechanical properties for well 2/4-17. Depth in ft

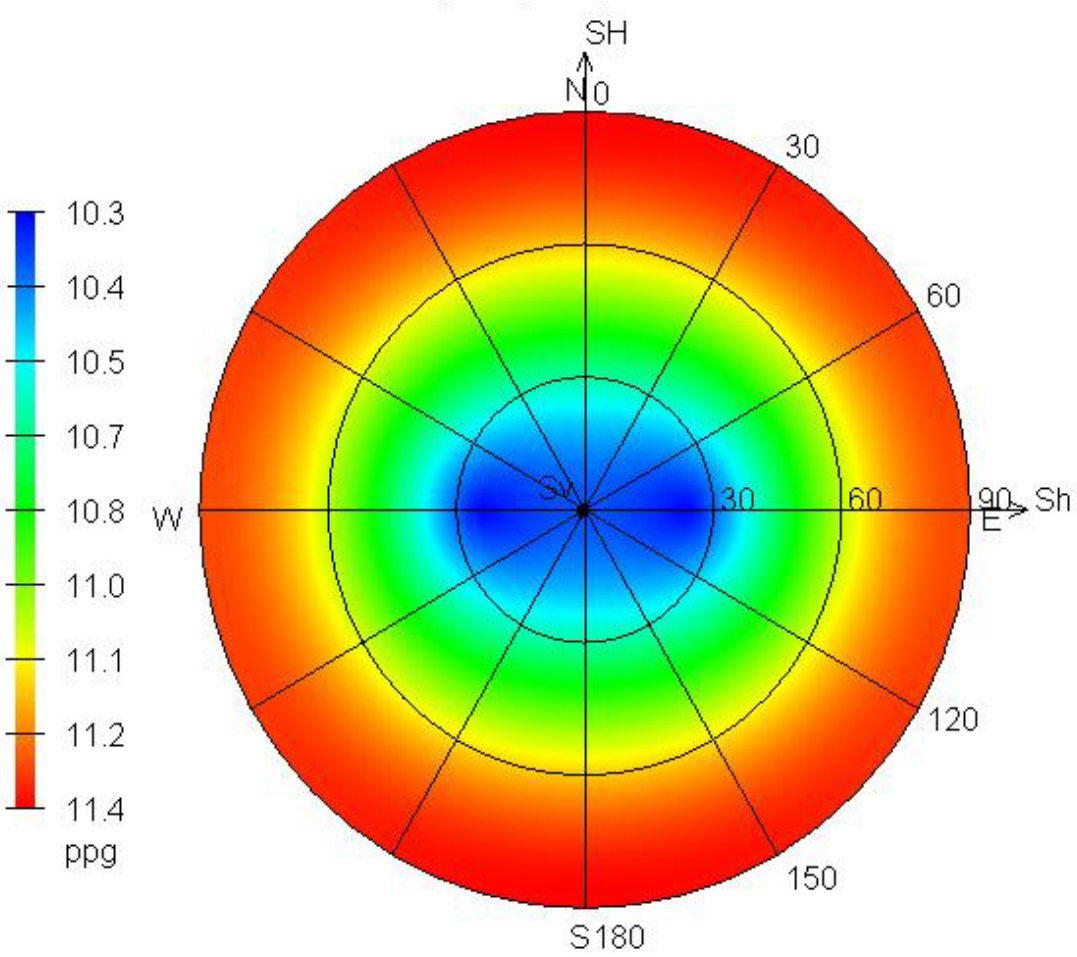

Figure 7.12. Hemisphere plot for well 2/4-17 at 5000ft

Table 7.3. Parameters used for safe wellbore trajectory analysis of well 2/4-17

Depth (ft)	5000
Failure criterion	Modified Lade
Overburden Gradient (ppg)	17.19
Pore Pressure Gradient (ppg)	7.49
Minimum Horizontal Stress Gradient (ppg)	15.72
Maximum Horizontal Stress Gradient (ppg)	16.03
Maximum Horizontal Stress Azimuth (ppg)	0.00
Poisson's ratio	0.46
Friction Angle (deg)	19.80
Cohesive Strength (psi)	522.05

7.4. Well 2/5-1

As described in section 6.6.4, the main source for calibrating the pressure gradients for well 2/5-1 is the mud weight design that was used to drill the well. Prior to performing the calibration, the curves are already quite close to the mud weights, the pore pressure lying under the mud weight and the shear failure gradient just exceeding the mud weight at a few depths, this is shown in Figure 7.13. By adjusting the end point of the normal compaction trend line from 100μs/ft to 115μs/ft, the shear failure gradient falls below the mud weight, allowing the mud weight design to lie within the safe drilling window. The calibrated curves are shown in Figure 7.14. Also, as seen for the previous wells, the margin between the shear failure gradient and the pore pressure increases.

The rock mechanical properties, seen in Figure 7.15, behave in a similar way as for the previous wells. For well 2/5-1, the unconfined compressive stress seems to vary more than previously. All three rock mechanic properties show an increase in values close to the wells TD.

For well 2/5-1, the hemisphere plot shown in Figure 7.16 shows a larger variation of mud weight in the maximum horizontal stress direction. The trend in which the mud weight varies is very similar to that of the previous wells.

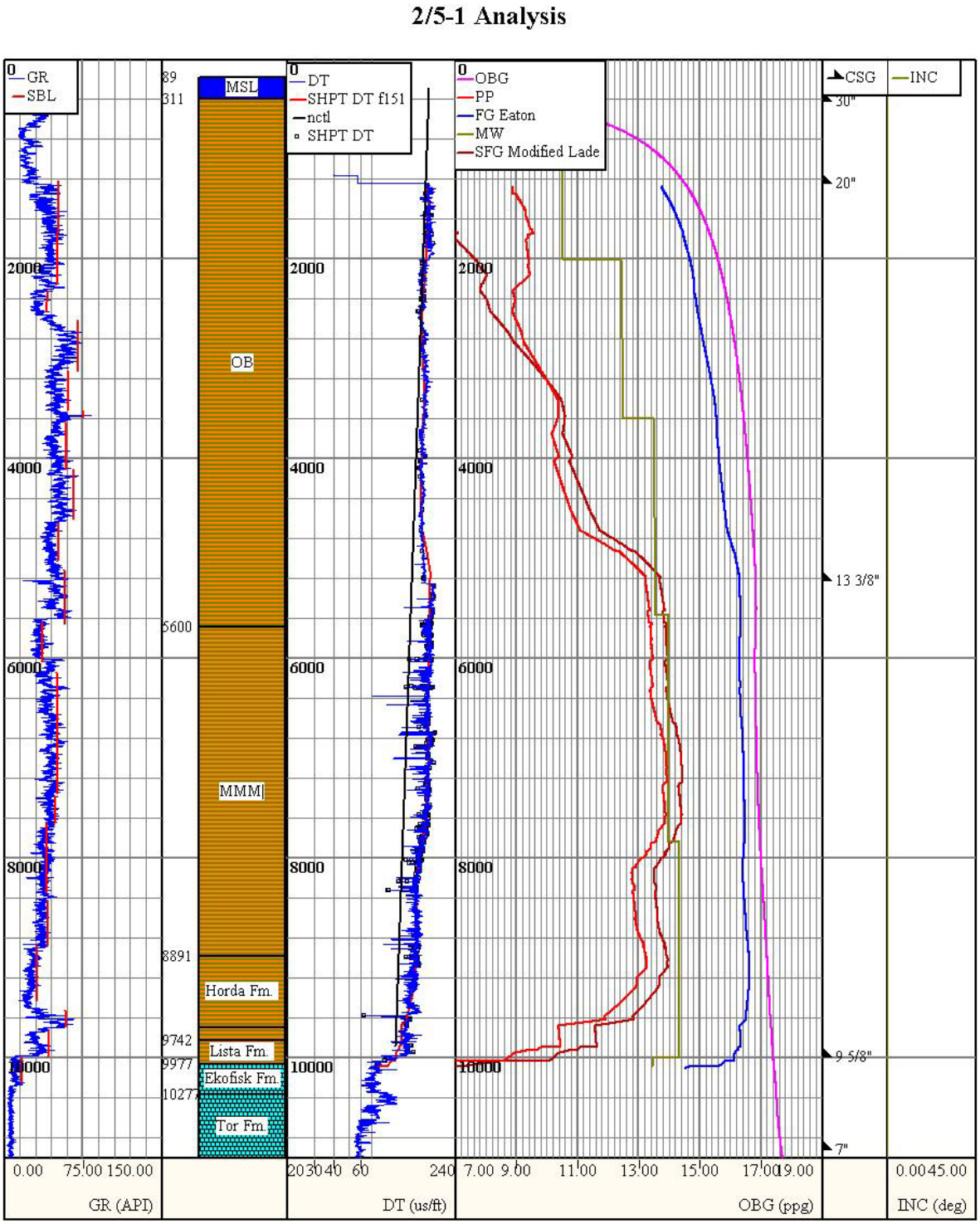

Figure 7.13. Modeled pressure gradients for well 2/5-1 prior to calibration. Depth in ft

2/5-1 Analysis

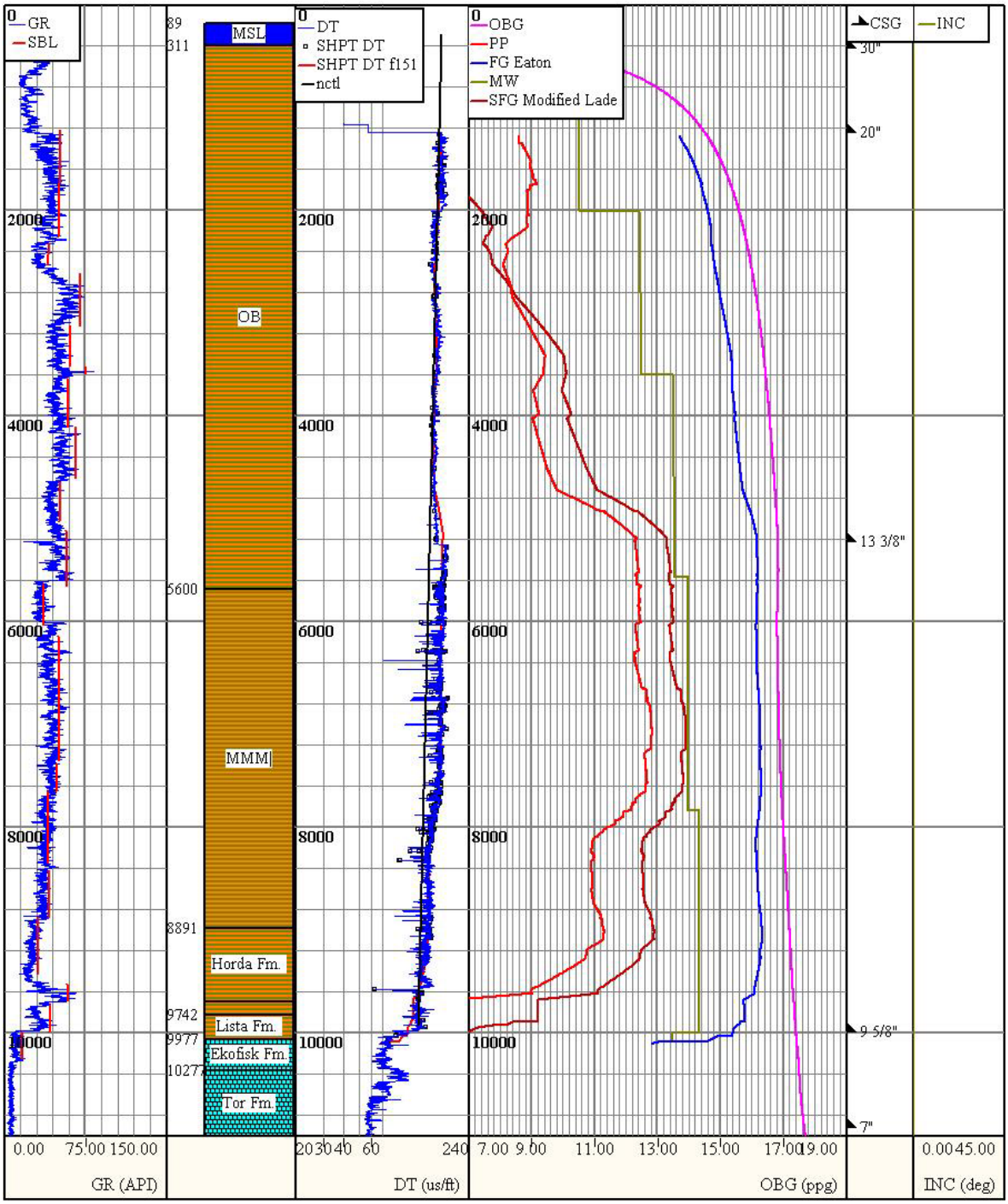

Figure 7.14. Modeled pressure gradients for well 2/5-1 post calibration. Depth in ft

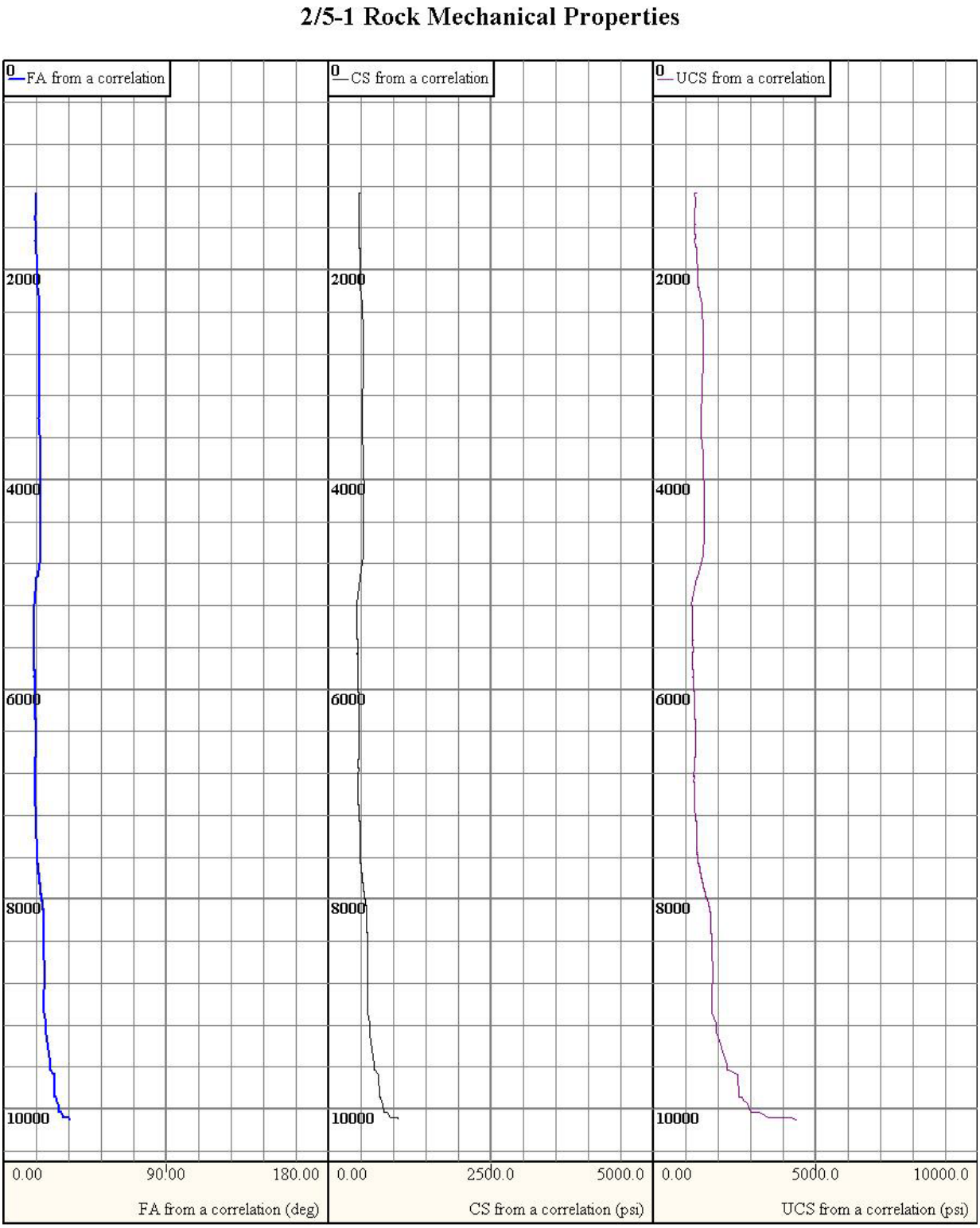

Figure 7.15. Rock mechanical properties for well 2/5-1. Depth in ft

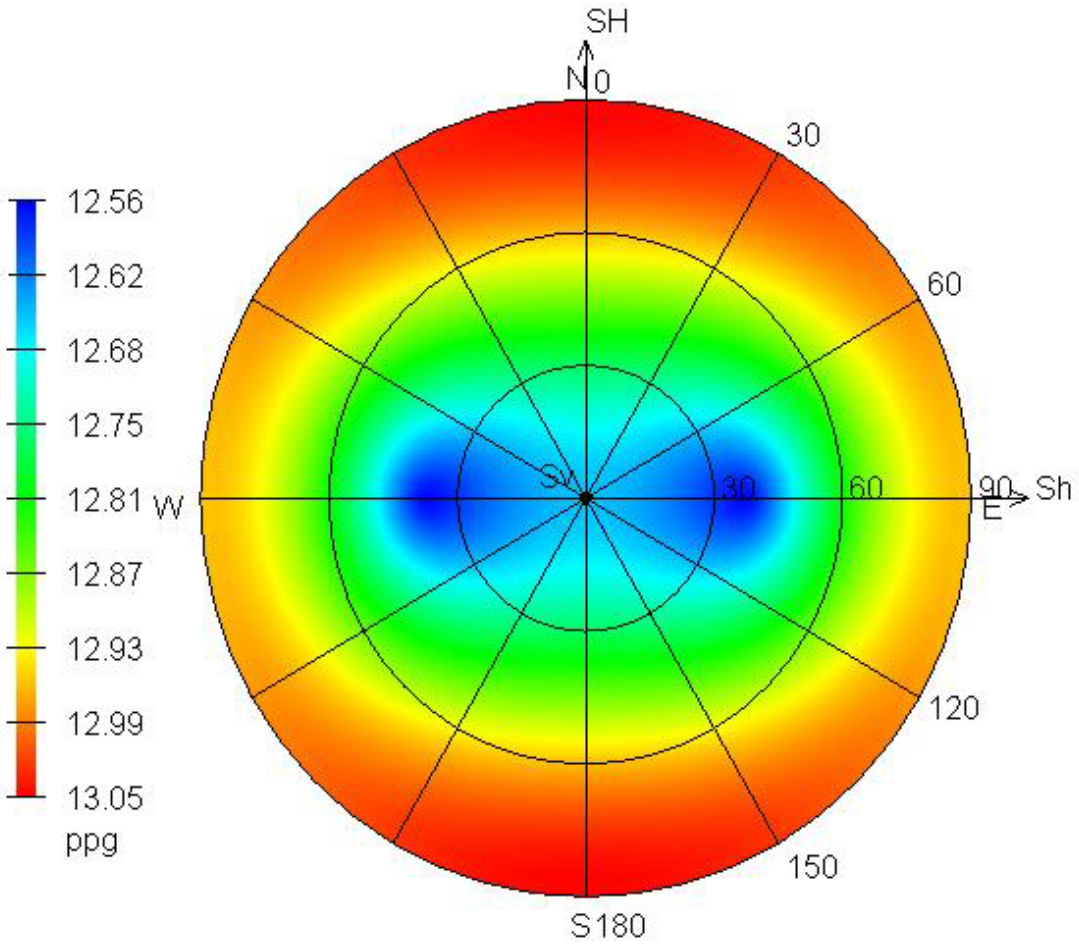

Figure 7.16 Hemisphere plot for well 2/5-1 at 5000ft

Table 7.4. Parameters used for safe wellbore trajectory analysis of well 2/5-1

Depth (ft)	5000
Failure criterion	Modified Lade
Overburden Gradient (ppg)	16.77
Pore Pressure Gradient (ppg)	11.60
Minimum Horizontal Stress Gradient (ppg)	16.03
Maximum Horizontal Stress Gradient (ppg)	16.35
Maximum Horizontal Stress Azimuth (ppg)	0.00
Poisson's ratio	0.46
Friction Angle (deg)	18.59
Cohesive Strength (psi)	487.76

7.5. Well 2/5-2

Figure 7.17 shows the pressure gradients as the log data predicts them to be. As for all the previous wells, except well 2/4-17, the main calibration source for well 2/5-2 is the mud weight design. The gradients prior to calibration are close to the mud weight, needing only a slight shift of the normal compaction trend line end point from 100µs/ft to 125µs/ft the shear failure gradient and the fracture gradient then allow the well to be drilled safely using the documented mud weights. The calibrated gradients are shown in Figure 7.18.

The rock mechanical properties derived from Lal's correlations show similar trends as for the previous wells as seen in Figure 7.19. The friction angle and the cohesive strength show a close to constant value until approximately 9000ft, where the trend deviates and the values increase towards well TD. The unconfined compressive strength is more fluctuating throughout the depth of the well, and also shows an increase in values towards TD.

Figure 7.20 shows the hemisphere plot for well 2/5-2, and similar to well 2/5-1 the plot shows a larger variation in the maximum horizontal stress direction. Also as seen previously, the required mud weight increases the further from the bulls' eye the well is.

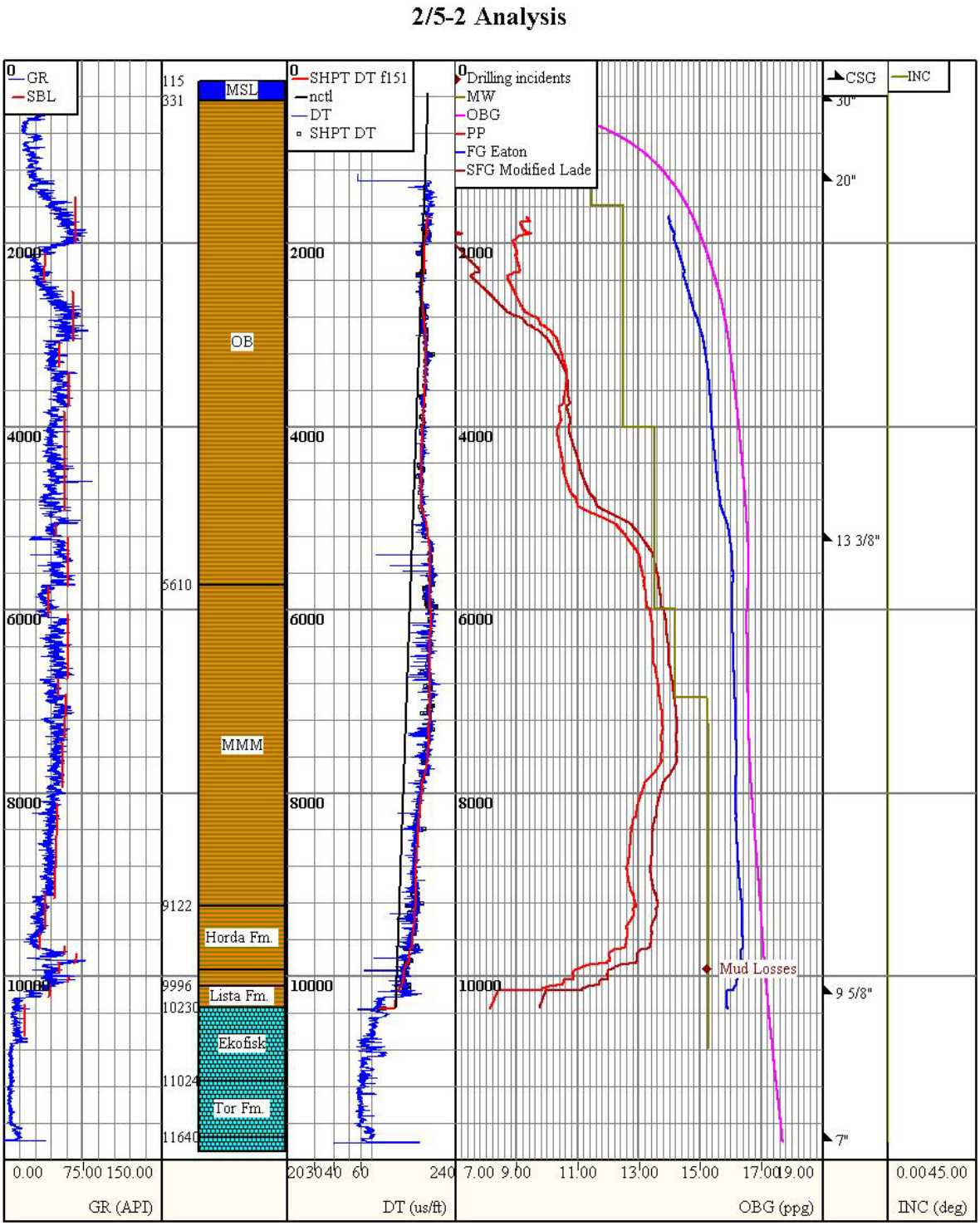

Figure 7.17. Modeled pressure gradients for well 2/5-2 prior to calibration. Depth in ft

2/5-2 Analysis

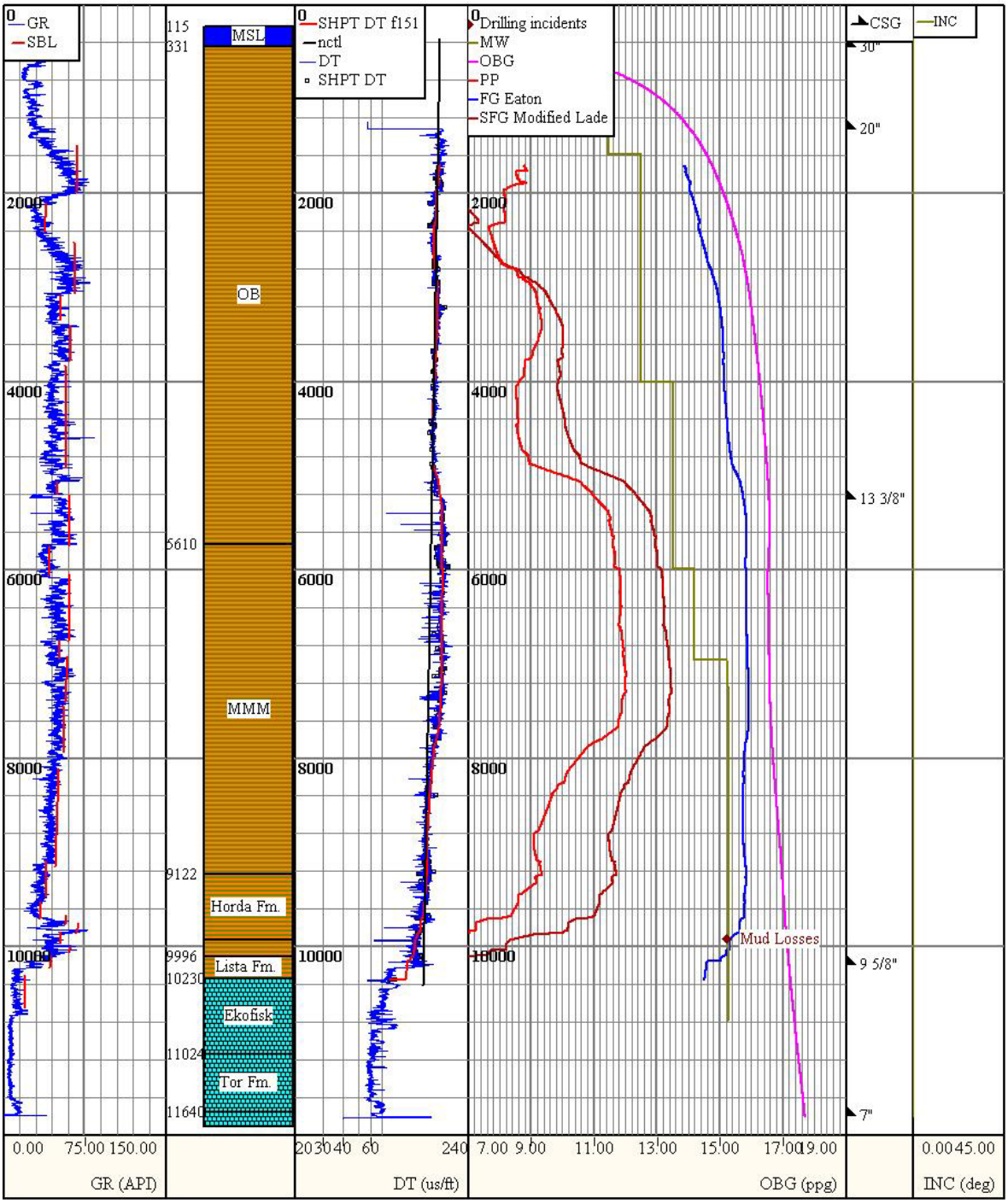

Figure 7.18. Modeled pressure gradients for well 2/5-2 post calibration. Depth in ft

2/5-2 Rock Mechanical Properties

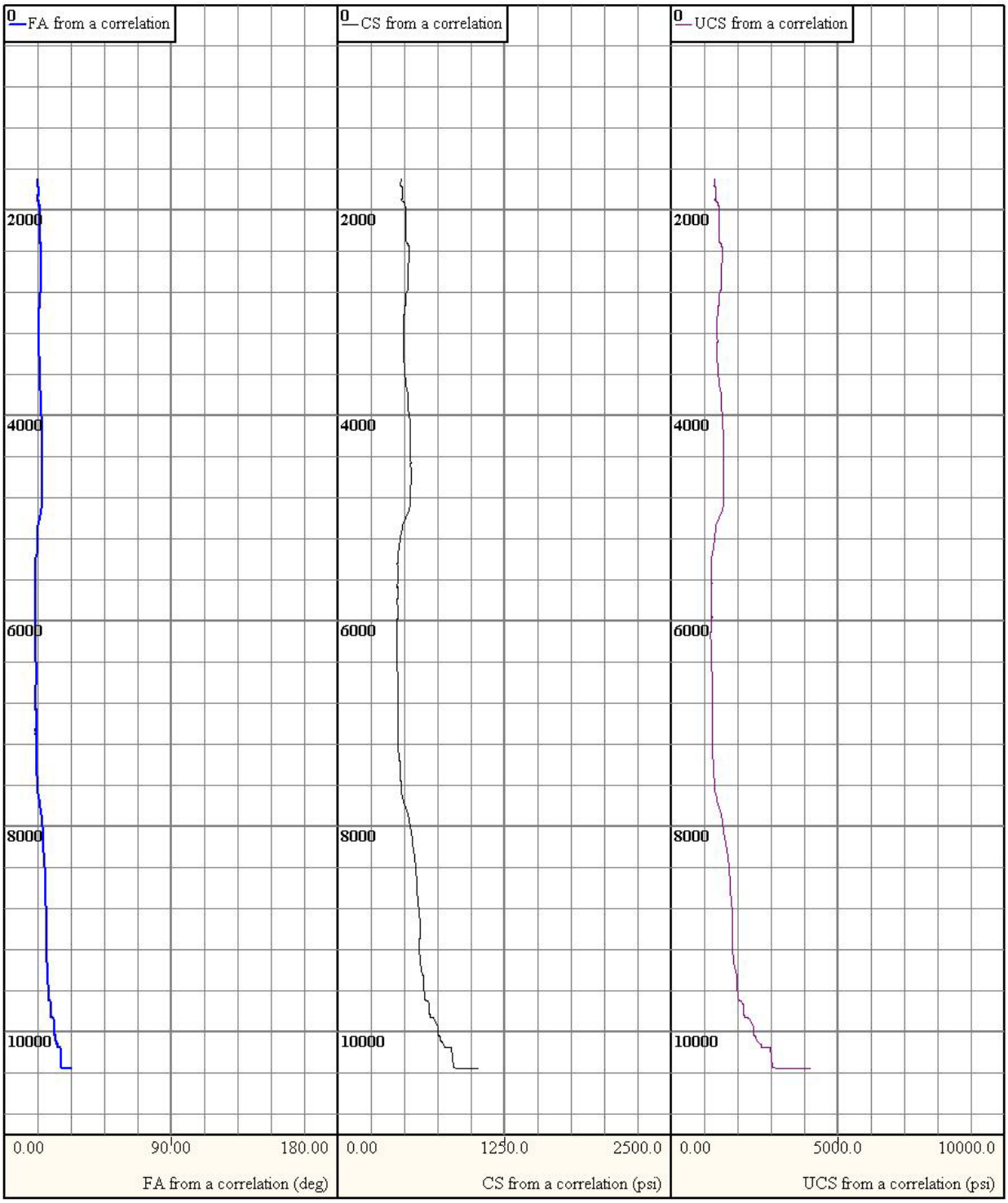

Figure 7.19. Rock mechanical properties for well 2/5-2. Depth in ft

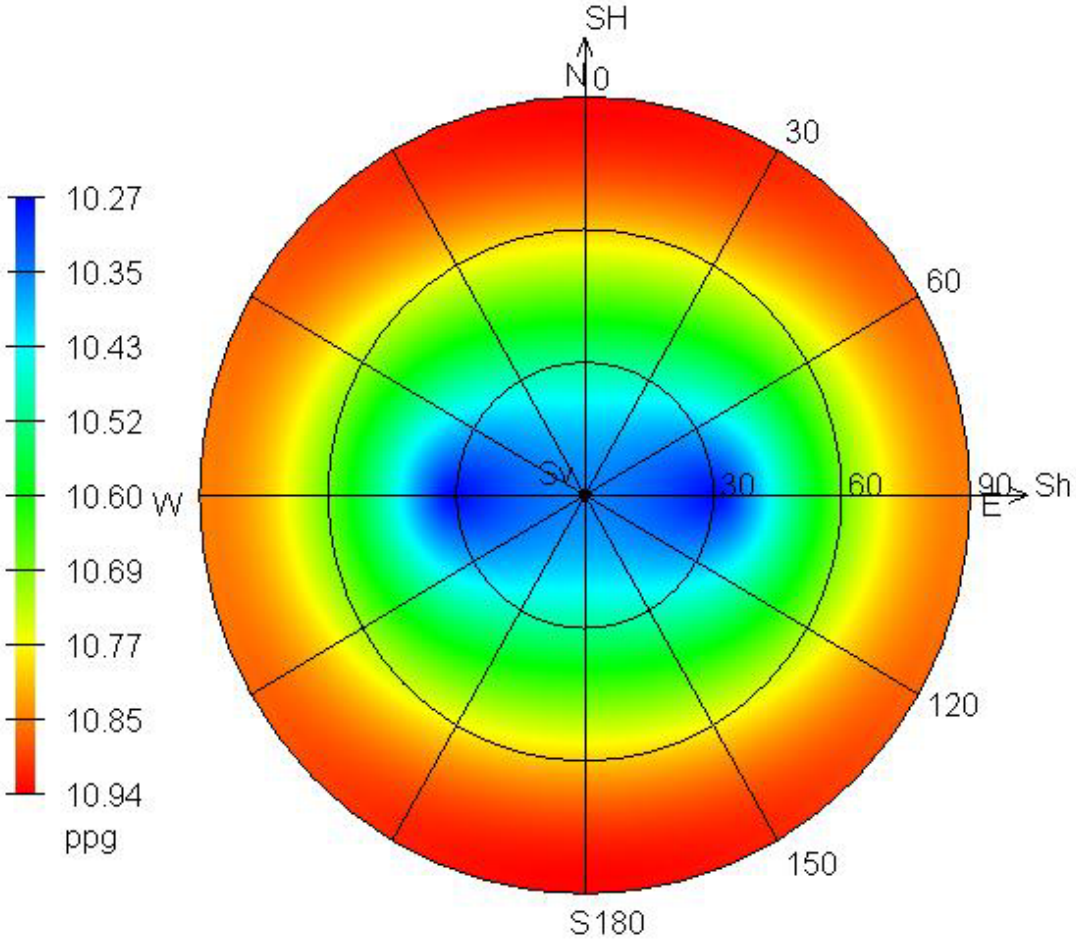

Figure 7.20. Hemisphere plot for well 2/5-2 at 4000ft

Table 7.5. Parameters used for safe wellbore trajectory analysis of well 2/5-2

Depth (ft)	4000
Failure criterion	Modified Lade
Overburden Gradient (ppg)	16.27
Pore Pressure Gradient (ppg)	9.60
Minimum Horizontal Stress Gradient (ppg)	15.28
Maximum Horizontal Stress Gradient (ppg)	15.59
Maximum Horizontal Stress Azimuth (ppg)	0.00
Poisson's ratio	0.46
Friction Angle (deg)	20.33
Cohesive Strength (psi)	537.45

7.6. Well 2/5-3

This is the well with no available calibration sources, as described in section 6.6.6. Thus calibration of the pore pressure gradient, fracture gradient and shear failure gradient was not possible for well 2/5-3. The primary modeled pressure gradients are the pressure gradients that will be used in the model, these are shown in Figure 7.21

In Figure 7.22 the rock mechanical properties for well 2/5-3 show quite little variation with depth, until close to the well TD where the values of the friction angle, cohesive strength and unconfined compressive stress increase.

Similar to the previous wells, well 2/5-3 hemisphere plot shows more variation in the direction of the maximum horizontal stress and an increase in the mud weight as the radial distance from the bulls' eye increases.

2/5-3 Analysis

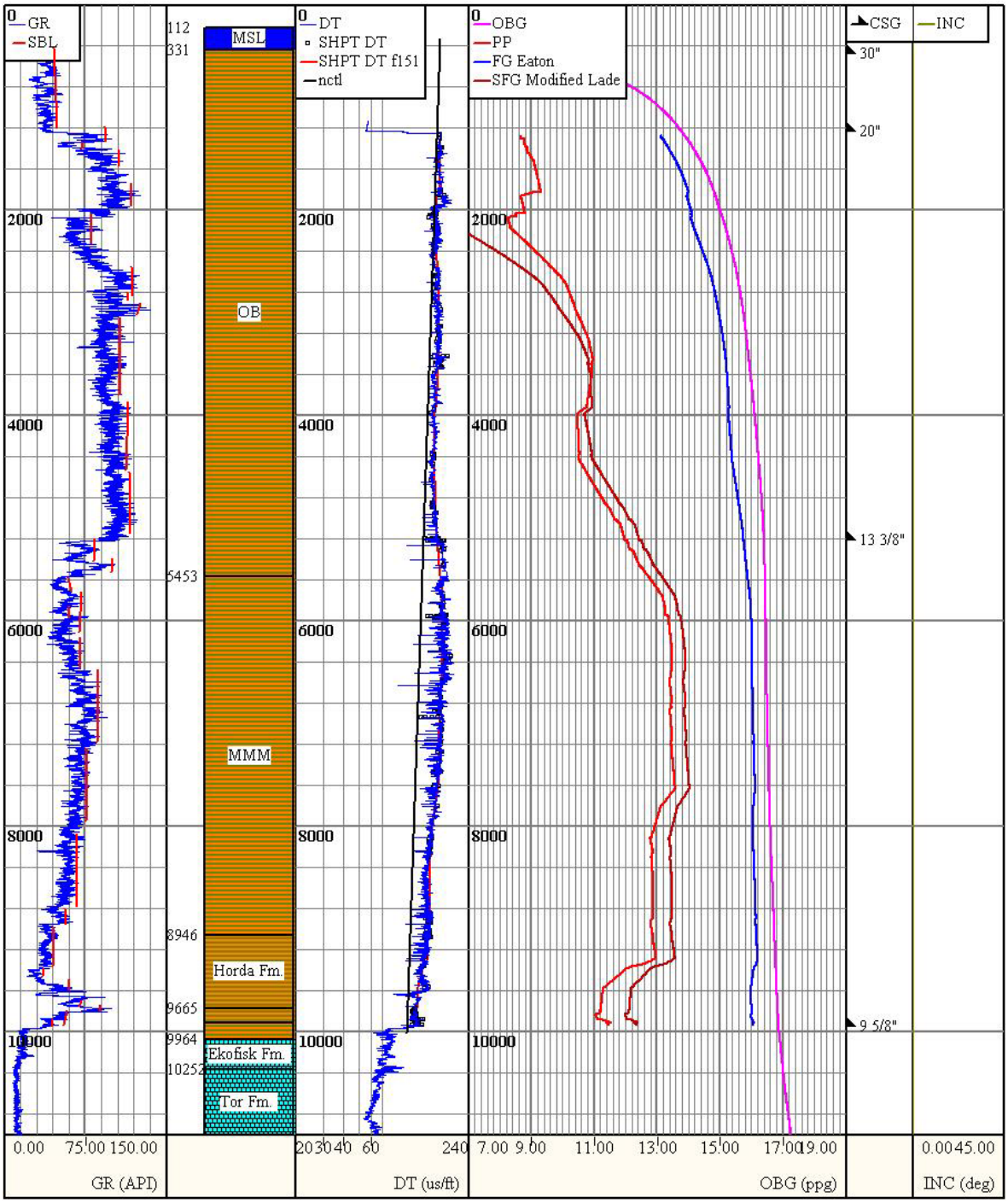

Figure 7.21. Modeled pressure gradients for well 2/5-3. Depth in ft

2/5-3 Rock Mechanical Properties

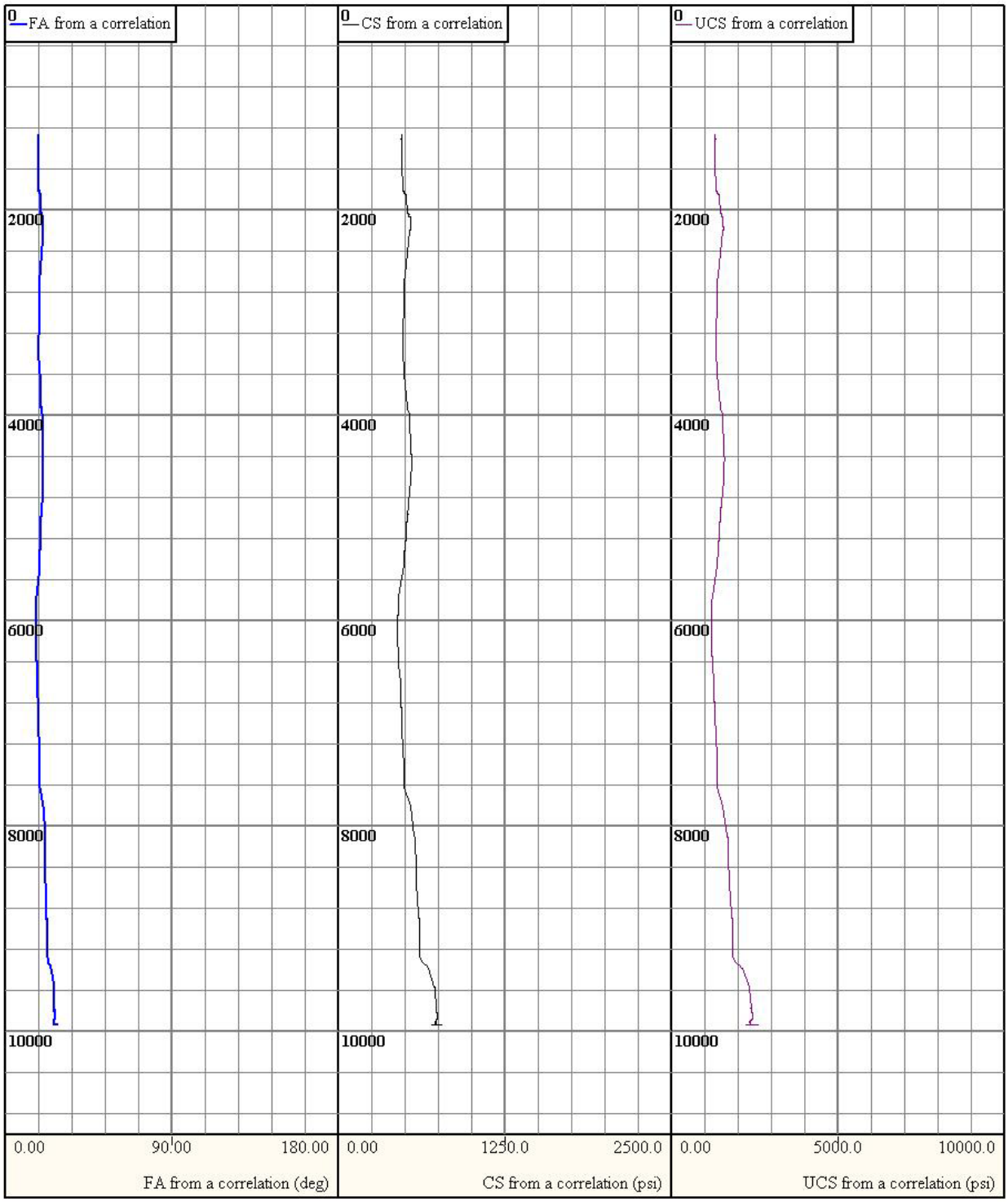

Figure 7.22. Rock mechanical properties for well 2/5-3. Depth in ft

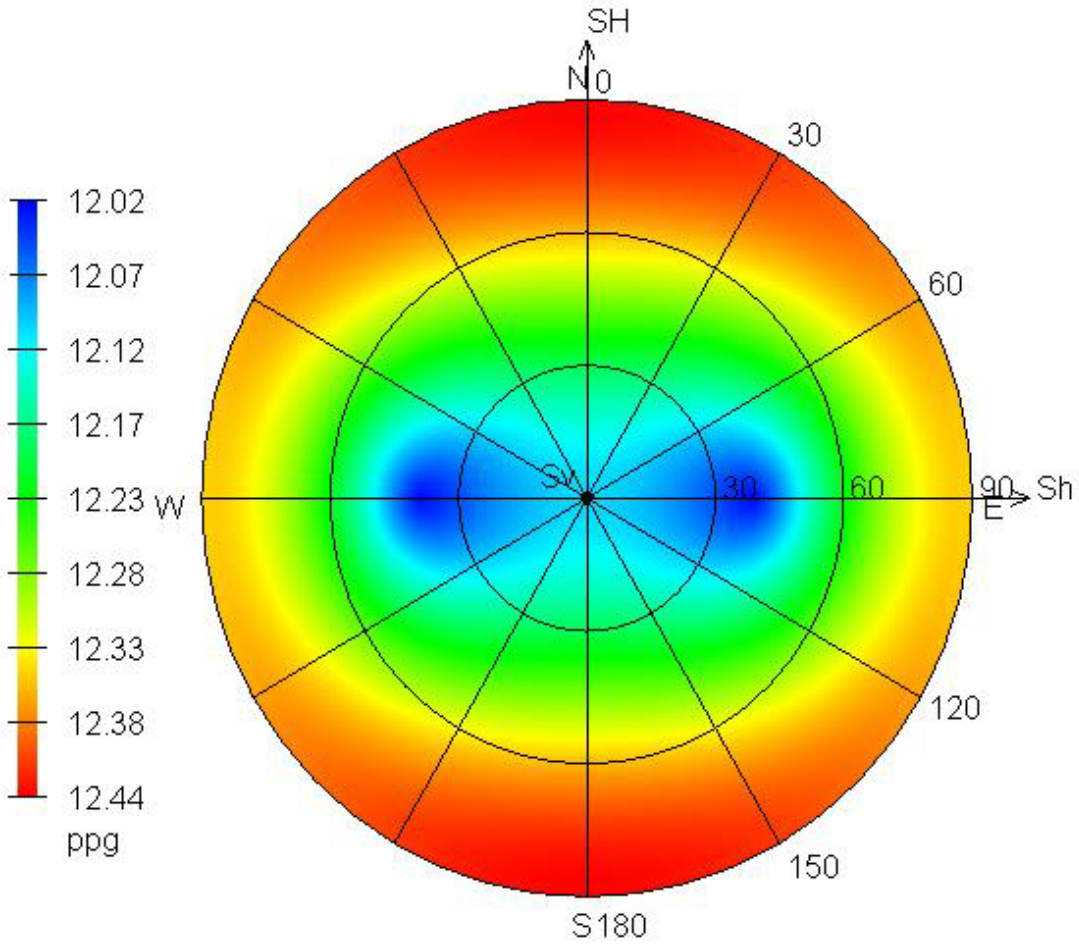

Figure 7.23. Hemisphere plot for well 2/5-3 at 5000ft

Table 7.6. Parameters used for safe wellbore trajectory analysis of well 2/5-3

Depth (ft)	5000
Failure criterion	Modified Lade
Overburden Gradient (ppg)	16.36
Pore Pressure Gradient (ppg)	11.65
Minimum Horizontal Stress Gradient (ppg)	15.67
Maximum Horizontal Stress Gradient (ppg)	15.98
Maximum Horizontal Stress Azimuth (ppg)	0.00
Poisson's ratio	0.46
Friction Angle (deg)	19.76
Cohesive Strength (psi)	521.08

8. Discussion

In areas where there has been little to no drilling activity, knowledge of the formation pressures is scarce, and well planners are basically drilling “blind”. The only available data may be seismic data, which implies that the estimates of pore pressure gradient, fracture gradient as well as the shear failure gradient are based on correlations which may be questionable. The model that has been built is the prediction of how the geopressure will behave in the Tor area, and is to be used when planning a well in the same area. The model must of course be updated in real time, to match observations made when drilling.

When performing the calibrations on the modeled pore pressure gradients, fracture gradients and shear failure gradients, the normal compaction trend line end point was shifted for all wells in order for the calibration points and pressure gradients to coincide. This indicates that the values used to create the normal compaction trend line were too low at the end point, meaning the formation is less compacted than first assumed. All but one of the normal compaction trend lines were corrected through calibration. Due to the lack of calibration sources for well 2/5-3, calibration was not possible for this well and thus the normal compaction trend line remains uncorrected.

As a result of shifting the normal compaction trend line towards higher values, the margin between the normal compaction trend line and the measured sonic log decreased, thus Eaton’s sonic method for predicting pore pressure will yield a lower value, as deduced from equation (7) in section 3.2.3. Also, as a result of the reduction in pore pressure, the failure gradient and shear failure gradient will be reduced accordingly. The magnitude of this reduction, or any reduction for that matter, is given by equation (26) and equation (38) in sections 3.3.3 and 4.1.3 respectively.

Well 2/4-17 shows a substantially larger decrease in the pressure gradient than the other wells, at around 6500ft the pore pressure has been reduced from 13ppg to 9ppg. For the other wells a decrease from approximately 14ppg to 12ppg was observed at the same depth. The reason for the large decrease of pore pressure in well 2/4-17 is unknown, and is a topic for further investigation.

The resulting operational drilling windows after calibration show substantially similar trends. For depths to 5000ft the drilling window is fairly wide, while for depths deeper than 5000ft the drilling window decreases and becomes narrower. This is the case for all the wells except well 2/4-17 where the drilling window is quite wide until a depth of approximately 7000ft. Keeping in mind that these wells have close to zero inclination, it is clear that with an inclined well the drilling window will be narrower and the margin between the shear failure gradient and the pore pressure will increase.

The rock mechanical properties that have been deduced by using Lal's equations for the six wells of current interest show the same trends. A close to constant value over the main part of the well depth may be observed, increasing in value over a short depth interval close to the wells total depth. The friction angle shows a close to constant value of 20° for all wells, a value shown to be common for shale (Horsrud, P., 2001). As for the cohesive strength and the unconfined compressive strength, these are values that may greatly vary depending on the shale. The values that were produced from Lal's equation in our case are in the range of 1000-2000 psi for the unconfined compressive strength and approximately 500 psi for the cohesive strength.

As for the safe wellbore trajectory analysis, this trend is evident for all of the wells. The hemisphere plots show the same tendency which is a greater variation on the mud weight in the direction of the maximum horizontal stress, thus showing the need for lower mud weight for drilling in the minimum horizontal stress direction, east to west. This is to be expected due to the horizontal stress ratio which is assumed to be 1.02, i.e. 2%. The higher this ratio is, the greater the difference will be regarding mud weight variation relative to horizontal stress direction. Of course, if the horizontal stress ratio is equal to one, the hemisphere plot will show close to concentric circles as there will be no difference of the horizontal stresses.

The hemisphere plots shown in section 7 show the maximum horizontal stress azimuth to be at 0°, this direction is the default value given by the software. In order to determine this value and reflect reality, the strike direction of drilling induced fractures can be determined, thus providing an estimation of the maximum horizontal stress direction.

When using the model built in this thesis, it must be decompressed or compressed to reflect the current formation depth intervals, thus providing the well planner with a pressure model that will be more than sufficient to determine the drilling window. Following the determination of the drilling window, the mud program can be designed and hydraulics can be run. When running hydraulics, different flow rates in the well are simulated by using appropriate software, resulting in the equivalent circulating densities (ECD) and down-hole pressures. On grounds of these results the casing setting depths may be determined. Of course the chosen mud weight must lie within the margin of the safe drilling window, and goal is to push the casing shoe depth further down allowing a deeper well.

As shown in section 6.5, choosing a different model to calculate the rock mechanical properties will have a substantial effect on the estimated shear failure gradient. This results in an element of uncertainty in the model. The shear failure gradient can however be validated by inspected cuttings from an incident where wellbore stability issues were encountered. The shape and size of the cuttings, i.e. if they are rounded or splintered, can provide information on whether or not the mud weight used exceeds the shear failure gradient. Also, by history matching and calibration of the model this element of uncertainty may be close to eliminated, meaning the model continues to be highly reliable. In order to increase the precision of the model, the number of offset wells used to build the model should be increased, leading to a better model which also implies more accurate predictions. However, it must be kept in mind that drilling itself is not a 100% exact science. When drilling a well, decisions must be made during the course of the actual drilling procedure. These decisions are based operational observations and incidents which must be acted on, and may lead to an alteration of the pre drilled estimate of a safe operational drilling window.

Prior to calibration, the geomechanical model based only on log and survey data is very conservative, and may not accurately describe reality. The estimation of the pressure gradients is dependent on each other, meaning the gradients are all sensitive to discrepancies in the provided log data. A quality check of the log data is therefore essential, to make sure that all values somewhat coincide with previous validated

measurements. In particular, if the density of the formation is wrongly estimated, this will lead to an erroneous estimate of the overburden gradient, which in turn will lead to an erroneous pore pressure gradient and fracture gradient estimation. A similar case is observed for the sonic log, due to the fact that this log has been used as the porosity indicating dataset, and the pore pressure estimation is based on the measured values departure from the normal compaction trend line, an erroneous sonic log measurement will result in an incorrect estimation of the pressure gradients. Hence, it is evident the pressure gradients are tremendously sensitive to inaccuracies in the log data.

For wildcat wells, where there is no prior information regarding the pressure situation within the formation, the predicted model will be very conservative, mainly basing itself on seismic data. As the development of a field begins, the number of offset wells drilled will increase. This means that data available for calibration will also increase, leading a reduction of uncertainty and an increase in accuracy of the field specific model. Most big fields on the Norwegian continental shelf are in their final phase, with the more complex and challenging wells left to be drilled and completed. For such a well, i.e. high pressure high temperature wells (HPHT) and/or wells with high inclination, the drilling window may be very tight. In some cases this drilling window is so tight it is questionable whether or not the well can be drilled. By calibrating the model using offset wells and thus fine tuning the pressure gradients, the drilling window may increase, allowing the well to be drilled.

Through calibration the model is validated and the uncertainty of the model is decreased. This validation is based on the data from calibration sources which may be a given value or simply indications that a gradient is inaccurate as described in section 6.6. Geomechanical modeling is not an exact science, and it is therefore of uttermost importance that the procedures yielding possible sources of calibration are consistent from well to well, i.e. that leak off tests are always performed correctly and that the correct values are selected from these. By eliminating the uncertainty of these measurements, the uncertainty of the model will also decrease, leading to a more precise geomechanical model.

One aspect that is important to keep in mind is that it is vital to have a fundamental understanding of all parts of the data acquisition. This means to understand the daily drilling reports, seismic data, geological data as well as the wellbore logs. An element of uncertainty in modeling arises when information from these different aspects is collected by different groups. This is due to unlike interpretations of technical terms and such that may lead to confusion and misunderstandings. In the light of this observation, it is clear that a fundamental understanding of all the previously mentioned aspects is necessary in order to properly build a geomechanical model.

It is also essential to understand what happens during drilling a well, meaning understanding of what mechanisms lead to the observed drilling incidents. Through combining the physical and operational observations with the theoretical model, the correct image of reality may be obtained and the well may be drilled as safely and cost efficient as possible.

9. Suggestions for Further Study

The 2D field specific model for the Tor field has been built based on data from six offset wells. For the further work of this project, future drilled wells should be added to the model, and newer wells that have been drilled in the area should be used to validate or invalidate the model. This will increase the precision of the model, and ultimately lead to a model that closely resembles reality.

The model that has been built in this thesis solves approximately 80% of all the drilling problems that may be encountered during drilling a well (Shaver, 2012). The problems that have been left unexplored in this work include the chemical and hydraulic issues and the changes they may induce in the near wellbore pressure. To solve these problems, a great amount of information and data is needed. Most of the problems regarding the chemically induced pressure effects have been solved in the industry by using oil based mud, which reduces the mud systems interaction with shale. For further investigation of the model and what impact various shale properties may have on the drilling window, the SINTEF developed software PSI may be used. PSI is an acronym, the full name of the software being “Preventing Shale Instabilities”. This software can investigate the effects of shale anisotropy, shale-fluid interactions as well as the capillary effects in shale and provide an estimate of the failure probability and shale failure gradient under various situations. In addition to this PSI allows the user to investigate the effect of well inclination and azimuth in combination with the previous mentioned shale properties. The Drillworks software also allows the user to observe the effect of inclination and azimuth, a feature that would be relevant in the case of planning a highly deviated well using the model that has been built.

10. Conclusions

The Greater Ekofisk area consists of several fields, amongst others the Tor field. By using offset well data from this field as well as offset well data from the South-East Tor field and Tjalve field, a 2D field specific linear elastic geomechanical model for the Tor field has been built, allowing for the estimation of pore pressure, fracture and shear failure gradients for future wells drilled in this field. There are several ways documented in the literature as to how these gradients are estimated, for the given situation of this work Eaton's sonic method was chosen for estimation of the pore pressure gradient, Eaton's method for the fracture gradient and the Modified Lade criterion for the shear failure gradient.

A great part of this work is calibrating of the model to operational observations, which involves fitting the estimated curves to real drilling incidents. The current model that has been built is highly reliable, and as mentioned it will become more accurate the more offset well data that is incorporated. This will lead to better and more precise predictions of the drilling window for future wells in the Tor field area.

The Tor field specific 2D geomechanical model shows how the pore pressure gradient, fracture gradient and the shear failure gradient will vary with depth. The model shows a wider drilling window for depths down to approximately 5000ft, becoming narrower and narrower as the depth approaches the wells total depth.

With this model it is hoped that reliable drilling windows can be estimated for the future wells in the Tor field area, thereby reducing drilling related problems and allowing the well to be drilled safely in a timely manner.

Bibliography

Baker Hughes Inc., 2011. *LIAG - Leibniz Institute for Applied Geophysics*. [Online] Available at: http://www.liag-hannover.de/fileadmin/user_upload/dokumente/FKPE/11.workshop/Wessling.pdf [Accessed 07 May 2012].

Berg, S., 2011. *Modelling of time dependent instabilities in shales on a real field case using PSI*. Project Work. Trondheim: NTNU.

Bourgoyne Jr., A.T., Millheim, K.K., Chenevert, M.E. & Young Jr., F.S., 1986. *Applied Drilling Engineering*. SPE Textbook Series.

Bowers, G.L., 1995. Pore Pressure Estimation From Velocity Data: Accounting for Overpressure Mechanisms Besides Undercompaction. *SPE, Drilling and Completion*, pp.89-95.

Bowers, G., 1999a. *State of the Art in Pore Pressure Estimation*. Report No. 1. Knowledge Systems, INC. DEA Project 119.

Bowers, G., 1999b. *State of the Art in Fracture Gradient Estimation*. Report No. 3. Knowledge Systems, INC. DEA Project 119.

Bowers, G.L., 2001. Determining an Appropriate Pore-Pressure Estimation Strategy. *Offshore Technology Conference*.

Breckels, & van Eekelen, H.A.M., 1982. Relationship Between Horizontal Stress and Depth in Sedimentary Basins. *Society of Petroleum Engineers of AIME*, pp.2191-99.

Cardu, M., Iabichino, G. & Mancini, R., 1989. A contribution to rock behavior under cyclic fatigue. In *Rock at Great Depth*. Rotterdam: Maury & Fourmaintraux. pp.77-83.

Cho, F. & Haimson, B.C., 1987. Effect of cyclic loading on circular openings - Results of a laboratory simulation. *28th US Symposium on Rock Mechanics*, pp.805-12.

ConocoPhillips Company, 2012. *The Greater Ekofisk Area*. [Online] Available at: http://www.conocophillips.no/EN/Norwegian%20shelf/Ekofisk/Pages/index.aspx [Accessed 03 March 2012].

Daines, S.R., 1980. The Prediction of Fracture Pressures for Wildcat Wells. *Society of Petroleum Engineers*. SPE 9081.

Daines, S.R., 1982. Prediction of Fracture Pressures for Wildcat Wells. *Journal of Petroleum Technology*, pp.863-72.

DiSiena, J.P. & Hilterman, F.J., 1994. Density Estimation From the Sonic Log: A Case Study. *Society of Exploration Geophysicists*.

Dutta, N., 1999. *Seismic Prediction of Geopressure: Some Basic Principles and the Best-Practice Methodology*. Report No. 2. Knowledge Systems, INC. DEA Project 119.

Eaton, B.A., 1969. Fracture Gradient Prediction and its Application in Oilfield Operations. *SPE-AIME*, pp.1353-60.

Eaton, B.A., 1975. The Equation for Geopressure Prediction from Well Logs. *Society of Petroleum Engineers*. SPE 5544.

Eaton, B.A. & Eaton, T.L., 1997. Fracture Gradient Prediction For The New Generation. *World Oil*, October. pp.93-100.

Ewy, R.T., 1999. Wellbore-Stability Predictions by Use of a Modified Lade Criterion. *SPE*.

Fjær, E. et al., 2008. *Petroleum Related Rock Mechanics*. 2nd ed. Elsevier.

Haavardstein, S., 2012. Personal Communication.

Halliburton, 2009. *Drillworks® Software Pro Training Manual, Predict and geostress.*. [Training manual] Version 5000.0.3.

Hobart, S., 1999. *Pre-Drill Overburden Estimation*. Report No. 4. Knowledge Systems, INC. DEA Project 119.

Horsrud, P., 2001. Estimating Mechanical Properties of Shale From Emperical Correlations. *SPE Drilling & Completion*. SPE 56017.

Hottmann, C.E. & Johnson, R.K., 1965. Estimation of Formation Pressures from Log-Derived Shale Properties. *Journal of Petroleum Technology*, 17(6), pp.717-22.

Hubbert, M.K. & Willis, D.G., 1957. Mechanics of Hydraulic Fracturing. *SPE 686*.

Islam, M.A., Skalle, P., Al-Ajmi, A.M. & Søreide, O.K., 2010. Stability Analysis in Shale through Deviated Boreholes using Mohr and Mogi-Coulomb Failure Criteria. *ARMA*.

Itasca, 2012. *Itasca Houston, Inc.: Expertise: Geomechanical Model*. [Online] Available at: http://www.itascahouston.com/geo_model.html [Accessed 29 April 2012].

Knowledge Systems, 2006a. *Knowledge Systems*. [Online] Available at: http://ks.wholewheatcreative.com/uploads/DrillworksPredict2.pdf [Accessed 10 Mars 2012].

Knowledge Systems, 2006b. *Knowledge Systems*. [Online] Available at: http://ks.wholewheatcreative.com/uploads/DrillworksGeostress2.pdf [Accessed 07 May 2012].

Lal, M., 1999. Shale Stability: Drilling Fluid Interaction and Shale Strength. *Society of Petroleum Engineers*.

Lashkaripour, G.R. & Dusseault, M.B., 1993. A Statistical Study on Shale Properties: Relationships Among Principal Shale Properties. In Li & Lo, eds. *Probabilistic Methods in Geotechnical Eng.* Balkema, Rotterdam, The Netherlands.

Li, S., George, J. & Purdy, C., 2012. Pore-Pressure and Wellbore-Stability Prediction to Increase Drilling Efficiency. *Journal of Petroleum Technology*, pp.98-101.

Matthews, W.R. & Kelly, J., 1967. How to predict formation pressure and fracture gradient. *The Oil and Gas Journal*, pp.92-106.

McLean, M.R. & Addis, M.R., 1990. Wellbore Stability: The Effect of Strength Criteria on Mud Weight Recommendations. *SPE 20405*.

Norwegian Petroleum Directorate, 2012a. *NPD FactMapSearch*. [Online] Available at: http://npdmap1.npd.no/website/NPDGIS/NPDSEARCH/default.htm [Accessed 03 March 2012].

Norwegian Petroleum Directorate, 2012b. *Norwegian Petroleum Directorate*. [Online] Available at: http://factpages.npd.no/factpages/Default.aspx?culture=nb-no&nav1=discovery&nav2=PageView|All&nav3=44084 [Accessed 03 March 2012].

Norwegian Petroleum Directorate, 2012c. *Norwegian Petroleum Directorate*. [Online] Available at: http://factpages.npd.no/factpages/Default.aspx?culture=nb-no&nav1=discovery&nav2=PageView|All&nav3=44090 [Accessed 03 March 2012].

Norwegian Petroleum Directorate, 2012d. *Norwegian Petroleum Directorate*. [Online] Available at: http://factpages.npd.no/factpages/Default.aspx?culture=nb-no&nav1=discovery&nav2=PageView|All&nav3=44066 [Accessed 03 March 2012].

Norwegian Petroleum Directorate, 2012e. *Norwegian Petroleum Directorate*. [Online] Available at: http://www.npd.no/en/Publications/Facts/Facts-2011/Chapter-10/Tor/ [Accessed 03 March 2012].

Osborne, M.J. & Swarbrick, R.E., 1997. Mechanisms for Generating Overpressure in Sedimentary Basins: A Reevaluation. *AAPG Bulletin*, June. pp.1023-41.

Owolabi, O.O., Okpobiri, G.A. & Obomanu, I.A., 1990. Prediction of Abnormal Pressures in the Niger Delta Basin Using Well Logs. *Society of Petroleum Engineers*. 21575.

Rocha, L.A.S. et al., 2004. Fracture Pressure Gradient in Deepwater. *SPE 88011*.

Schlumberger, 2012. *Schlumberger Oilfield Glossary*. [Online] Available at: http://www.glossary.oilfield.slb.com/ [Accessed 15 February 2012].

Shaver, M., 2012. Personal Communication.

SPE, 2011. *SPE E&P Glossary*. [Online] Available at: http://www.spe.org/glossary/wiki/doku.php/terms:ballooning_drilling [Accessed 07 May 2012].

Swarbrick, R.E., 2001. Pore-Pressure Prediction: Pitfalls in Using Porosity. *Offshore Technology Conference*.

Tang, H. et al., 2011. Worldwide Pore Pressure Prediction: Case Studies and Methods. *SPE 140954*.

Ward, C.D., Coghill, K. & Broussard, M.D., 1995. Brief: Pore- and Fracture-Pressure Determinations: Effective-Stress Approach. *JPT*, pp.123-24.

Yassir, N. & Addis, M.A., 2002. Relationships between Pore Pressure and Stress in Different Tectonic Settings. In A.R. Huffman & G.L. Bowers, eds. *Pressure regimes in sedimentary basins and their prediction: AAPG Memoir 76*. pp.79-88.

Zhang, J., Standifird, W. & Lenamond, C., 2008. Casing Ultradeep, Ultralong Salt Sections in Deep Water: A Case Study for Failure Diagnosis and Risk Mitigation in Record-Depth Well. *SPE 114273*.

Appendix A – Nomenclature

C	Conductivity [millimhos]
CS	Cohesive Strength [MPa] or [psi]
C_0	Unconfined Compressive Strength [MPa] or [psi]
d	Corrected d exponent [d-units]
D	Depth [ft]
D_w	Water depth [ft]
D_A	Depth of interest in abnormal pressure interval [ft]
D_N	Normal equivalent depth, corresponding to D_A [ft]
DP	Drucker-Prager
E	Young's modulus [GPa]
FA	Friction angle [°]
FG	Fracture Gradient [ppg]
G	Shear modulus [GPa]
g	Gravitational constant
G_0	Overburden Gradient [psi/ft]
G_H	Normal Hydrostatic Gradient [psi/ft]
HPHT	High Pressure High Temperature
K_B	Ratio used in Daines equation
K_{eff}	Effective stress ratio
K_E	Ratio used in Eaton's equation
K_{HW}	Ratio used in Hubbert & Willis' equation
K	Porosity decline constant [1/ft]
MC	Mohr Coulomb
ML	Modified Lade
MWD	Measurement While Drilling
NCS	Norwegian Continental Shelf
PPG	Pore Pressure Gradient [ppg]
P_w	Well pressure [MPa] or [psi]
$p_{confining}$	Confining pressure [MPa] or [psi]
p_f	Pore pressure [MPa] or [psi]

p_{fn}	Normal pore pressure [MPa] or [psi]
p_{ff}	Fracture extension pressure [MPa] or [psi]
R	Resistivity [ohm-m]
SFG	Shear Failure Gradient [ppg]
Δt	Interval transit time [microsecond/ft]
TD	Total Depth
T_0	Tensile strength [MPa] or [psi]
UCS	Unconfined Compressive Strength [MPa] or [psi]
v_p	P-wave velocity normal to bedding [km/s]
V	Velocity [ft/sec]
β	Failure angle [°]
μ	Coefficient of internal friction
σ	Stress [MPa] or [psi]
σ'	Effective stress [MPa] or [psi]
σ_{ob}	Overburden stress [MPa] or [psi]
σ_t	The superposed horizontal tectonic stress [MPa] or [psi]
σ_v	Vertical/overburden stress [MPa] or [psi]
σ_H	Maximum horizontal stress [MPa] or [psi]
σ_h	Minimum horizontal stress [MPa] or [psi]
σ_n	Normal vertical matrix stress [MPa] or [psi]
σ_z	Axial stress [MPa] or [psi]
σ_θ	Hoop stress [MPa] or [psi]
σ_r	Radial stress [MPa] or [psi]
σ_1	Maximum principal stress [MPa] or [psi]
σ_2	Intermediate principal stress [MPa] or [psi]
σ_3	Minimum principal stress [MPa] or [psi]
ρ	Density [g/cc]
ρ_b	Bulk density [g/cc] or [lbm/gal]
ρ_{sw}	Seawater density [g/cc] or [lbm/gal]
ρ_g	Grain density [g/cc] or [lbm/gal]
$\tau_{\theta z}$, τ	Shear stress [MPa] or [psi]
ϕ_0	Surface porosity [-]

ϕ	Porosity [%]
φ	Friction angle [°]

NOTE: All equations are given in consistent units, i.e. oil field units or SI units.